COO-1177-16

TURBULENT FREE CONVECTION IN NEAR CRITICAL WATER*

by

J. R. Larson

R. J. Schoenhals

Purdue Research Foundation

Lafayette, Indiana

Contract No. AT(11-1)-1177

August 1964

*Work reported herein formed the basis of a Ph.D. thesis in Mechanical Engineering at Purdue University.

DISCLAIMER

ACKNOWLEDGMENT

I wish to thank my major professor, Dr. R. J. Schoenhals for his guidance and many suggestions throughout the course of this work;

staff members and fellow students of the School of Mechanical Engineering for many tangible and intangible contributions;

and to the Argonne National Laboratory of the United States Atomic Energy Commission for the financial support making the investigation possible.

TABLE OF CONTENTS

Page

LIST OF TABLES

LIST OF ILLUSTRATIONS

ABSTRACT

Larson, Jay Reinhold. Ph.D., Purdue University, August 1964. Turbulent Free Convection in Near Critical Water. Major Professor: R. J. Schoenhals. Heat transfer from a vertical flat plate by turbulent free convection to water near its thermodynamic critical point was studied analytically and experimentally. An analytical method was developed to predict the magnitude and trend of the heat transfer coefficient in this region. This method of solution involved an integral technique whereby the boundary layer equations were integrated across the boundary layer. The method included assumptions of Reynolds analogy, the Blasius wall shear stress, and suitable velocity and temperature profiles. The energy equation was written in terms of enthalpy in order to avoid certain difficulties associated with the highly variable properties in the critical region.

Experimental measurements were made of the heat flux from a platinum ribbon suspended in a pressure vessel containing the test water. The ribbon was heated electrically by direct current. The temperature of the ribbon was determined by resistance measurement and comparison with a previous calibration of the resistance-temperature curve of the test section. The temperature of the bulk fluid was determined by use of a platinum resistance thermometer.

The experimental results indicate reasonable agreement with the analytical prediction. A correlation was also developed which gives reasonable predictions of the data in terms of the usual dimensionless parameters.

INTRODUCTION

Heat transfer in the near critical region of water has been of interest for some time. Steam boilers and nuclear reactors are approaching or already exceed the pressures and temperatures of the critical point. Experimental data is necessary to confirm existing heat transfer correlations or to devise new ones for design calculations. The critical region is also of interest because of the variation of the thermodynamic and transport properties in a narrow temperature band. These property changes cause the coefficient of heat transfer to become very large as the critical point is approached and thus might permit the removal of large quantities of heat from a physically small heat source.

Free convection is of universal interest in the removal of heat because its inherent mechanism eliminates the need for pumps with their cost, maintenance, and resultant power loss as well as increasing system reliability. In this work there were three major objectives: the first one was to establish an analytical model and method for the prediction of heat transfer in this region; the second one was to experimentally measure actual heat transfer data supporting the analytical work; and the third was to provide a simple method of presentation of the results in a form convenient for design purposes. The geometry chosen for this investigation was a vertical flat plate.

An integral technique was employed to obtain an analytical solution of the problem. The equations of momentum and energy were

integrated across the boundary and the heat transfer coefficient was obtained. The method included the assumptions of Reynolds analogy, the Blasius wall shear stress, and suitable velocity and temperature profiles. Because of the complexity of expressions required to describe the variations in properties with temperature, numerical integration was employed. More sophisticated techniques and analogies are commonly used in the study of forced turbulent convection. However, until better experimental knowledge exists of the velocity and temperature variation across the boundary layer these techniques will be difficult to apply in free convection.

The experimental apparatus consisted of a platinum ribbon or foil placed inside a pressure vessel. The ribbon was heated electrically by direct current. During operation voltage was measured at several points along the length to determine local heat generation and a local temperature from a previous temperature-resistance calibration. The temperature of the ambient fluid was determined by a platinum resistance thermometer. The local heat transfer coefficient was determined from the relationship

$$h_c = \frac{Q}{A'\Delta t}$$

where Q was the heat generation, A' was the area of the ribbon section, and Δt was the temperature difference between the ribbon and the bulk fluid.

The experimental results were compared to the analytical prediction and similar trends and magnitudes were found. Some 77 data points representing a range of temperature and temperature differences for both

3240 and 3300 psia were correlated best by

$$Nu = 0.0872\, Gr'^{\frac{1}{3}}\, Pr^{0.247} \left(\frac{t_\infty}{t_w - t_\infty}\right)^{0.137}$$

where all properties not specified were evaluated at the bulk temperature. The average error of this relation was about 15 percent.

LITERATURE SURVEY

Work in the Critical Region

Many investigators have taken experimental data for forced convection in near critical water. Some have also made analytical studies of this problem in an attempt to explain the increase in heat transfer in this critical region. A discussion of this work and the pertinent references are given in Touba (29).

Fewer people have made studies of near critical fluids in free convection. Schmidt, Eckert, and Grigull (20) experimented with near critical ammonia contained in a thermal-syphon loop. Very large coefficients of heat transfer were obtained but no correlation was attempted due to lack of accurate knowledge of the thermal properties. Doughty and Drake (3) conducted experiments using a platinum wire immersed in near critical Freon 12. Most of their data was expressed as plots of heat flux versus temperature difference. A peaking of the heat transfer coefficient was shown at critical conditions.

Griffith and Sabersky (8) also conducted experiments on near critical Freon 14, from a wire. They photographed some flow patterns at high temperature differences which they believed were due to bubble formations. They concluded that these bubbles confirmed a previous postulation made to explain the high rates of heat transfer observed in near critical water in forced convection.

Holt (11) carried out experiments with water over a wide range of temperature and pressure using a heated wire and also a one-eighth inch high vertical ribbon. Because of the small height of the ribbon, none of his data was in the accepted turbulent regime of free convection, although boiling did occur.

Bonilla and Sigel (2) experimentally studied free convection from a horizontal plate with n-pentane as the test fluid. Their experiment was conducted at pressures both below and above the critical point with large temperature differences, i.e., 60 degrees Fahrenheit to several hundred degrees Fahrenheit. The resultant data was correlated by the expression

$$Nu \propto Ra^{1/3}.$$

All properties were evaluated at the film temperature except for $\beta \Delta t$, which was expressed by either

$$\beta \Delta t = 2 \left(\frac{v'_w - v'_\infty}{v'_w + v'_\infty} \right)$$

or

$$\beta \Delta t = \log_e \left(\frac{v'_w}{v'_\infty} \right).$$

The large experimental temperature differences probably reduced the effect of the large property changes that occur in a small temperature range. Holman and Boggs (10) experimentally studied free convection heat transfer to Freon 12 in a closed loop over a wide range of tem-

peratures and pressures. Their data was fairly well described by a dimensionless correlation derived for a thermal-syphon with constant properties of the form

$$\frac{Nu\,Gr}{Pr} = C' Re^{K'}$$

where C' and K' were constants. The average bulk temperature was used to evaluate the thermodynamic properties which were not well known. The average temperature differences between the wall and the fluid were not stated but were probably large. This would tend to average and minimize the effect of large property changes over a small temperature interval.

Van Putte (33) studied free convection in a closed loop and noticed an oscillation phenomenon as did Holman at near critical temperature and pressure. Van Putte was unable to correlate his data using common forced convection correlations.

Fritsch (5) made measurements from a one-eighth inch high vertical ribbon in near critical water at temperature differences of less than 30 degrees Fahrenheit. His data compared favorably with an exact solution for laminar free convection including the effects of variable specific heat and density. Thermal conductivity and viscosity were considered constant. He concluded that by accounting for the effect of property variations the accepted methods of obtaining heat transfer solutions would be satisfactory for near critical fluids as well as for fluids with small property changes.

Simon (26) experimentally studied laminar free convection in near critical carbon dioxide from a vertical plate and a horizontal cylinder.

A Mach Zender interferometer was utilized to obtain the density gradient in the boundary layer and density at the wall. The wall temperature and temperature profiles were then found from thermodynamic data. His experiments were conducted with temperature differences smaller than 0.02 degrees Centigrade. The flat plate results were satisfactorily correlated by

$$\frac{q'' \frac{L}{2}}{\rho_c k_c \frac{\partial T}{\partial \rho}\Big|_p} \left(\frac{T - T_c}{T_c}\right) \propto \frac{Ra'}{\left(\frac{\mu C_p}{k_c}\right)^{1/2}} .$$

The heat flux was q'', $\frac{L}{2}$ was half the plate height, and properties with the subscript "c" were evaluated at the critical point. Simon also visually noted many interesting and unusual flow patterns in the critical region.

Theoretical Free Convection Work

One of the first attempts to derive an analytical expression for the coefficient of heat transfer in turbulent free convection was made by Eckert and Jackson (4). Their approach consisted of integrating the momentum and energy flux across the sides of a control volume along a prescribed velocity and temperature profile. They also utilized Reynolds analogy to relate the wall heat flux to the wall shear stress. The Blasius wall shear expression developed for forced convection was used to complete the derivation. They further restricted their solution to an incompressible fluid whose properties (all excepting density) were independent of temperature. The geometry chosen was that of a vertical flat plate. To clarify the details, the procedure will be briefly outlined.

Consider the volume element in Figure 1. By summing the momentum flux, the wall shear force, and the pressure force, the momentum balance on the control volume was

$$\frac{\partial}{\partial x}\left(\int_0^b \frac{\rho}{g} u^2 \, dy\right) = -\int_0^b \rho \, dy - b\frac{dp}{dx} - \tau_w .$$

Notice that ρ in this equation is in units of lb./ft.^{3} instead of slugs as used by Eckert. There was no momentum contribution across the right hand boundary since the velocity u was assumed zero beyond the disturbance thickness, δ .

The pressure change was due only to the hydrostatic head, thus,

$$\frac{dp}{dx} = -\rho_\infty .$$

The volumetric coefficient of expansion is defined as

$$\beta = \frac{1}{v'}\frac{\partial v'}{\partial t} = -\frac{1}{\rho}\frac{\partial \rho}{\partial t} \qquad \text{for constant pressure.}$$

For the case where the density change is small compared to the magnitude of the density and where β is nearly independent of temperature, the previous relationship may be integrated and expanded in a series yielding

$$\beta = \frac{\rho_\infty - \rho}{\rho}\left(\frac{1}{t - t_\infty}\right) .$$

With these relationships the momentum equation was

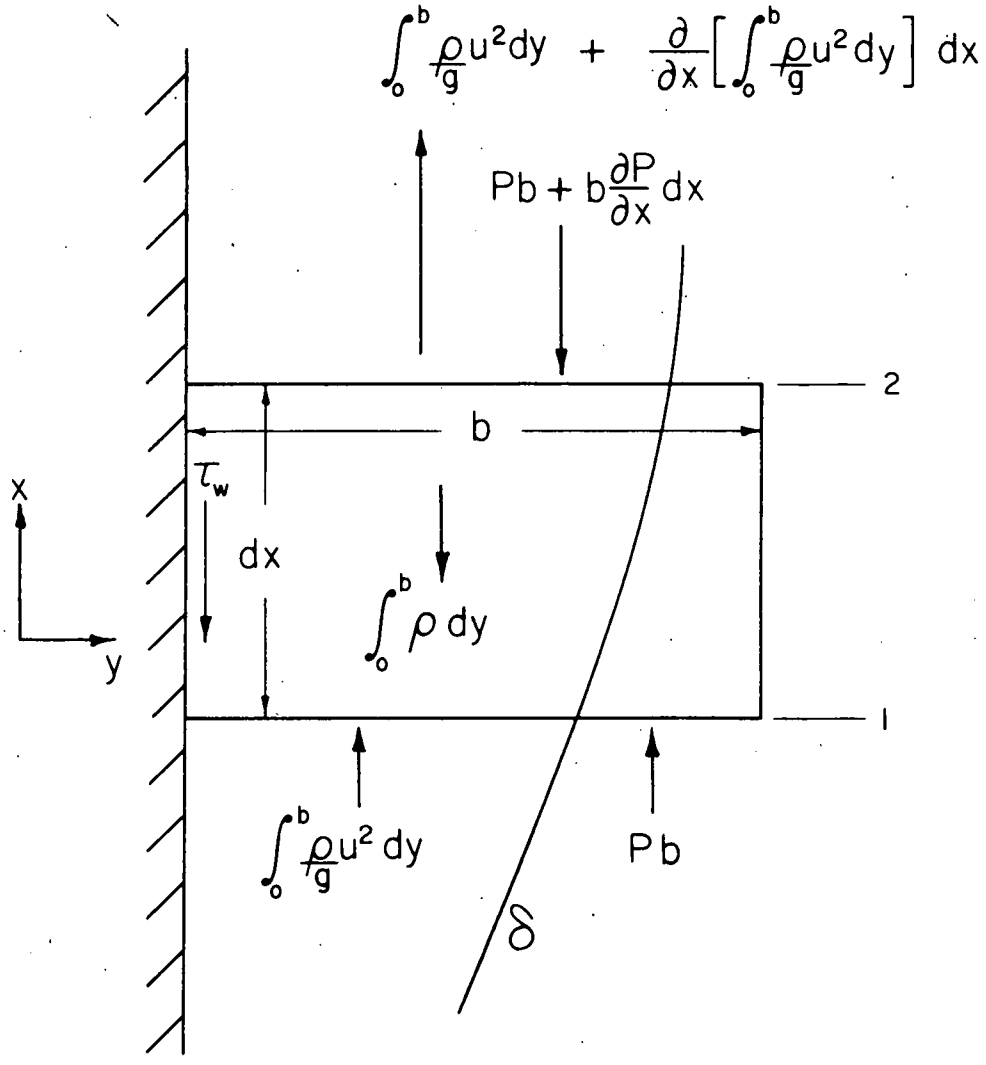

FIG. 1 CONTROL VOLUME FOR MOMENTUM ANALYSIS

$$\rho \frac{\partial}{\partial x} \int_0^b u^2 dy = g\rho\beta \int_0^b (t - t_\infty) dy - g\tau_w .$$

The energy equation was found from the elemental volume shown in Figure 2. Summing the heat convected from the element and the heat conducted into the element at the wall yielded

$$q''_w = \rho C_p \frac{\partial}{\partial x} \int_0^b (t - t_\infty) u \, dy .$$

In obtaining the energy convected across the right boundary the velocity across the boundary was needed and was found from the continuity of mass equation written as

$$v_{y=b} = - \int_0^b \frac{\partial u}{\partial x} \, dy .$$

For expressions describing the velocity and temperature profiles, Eckert and Jackson used earlier experimental work of Griffiths and Davis (9). The velocity and temperature profiles could be closely approximated by the one-seventh power law which is used extensively in forced convection. The expressions used were

$$u = u_1 \left(\frac{y}{\delta}\right)^{1/7} \left(1 - \frac{y}{\delta}\right)^4, \text{ and } \quad t - t_\infty = (t_w - t_\infty)\left[1 - \left(\frac{y}{\delta}\right)^{1/7}\right] .$$

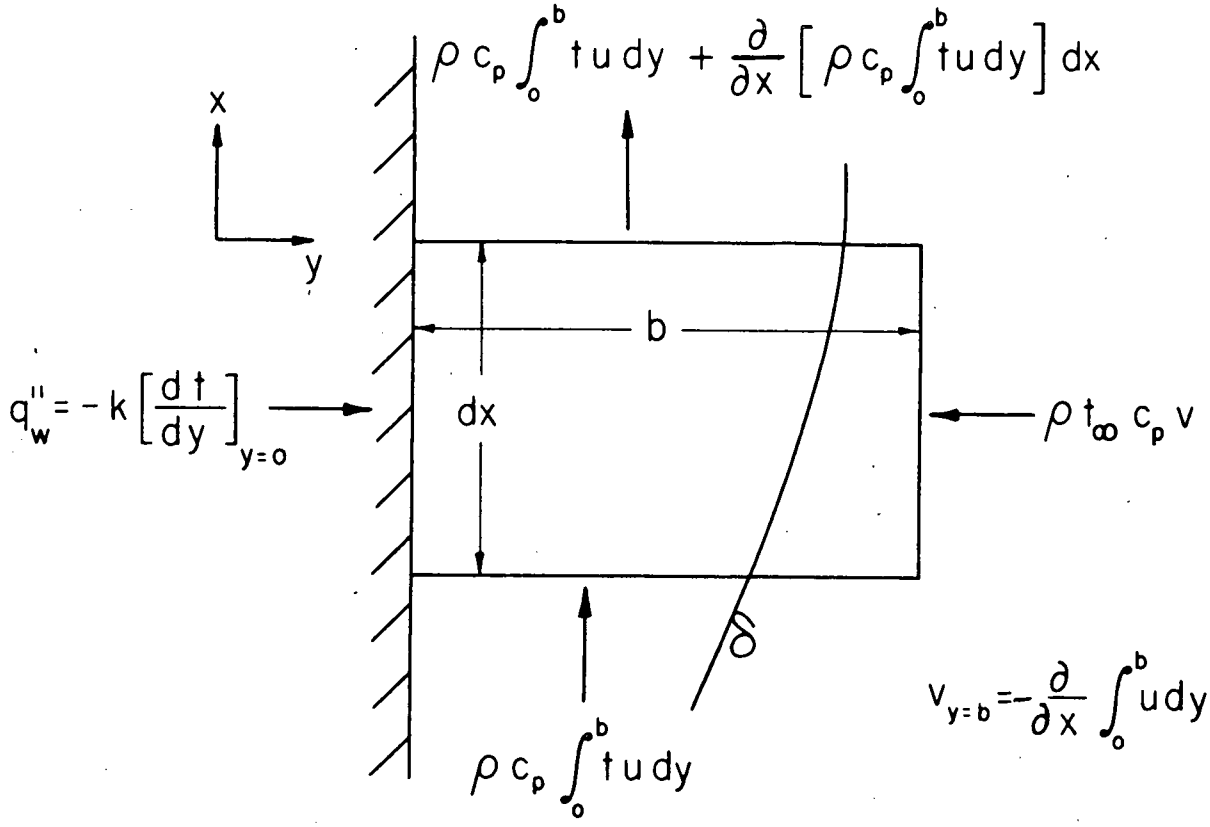

FIG. 2 CONTROL VOLUME FOR ENERGY ANALYSIS

The profiles are shown in Figure 3. The velocity u_1 was the value u would take at δ if the one-seventh power velocity law held completely across the boundary layer. It was the equivalent characteristic stream velocity for which the velocity profile near the wall takes the same shape as in forced convection. Implicit in the choice of profiles was the assumption that the velocity and temperature disturbance thicknesses were nearly the same. This is approximately true for a Prandtl number near unity as illustrated in the exact solution for the laminar case by Ostrach (17).

Because of the similarity of the free convection velocity profile to the universal one-seventh power profile of forced convection, Eckert and Jackson assumed the Blasius shear expression developed for forced convection would hold true for the wall shear in free convection. For the one-seventh power velocity profile the Blasius expression is

$$\tau_w = 0.0225 \frac{\rho}{g} u_1^2 \left(\frac{\nu}{u_1 \delta}\right)^{1/4} .$$

To relate the wall shear to the wall heat flux Reynolds analogy, in the form

$$\frac{q''}{\tau} = -g C_p \frac{dt}{du} ,$$

was borrowed from forced convection theory. This assumed a Prandtl number of unity. However, a correction factor of $Pr^{-2/3}$ was applied as has been done for forced convection to make the analogy agree with experimental results over a wide range of Prandtl numbers. Thus

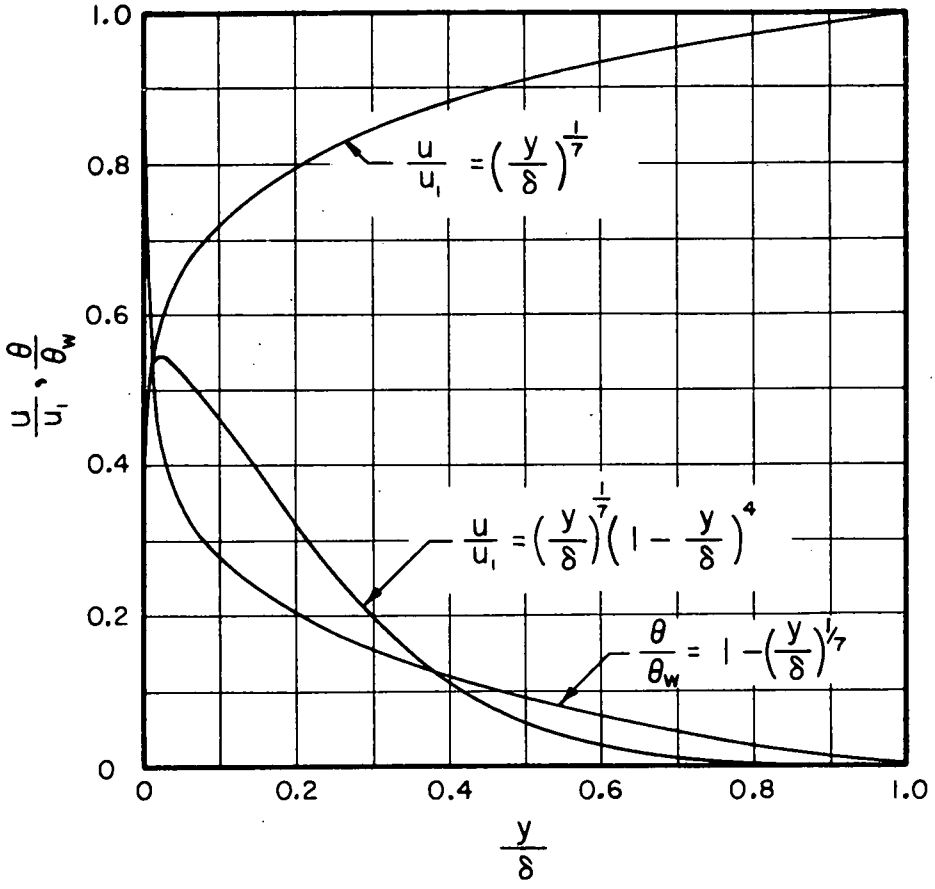

FIG. 3 DIMENSIONLESS VELOCITY AND TEMPERATURE PROFILES BASED ON DATA OF GRIFFITHS AND DAVIS

Eckert and Jackson developed the relationship

$$q_w'' = g \tau_w C_p \frac{\theta_w}{u_1} Pr^{-2/3} .$$

Evaluating the integrals with the aid of the specified profiles and substituting the shear stress and heat flux expressions into the energy equation, they obtained

$$0.523 \frac{d}{dx}\left(u_1^2 \delta\right) = 0.125 g \beta \theta_w \delta - 0.0225 u_1^2 \left(\frac{\nu}{u_1 \delta}\right)^{1/4}$$

and

$$0.0366 \frac{d}{dx}\left(u_1 \delta\right) = 0.0225 u_1 \left(\frac{\nu}{u_1 \delta}\right)^{1/4} Pr^{-2/3} .$$

The characteristic velocity u_1 and disturbance thickness δ are functions of x only. The two equations were solved by the substitutions,

$$u_1 = C_1 x^m \quad \text{and} \quad \delta = C_2 x^n .$$

Since the equations are valid for any x, the exponent of x for all terms in either equation must be identical. Thus the values m equal to one-half and n equal to seven-tenths were obtained. The constants C_1 and C_2 were then evaluated, and u_1 and δ were explicitly determined.

The local heat transfer coefficient was then found from the Reynolds relationship to be

$$h_c = \frac{q''_w}{\theta_w} = 0.0225\, \rho\, C_p\, u_1 \left(\frac{\nu}{u_1 \delta}\right)^{1/4} Pr^{-2/3} .$$

By addition of the proper variables, a local Nusselt number was developed to be

$$Nu = 0.0295 \left[\frac{Gr}{1 + 0.494\, Pr^{2/3}}\right]^{2/5} Pr^{7/15} .$$

From this expression the local coefficient was found to vary as $x^{0.2}$; thus the average coefficient was determined as

$$h_{c_{ave}} = \frac{h_{c_{local}}}{1.2} ,$$

and the average Nusselt number was determined as

$$Nu_{ave} = \frac{Nu_{local}}{1.2} .$$

This result was shown to agree well with experimental data, particularly for a Pr of unity.

An analysis for a vertical plate assuming a uniform heat flux was made by Siegel (25). His assumptions and the method of solution were basically the same as those of Eckert (4). The result for free turbulent flow was nearly the same as obtained for the isothermal wall, and was

$$Nu_{ave} = 0.0246 \left[\frac{Gr}{1 + 0.444\, Pr^{2/3}} \right]^{2/5} Pr^{7/15} .$$

where the Grashof number was based on an average temperature difference.

An attempt at a more realistic approach was made by Bayley (1) for a constant property incompressible fluid. He divided the boundary layer into two parts, a viscous sublayer and a turbulent outer layer. To account for an intermediate buffer layer the hydraulic sublayer thickness of $y^+ = 12$, determined from forced convection experimental measurements, was increased by half of the buffer layer to arrive at a thermal sub-layer thickness. The thickness of the thermal sub-layer was then

$$y^+ = \frac{y}{2} \left(\frac{g \tau_w}{\rho} \right)^{1/2} = 15 .$$

From this assumption, fractional temperature drops were computed in each layer and related. The temperature relationships were then substituted into the integral form of the boundary layer equations as written previously. The equations were solved for velocity and the disturbance layer thickness yielding expressions for the coefficient of heat transfer and Nusselt number.

Like Eckert and Jackson, Bayley assumed identical thicknesses for the thermal and velocity boundary layers. He stated that although

they are in reality different for Pr not equal to one, in free convection the fluid motion is caused by the temperature difference and therefore the actual difference in thickness is unimportant. Reynolds analogy, and the Blasius shear expression were also borrowed from forced convection theory. The velocity and temperature profiles, characterized by the one-seventh law were likewise used. To calculate an eddy diffusivity needed in Reynolds analogy, Bayley used the mixing length theory developed by Von Karman.

Bayley numerically evaluated his results for air (Pr = .73) and mercury (Pr = 0.01). His results for air could be well correlated by the expression

$$Nu = 0.10 \left(Gr\ Pr \right)^{1/3}$$

and closely checked experimental results of Saunders (24).

Next Waibler (36) made an analysis of the constant property problem using an approach similar to that used by Eckert and Jackson. He pointed out that the results obtained by Eckert and Jackson were not in agreement with the bulk of experimental data; specifically, experimental data could be correlated better by a Grashof number to the one-third power than by the two-fifths power. He also showed that the characteristic one-third power for turbulent flow could be obtained by modifying the exponential constant of the Blasius shear expression from one-fourth to one-half.

The constants in the Blasius shear expression have been shown to vary with the exponent of the velocity profile describing forced flow, viz.,

$$\frac{u}{u_1} = \left(\frac{y}{\delta}\right)^{1/n} .$$

Thus for an exponent of one-half in the Blasius expression, the corresponding value of n would be closer to three or four. With this Waibler argued that the one-seventh power characteristic velocity profile was not correct for turbulent free convection.

Fujii (6) derived several solutions for the constant property free convection problem at high GrPr numbers. In one case he used the laminar form of the boundary layer equations, i.e., wall shear stress expressed as equal to

$$\tau_w = \frac{\mu}{g}\left(\frac{\partial u}{\partial y}\right)_{wall} .$$

His equations were integrated using temperature and velocity profiles broken into two parts, a viscous sublayer and a turbulent outer layer. Using the same value for eddy diffusivity as used by Bayley, he obtained a solution characterized by the one-fourth power of the Grashof number which corresponded to experimental data he had obtained with ethylene glycol at GrPr values from 10^{10} to 10^{11}.

Another solution was obtained by integrating the turbulent form of the boundary layer equations, i.e., Blasius equation used for the wall shear stress. The constants a and N in the shear stress equation

$$\tau_w = a\frac{\rho}{g} u^2 \left(\frac{\nu}{u\delta}\right)^N$$

were left as unknowns. They were later determined, using previous experimental data from a derived expression relating these constants to a Reynolds number with properties and distance evaluated at the sublayer-outer layer interface. The values of these constants, a and N, for the shear stress expression were found to be identical to those in use for the one-seventh power law velocity profile, the shape of which was a necessary assumption in the analysis.

Fujii did not correct the relationship between heat flux and wall shear stress for the effect of variable Prandtl numbers as was done by Eckert. Instead he multiplied his final result by $Pr^{-2/3}$ and thus obtained a slightly different form given by

$$Nu \propto Gr^{2/5} Pr^{1/3}.$$

Experimental Free Convection Work

Experimental work in turbulent free convection has been carried out by a number of investigators. Most of the effort has been restricted to correlating the heat transfer coefficient in terms of the applicable dimensionless parameters. Very few have attempted to measure velocity and temperature profiles.

Turbulent Free Convection Correlations

The first evidence of the turbulent free convection coefficient being independent of a length parameter, i.e., $Nu \simeq Gr^{1/3}$, was produced by Griffiths and Davis (9). Their apparatus consisted of a nine foot wall made up of individually electrically heated sections

placed in air. A uniform wall temperature was obtained by varying the heat imput to the individual sections. By plotting the heat input versus height they ascertained that above a certain height the heat flux input remained constant when a constant wall-ambient air temperature difference was imposed. This meant the heat transfer coefficient was independent of distance beyond this height. This was also perhaps the first indication of the turbulent mechanism in free convection.

Saunders (22) investigated free convection in air over a wide range of Grashof numbers. This was accomplished by enclosing a uniformly electrically heated plate inside a pressure vessel. Thus the air density was used as the controlled variable instead of length or temperature difference. A plot of his data showed that the Nusselt number varied with the one-third power of the Grashof number in the turbulent region.

Saunders (23) also investigated free convection from a vertical plate in water. He found his data in the turbulent region was well correlated by

$$Nu = 0.17 (Gr\,Pr)^{1/3}.$$

The origin of turbulence was also investigated optically and found to occur at about $GrPr = 2 \times 10^9$.

Touloukian (30) investigated free convection to water and ethlyene glycol at high Grashof numbers using an electrically heated vertical cylinder. A correlation of the form

$$Nu = 0.0674 (Gr\,Pr^{1.29})^{1/3}$$

fitted all data very closely.

Waibler (36) investigated free convection to water from a ten foot vertical wall heated by condensing steam. Traps were placed at various heights to collect the condensation and thus provide a method of determining the local wall heat flux. His data was best correlated by

$$Nu = 0.795 (Gr\ Pr)^{0.285}$$

in the turbulent region.

Tuan (31) measured turbulent local heat transfer coefficients from a vertical cylinder to water. The cylinder was kept isothermal by varying power to individual internal heating elements. Thus local coefficients could be obtained quite well. His work was correlated by an expression

$$Nu = 0.0664 (Gr\ Pr)^{0.39}.$$

Jakob (12) and McAdams (14) both recommend a correlation of the form

$$Nu = 0.13 (Gr\ Pr)^{1/3}$$

based on experimental evidence of several investigators.

Velocity and Temperature Measurements

In all turbulent convection work a good knowledge of the velocity and temperature profiles is essential for a complete theoretical analysis of the problem. Temperature profiles may be found with relative ease, at least near the wall, by use of a small thermocouple. In the outer portion of the boundary layer large fluctuations occur which require

averaging to obtain a profile. Velocity profiles are much more difficult to obtain. The hot wire anemometer used extensively in forced air flow is not easily adapted to cope with a superimposed thermal layer found in free convection.

For measurements along a vertical wall in air, Griffiths and Davis (9) used a small platinum wire in one leg of a wheatstone bridge arrangement. With a small current flowing through this wire, the instrument acted as a resistance thermometer when placed in the boundary layer flow. For a larger current flow, the instrument became a hot wire anemometer. These investigators attempted to eliminate the temperature profile variation effect on velocity measurements by operating with a constant temperature difference between the wire and the air.

A plot of their temperature data showed some inconsistency. The temperature data in the outer layer did not smoothly approach the stated infinite bulk temperature value. Instead the temperature became nearly constant at a level considerably above the bulk temperature. Eckert and Jackson stated that these measurements were inconsistent but used them in their analysis since they were the only ones available.

Waibler (36) obtained velocity measurements in water by means of small probes used to detect total and static pressure. The leads from these probes were connected to two chambers containing floats. A cross arm with a mirror was supported by the floats. The difference in the water level, i.e., velocity head, was determined by sighting on the image of a surveyor's rod as seen in the mirror through a level. By placing the rod and level some distance from the mirror, a very small difference could be readily detected. His velocity measurements

were well correlated by n equal to three near the plate and by n equal to six near the outer edge of the boundary layer.

Van Dyke (32) obtained temperature profiles in water and ethylene glycol over a wide range of Prandtl numbers. He showed that a typical profile could be well represented by the relationship

$$\theta = \theta_w (1-\eta)^3 .$$

Other of his profiles could be better represented by a higher power value. None of his profiles corresponded to the universal one-seventh power law of forced convection. His apparatus consisted of a vertical cylinder which was kept at isothermal conditions by varying electrical heat input to a series of internal heating elements. A fine wire thermocouple was accurately positioned by means of a rigid probe and attached dial indicator.

Fujii (6) obtained temperature profiles in water and ethylene glycol in the fully turbulent region and in the region of transition. His apparatus was a cylinder similar in design to Van Dyke's. These profiles were non-dimensionalized in the y direction by the parameter

$$\eta = \frac{Nu_x \, y}{2x} .$$

No attempt was apparently made to correlate them against $\frac{y}{\delta}$. A replot of Fujii's curves indicated that the profile given for the vortex street could be represented approximately by

$$\theta = \theta_w (1-\eta)^3$$

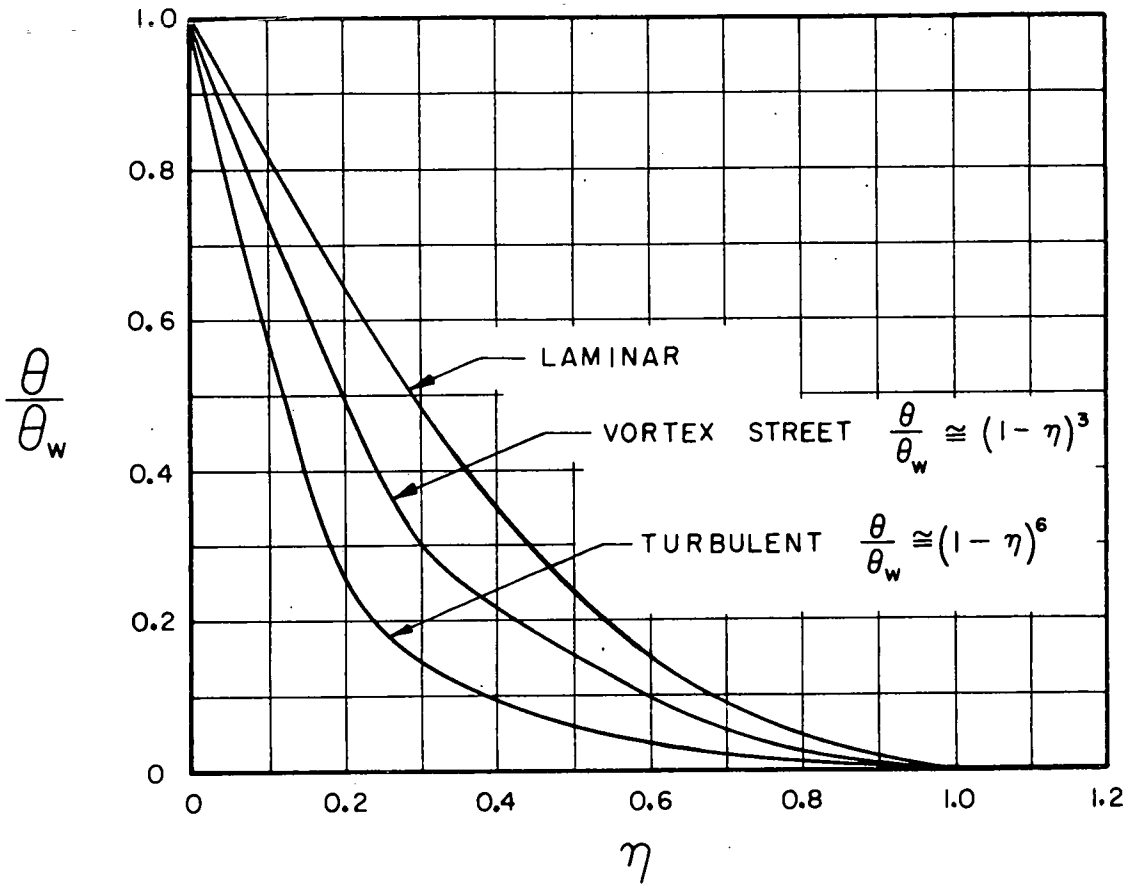

FIG. 4 TEMPERATURE PROFILES BASED ON DATA OF FUJII

and the fully turbulent region by

$$\theta = \theta_w (1-\eta)^6.$$

Summary

The limited analytical study of turbulent free convection has been largely based on assumptions that have been proven successful in the prediction of turbulent forced convection. These free convection predictions have given fair agreement with experimental results obtained in fluids of near constant properties. However, the experimental evidence of turbulent free convection indicates the temperature and velocity profiles across the boundary layer and Blasius wall shear stress are not the same as found in forced flow. Modification of these parameters in the analytical model should give better correspondence to physical reality.

ANALYSIS

Constant Property Problem

Early in the 20th century, from analysis of existing data, Blasius formulated an empirical equation relating a dimensionless friction coefficient to the Reynolds number for the case of flow inside smooth tubes. The equation was

$$\lambda = 0.3164\, Re^{-1/4}. \tag{1}$$

Now from a force balance on an elemental volume in a tube, the wall shear stress may be expressed in terms of pressure drop per unit length $\Delta P/L$ and tube radius r as

$$\tau_w = \frac{\Delta P}{L}\frac{r}{2}.$$

The friction coefficient for flow in a tube is commonly defined by

$$\frac{\Delta P}{L} = \frac{\lambda}{2r}\left(\frac{1}{2}\frac{\rho}{g}\bar{u}^2\right)$$

where $\bar{u}$ is the average velocity. From these last two relations the wall shear may be expressed as

$$\tau_w = \frac{1}{8}\lambda\frac{\rho}{g}\bar{u}^2. \tag{2}$$

Prandtl was the first to substitute equation (1) into (2) and obtained

$$\tau_w = 0.03325 \frac{\rho}{g} \bar{u}^{7/4} \left(\frac{\nu}{r}\right)^{1/4} . \qquad (3)$$

By relating the average velocity to the maximum velocity, $\bar{u} = 0.8\, u_m$ for a velocity profile characterized by the one-seventh power law, the expression

$$\tau_w = 0.0225 \frac{\rho}{g} u_m^2 \left(\frac{\nu}{u_m r}\right)^{1/4} \qquad (4)$$

was obtained. This is the universal expression for the wall shear stress in forced flow. Using the friction velocity $v^* = \left(\frac{g}{\rho}\tau_w\right)^{1/2}$ the wall shear stress became

$$\tau_w = \frac{\rho}{g} v^{*2} .$$

Equation (4) was rearranged to form

$$\frac{u_m}{v^*} = 8.74 \left(\frac{v^* r}{\nu}\right)^{1/7} \qquad (5)$$

which is valid for Reynolds numbers up to about 10^5 where the one-seventh power law velocity profile is valid.

For other Reynolds numbers, Nikuradse found the one-seventh profile was not valid; also, the Blasius formulation for the friction coefficient yielded values which were too low.

A more general form of equation (5) may be written as

$$\frac{u}{v^*} = C_{(n)}\left(\frac{v^* y}{\nu}\right)^{1/n} \qquad (6)$$

where $C_{(n)}$ is a constant depending on the parameter n. The value of n corresponds to the value by which the velocity profile may be characterized. Thus in forced flow for Reynolds numbers beyond 10^5, n becomes eight, nine, or even ten. The value of the constant $C_{(n)}$ which varies linearily over this range of n is shown in Figure 5 .

This general form is applicable to flat plate flow as well as tubes; also, the value of the distance y chosen need not be the exact boundary layer thickness but may be any intermediate value. The velocity u then corresponds to the distance chosen.

This data for $C_{(n)}$ is extrapolated to lower values which gives $C_{(n)} = 5.1$ for $n = 3$. This value was used in the present work to develop another relation for the constant property case.

Although the basic mechanism of free convection flow is different from forced flow, it may be assumed that the general relationship previously developed for the wall shear stress is valid for free convection. Thus for a velocity profile characterized by the one-third power, n equals three and the constant $C_{(n)}$ must be determined.

From the arguments and data of Waibler (36), and data of Van Dyke (32), temperature and velocity profiles other than the classical universal ones seem probable. As a first step in the solution of the problem with variable properties the integral technique, as used by

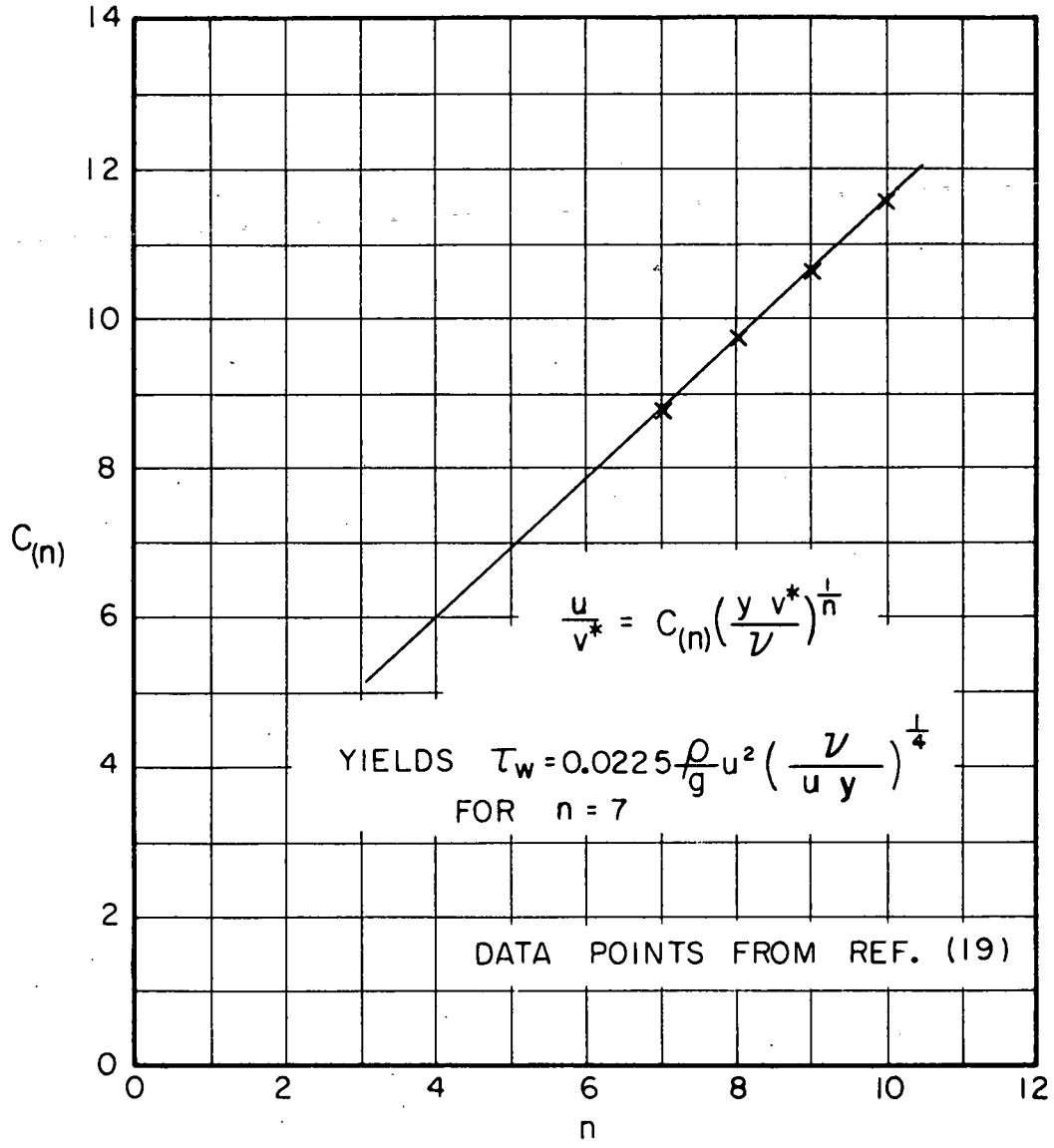

FIG. 5 BLASIUS LAW CONSTANT $C_{(n)}$

Eckert (4), was applied to the constant property case using the velocity and temperature profiles as suggested by Waibler and Van Dyke.

With the use of the integral method, a relationship between the heat transfer and momentum transfer is needed. The first and simplest relation developed for this purpose is Reynolds analogy. It has been the most widely and successfully used relation in forced convection and was therefore a logical choice for the free convection problem.

The expression for heat flux in a boundary layer may be written as

$$q'' = -\rho C_p \left(\frac{k}{\rho C_p} + \epsilon_H \right) \frac{\partial t}{\partial y}$$

where ϵ_H is the eddy diffusivity of heat, a contribution due to the turbulent mixing phenomena. The shear stress may be written as

$$\tau = \frac{\rho}{g} \left(\nu + \epsilon_M \right) \frac{\partial u}{\partial y}$$

where ϵ_M is the eddy diffusivity of momentum due also to turbulence. Taking the ratio of these expressions, the equation is

$$\frac{q''}{\tau} = -g C_p \frac{\left(\frac{k}{\rho C_p} + \epsilon_H \right)}{\left(\nu + \epsilon_M \right)} \frac{\partial t}{\partial u} .$$

The ratio ϵ_m/ϵ_H is known as a turbulent Prandtl number. A study of the boundary layer equations for forced turbulent flow show that for the case of negligible pressure gradient and viscous dissipation, the momentum and energy equations are identical if the normal and turbulent Prandtl numbers are unity. As a result the temperature and velocity profiles are identical for this case. Identical profiles mean that the derivative dt/du is a constant across the boundary layer and that the ratio of heat flux to shear stress is also constant so that

$$\frac{q''}{\tau} = \frac{q_w''}{\tau_w} \quad .$$

Experimental data for forced convection indicates that better results are obtained by considering ϵ_m/ϵ_H as unity (13). Thus it is also a logical assumption for free convection and is used in the following development. To continue further, it is necessary to take the normal Prandtl number as unity. Thus $\frac{k}{\rho C_p}$ equals ν and if the velocity and temperature profiles are similar*, the equation becomes

$$\frac{q_w''}{\tau_w} = -g\, C_p \frac{dt}{du} \quad .$$

This may be integrated across the boundary layer yielding

$$\frac{q_w''}{\tau_w} = g\, C_p \frac{(t_w - t_\infty)}{u_1} \quad .$$

---

* For free convection the assumption of the normal and turbulent Prandtl numbers equaling unity does not result in identical velocity and temperature profiles because the equations are not identical.

A correction factor of $Pr^{-2/3}$ when applied to the forced convection Stanton number has yielded good results for heat transfer coefficients over a wide range of Prandtl numbers. As this form of Reynolds analogy can be arranged to obtain a Stanton number, the Prandtl correction factor was applied to the free convection development.

Examining typical free convection velocity and temperature profiles, i.e., Figures 6 and 7, it is obvious that the similarity requirement is not met since the velocity reaches a maximum and then decreases with distance from the fixed wall. Considering only the portion of the profiles between the wall and the point where the velocity reaches a maximum, the similarity is seen to be much better. Because of this observation, two methods of utilizing Reynolds analogy were attempted. They were the model where the entire boundary layer was considered, and a modification where only the boundary layer between the wall and point of maximum velocity was considered. The approach illustrated next is the model where the entire boundary layer was considered. The two results are compared later.

Going through the procedure of evaluating the integral equations and solving for h_c in much the same manner as Siegel (25), the expression

$$Nu = 0.121 \left[\frac{Gr}{1 + 0.976\, Pr^{2/3}} \right]^{1/3} Pr^{5/9} \qquad (7)$$

was obtained. This is compared to Siegel's expression in Figure 8. Results given by Saunders (24) and McAdams (14) are shown as well. The procedure leading to equation (7) is fully developed in Appendix B.

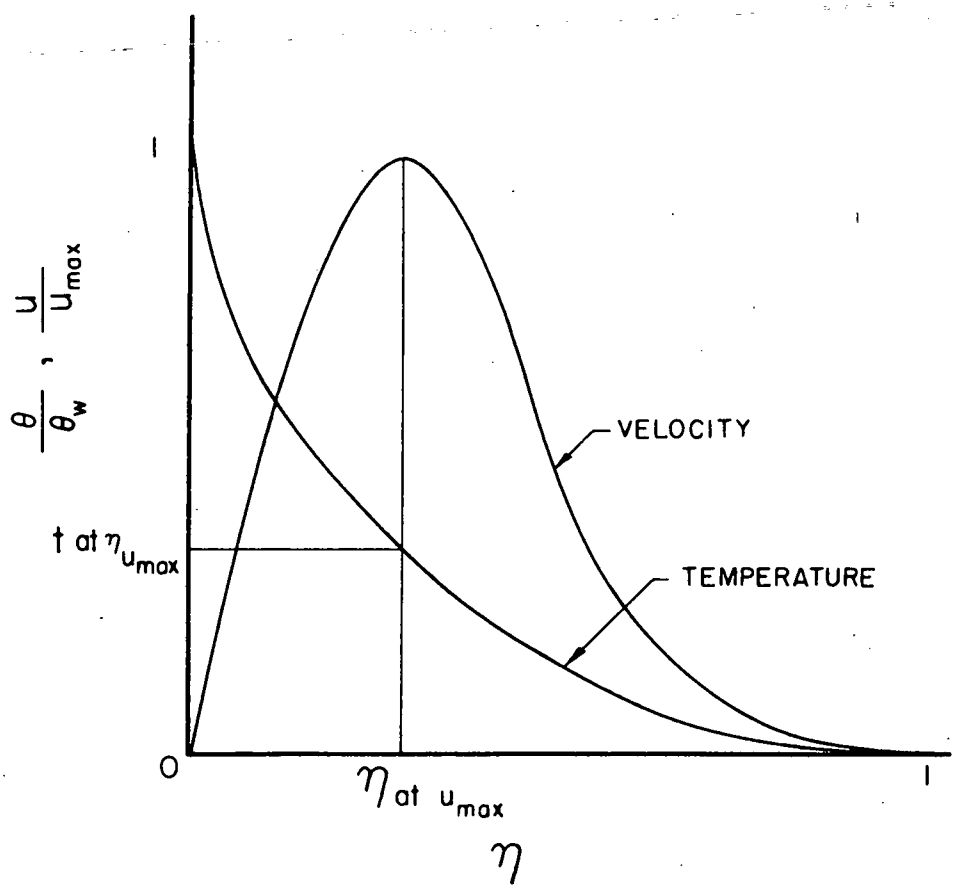

FIG. 6 TYPICAL FREE CONVECTION VELOCITY AND TEMPERATURE PROFILES

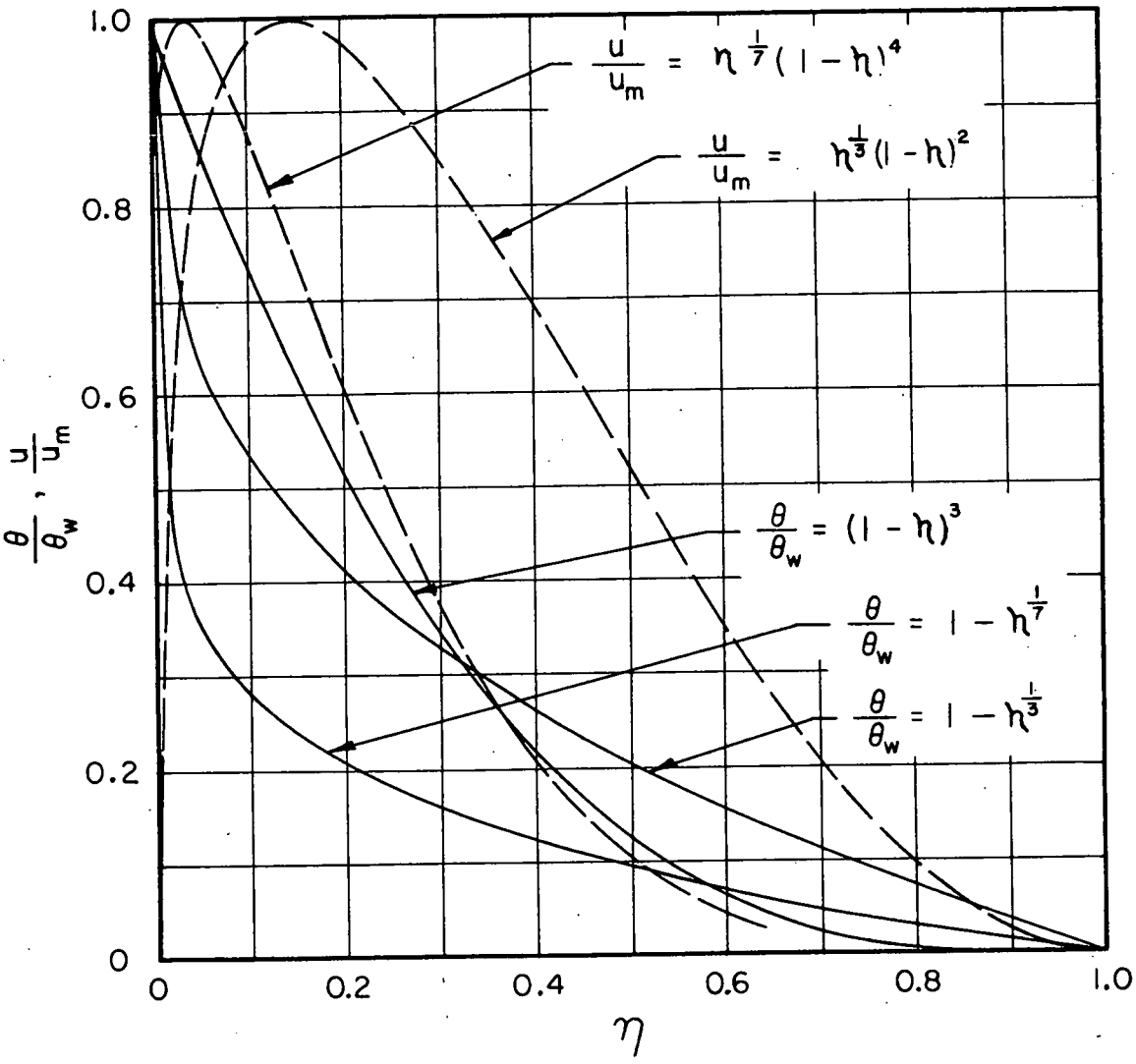

FIG. 7 COMPARISON OF TEMPERATURE AND VELOCITY PROFILES

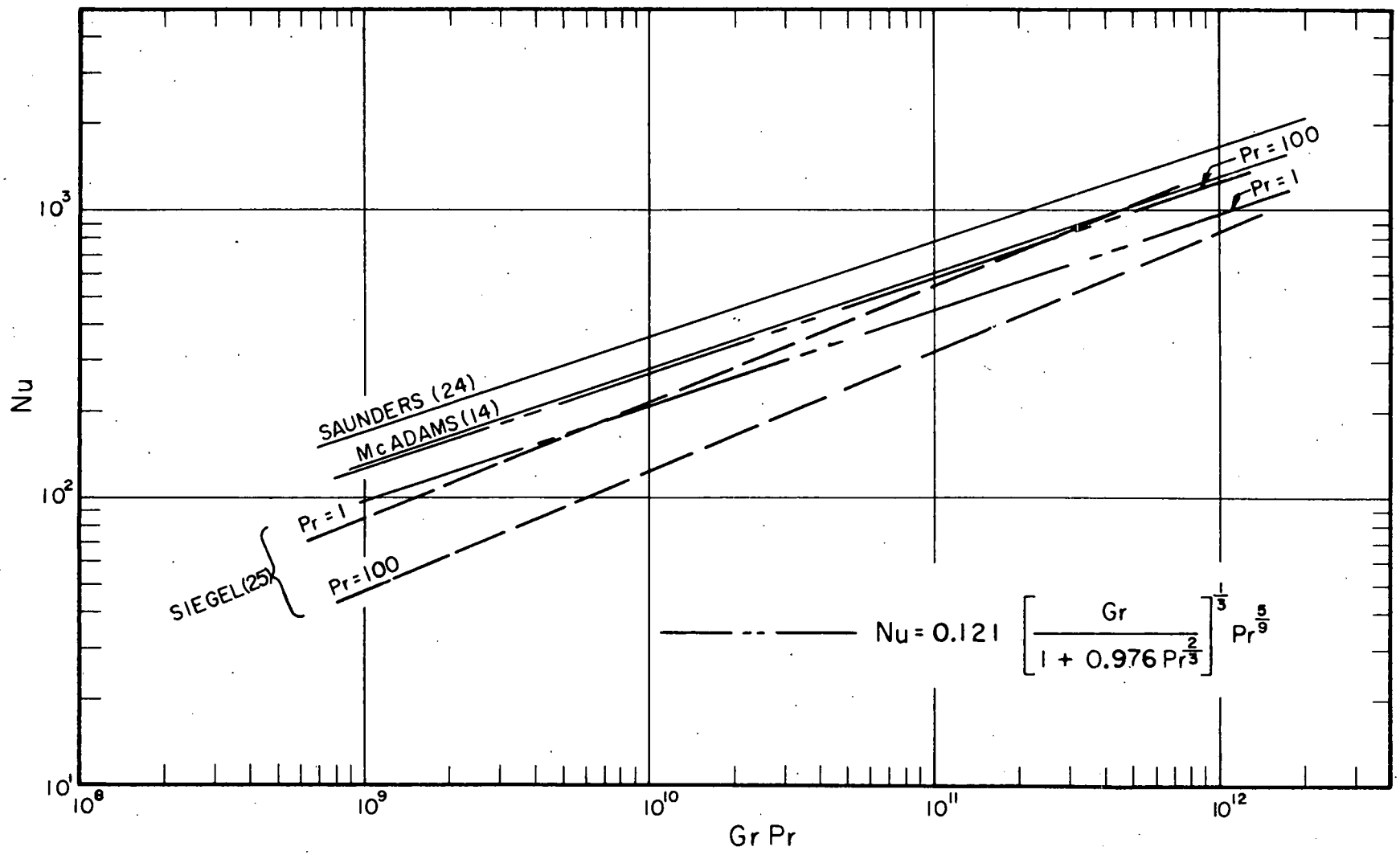

FIG. 8 CORRELATION OF CONSTANT PROPERTY SOLUTION COMPARED TO OTHER RESULTS

This derived expression for the Nusselt number gives values which are generally low as compared to experimental data which has been well correlated by Saunders (23) and others with the equation

$$Nu = 0.17 \left(Gr\, Pr \right)^{1/3}.$$

This could be partially due to the value chosen for $C_{(n)}$. The value chosen was obtained by extrapolating data for other characteristic profiles.

By choosing a value of $C_{(n)} = 3.5$, the same procedure yields a result slightly different from that of equation (7). This result is

$$Nu = 0.177 \left[\frac{Gr}{1 + 0.978 Pr^{2/3}} \right]^{1/3} Pr^{5/9}.$$

This expression compares very well with the accepted correlation of experimental results especially for Prandtl numbers somewhat above ten.

Variable Property Problem

In the constant property case of turbulent free convection, a control volume was utilized and the momentum and energy fluxes were integrated at the boundaries of the volume to obtain energy and momentum balances. For the problem considering variable properties, the boundary layer equations are integrated directly across the boundary layer to illustrate the problem in greater detail. This method of development is generally the same as the constant property case but considers all properties as variables.

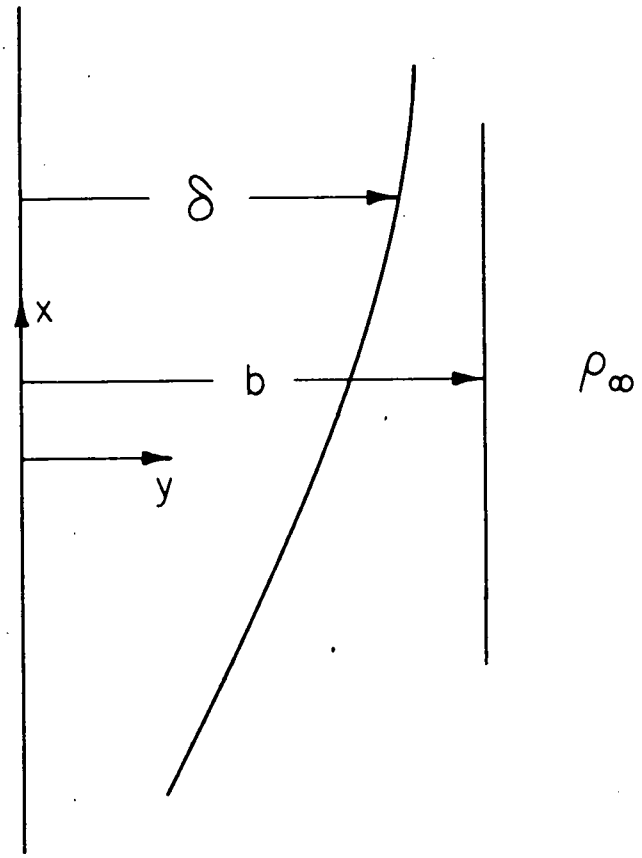

FIG. 9 BOUNDARY LAYER NOMENCLATURE

The equation of momentum for a boundary layer in turbulent flow may be written as

$$\frac{\rho}{g}\left(u\frac{\partial u}{\partial x}+v\frac{\partial u}{\partial y}\right)=X-\frac{dP}{dx}+\frac{\partial}{\partial y}\left[\left(\frac{\mu}{g}+\frac{\rho}{g}\epsilon_M\right)\frac{\partial u}{\partial y}\right]. \quad (9)$$

This general form of Prandtl's boundary layer equation assumes two dimensional flow where all properties may be variables. The contribution of momentum transfer due to turbulence is included in the eddy diffusivity of momentum ϵ_M.

With no pressure drop due to forced flow, the gradient of pressure is due only to the hydrostatic pressure of the height of the fluid and

$$\frac{dP}{dx}=-\rho_\infty .$$

The only body force acting is the normal gravitational one and is

$$X=-\rho .$$

Substituting these expressions into equation (9) and integrating from the wall to a point external to the boundary layer (see Figure 9) gives

$$\int_0^b\left(\rho u\frac{\partial u}{\partial x}+\rho v\frac{\partial u}{\partial y}\right)dy=\int_0^b g\left(\rho_\infty-\rho\right)dy+\int_0^b\frac{\partial}{\partial y}\left[\left(\mu+\rho\epsilon_M\right)\frac{\partial u}{\partial y}\right]dy. \quad (10)$$

The last integral becomes

$$(\mu + \rho\epsilon_M)\frac{\partial u}{\partial y}\Big|_0^b = -(\mu + \rho\epsilon_M)\frac{\partial u}{\partial y}\Big|_{y=0} = -g\tau_w$$

since the velocity gradient is zero beyond the disturbance thickness δ.

Integrating the second term of the left integral of equation (10) by parts gives

$$\int_0^b \rho v \frac{\partial u}{\partial y}\, dy = \rho u v\Big|_0^b - \int_0^b u \frac{\partial \rho v}{\partial y}\, dy ,$$

and, since $u = o$ at $y = o$ and at $y = b$, the first term drops out. Using the equation of continuity

$$\frac{\partial \rho u}{\partial x} + \frac{\partial \rho v}{\partial y} = 0 ,$$

the remaining integral is

$$-\int_0^b u \frac{\partial \rho v}{\partial y}\, dy = \int_0^b u \frac{\partial \rho u}{\partial x}\, dy .$$

This is substituted back into equation (9) yielding

$$\int_0^b \frac{\partial \rho u^2}{\partial x}\, dy = g\int_0^b (\rho_\infty - \rho)\, dy - g\tau_w$$

since the left integral is a perfect differential.

Making a change in variable by defining $\eta = y/\delta$ and changing the limit of integration from b to δ, the integral limits are

$$y = 0 \Rightarrow \eta = 0 \ , \quad \text{and} \quad y = \delta \Rightarrow \eta = 1 \ .$$

The equation then becomes

$$\frac{\partial}{\partial x}\left(\delta \int_0^1 \rho u^2 d\eta\right) = g\delta \int_0^1 (\rho_\infty - \rho) d\eta - g\tau_w \ . \quad (11)$$

A velocity profile is defined in the form

$$u = u_1 F(\eta)$$

where u_1 is the equivalent stream velocity and $F(\eta)$ is a shape parameter. With this form substituted, the momentum equation is

$$\frac{\partial}{\partial x}\left(\delta \int_0^1 \rho u_1^2 F(\eta)^2 d\eta\right) = g\delta \int_0^1 (\rho_\infty - \rho) d\eta - g\tau_w \ . \quad (12)$$

The equation of energy for boundary layer flow in terms of enthalpy is written as (see Appendix C)

$$\rho\left(u\frac{\partial h}{\partial x} + v\frac{\partial h}{\partial y}\right) = \frac{\partial}{\partial y}\left[\left(k + \rho C_p \epsilon_H\right)\frac{\partial t}{\partial y}\right] \quad (13)$$

where the effect of viscous work and work against gravity have been neglected. This equation is integrated across the boundary layer as before. The right side of this equation yields

$$\int_0^b \frac{\partial}{\partial y}\left[\left(k+\rho C_p \epsilon_H\right)\frac{\partial t}{\partial y}\right]dy = \left(k+\rho C_p \epsilon_H\right)\frac{\partial t}{\partial y}\Big|_0^b = -k\frac{\partial t}{\partial y}\Big|_{y=0} = q''_w ,$$

as the temperature gradient is zero beyond δ, and the eddy diffusivity is zero at the wall.

Replacing h by the enthalpy difference, $(h-h_\infty)$ equal to H, the second term in the left integral of equation (13) is integrated by parts and yields

$$\int_0^b \rho v \frac{\partial H}{\partial y}\, dy = \rho v H\Big|_0^b - \int_0^b H \frac{\partial \rho v}{\partial y}\, dy .$$

Since H=o at y=b, and v=o at y=o, the first term drops out. Using the continuity equation as previously, the left side of equation (13) becomes a perfect differential and is written as

$$\int_0^b \frac{\partial \rho u H}{\partial x}\, dy = q''_w .$$

Making the change in variables $\eta = y/\delta$ the equation becomes

$$\frac{\partial}{\partial x}\left(\delta \int_0^1 \rho u H\, d\eta\right) = q''_w . \qquad (14)$$

Before substituting an assumed temperature profile into this equation, the thermodynamic relationship between temperature and enthalpy,

$$dh = \left(\frac{\partial h}{\partial t}\right)_p dt + \left(\frac{\partial h}{\partial P}\right)_t dP ,$$

was considered. This relationship holds if thermodynamic equilibrium is a valid assumption. However, metastable conditions have been found to exist at pressures slightly above the critical point which indicate that this equilibrium may not always be present (26).

Pressure across the boundary is almost constant. Also the difference in pressure due to the hydrostatic head variation is small. Therefore enthalpy dependence on pressure is very small and is neglected leaving enthalpy as a function of temperature only (See Appendix C).

The temperature profile is specified by

$$\theta = \theta_w G(\eta)$$

with $G_{(\eta)}$ being a shape parameter of the temperature. Enthalpy at constant pressure is expressed as

$$h = h\,[t(\eta)]$$

and must be computed for each temperature profile.

After substituting the velocity relationship into the energy equation it becomes

$$\frac{\partial}{\partial x}\left(\delta \int_0^1 \rho\, u_1 F(\eta) H\, d\eta\right) = q''_w . \qquad (15)$$

From the previous development the wall shear stress for a velocity profile characterized by the one-third power law was

$$\tau_w = a \frac{\rho}{g} u^2 \left(\frac{\nu}{u y}\right)^{1/2} .$$

where the constant a depends on the exact value of $C_{(n)}$ used. Using the integrated average of density and viscosity over this portion of the boundary layer, the equation becomes

$$g \tau_w = \frac{a u_1^{3/2}}{\delta^{1/2}} \int_0^1 \rho \nu^{1/2} \, d\eta . \qquad (16)$$

To apply Reynolds analogy to the variable property problem, it is convenient to initially consider variable property forced convection. When pressure gradients are negligible, enthalpy may be considered as a function of temperature only and

$$dh = \left(\frac{\partial h}{\partial t}\right)_p dt = C_p \, dt .$$

Temperature is a function of the coordinate y, thus enthalpy is also a function of y and

$$\frac{\partial h}{\partial y} = C_p \frac{\partial t}{\partial y} .$$

Substituting this expression in the energy equation (13) and rewriting the momentum equation (9) without the pressure gradient and body force, the two equations become

$$\rho\left(u\frac{\partial u}{\partial x}+v\frac{\partial u}{\partial y}\right)=\frac{\partial}{\partial y}\left[\rho(\nu+\epsilon_M)\frac{\partial u}{\partial y}\right]$$

and

$$\rho\left(u\frac{\partial h}{\partial x}+v\frac{\partial h}{\partial y}\right)=\frac{\partial}{\partial y}\left[\rho\left(\frac{k}{\rho C_p}+\epsilon_H\right)\frac{\partial h}{\partial y}\right].$$

These equations are forced convection energy and momentum equations considering all properties as variables.

If the normal and turbulent Prandtl numbers are unity, the equations are identical yielding identical enthalpy and velocity profiles. By the same arguments as used in the constant property development, the analogy may be expressed as

$$\frac{q_w''}{\tau_w}=-g\frac{dh}{du}.$$

As in the previous development, it is necessary to assume the normal and turbulent Prandtl numbers as unity and profiles similar in shape. Thus the analogy may be integrated across the boundary layer as was done for the constant property case. Multiplying the analogy by the integrated average of the Prandtl number correction

factor over this interval, the final expression becomes

$$\frac{q_w''}{\tau_w} = g\,\frac{(h_w - h_\infty)}{u_1}\left(\int_0^1 Pr\ d\eta\right)^{-2/3}. \qquad (17)$$

Before continuing the following substitutions are made for simplicity, viz.,

$$V_1 = \left(\int_0^1 Pr\, d\eta\right)^{-2/3},$$

$$W = \int_0^1 \rho F(\eta)^2\, d\eta,$$

$$X_1 = g\int_0^1 (\rho_\infty - \rho)\, d\eta,$$

$$Y = \int_0^1 \rho v^{1/2}\, d\eta,$$

and

$$Z = \int_0^1 \rho F(\eta) H\, d\eta.$$

Next, the shear stress expression and Reynolds analogy are substituted into the momentum and energy equations (12) and (15) which yield

$$\frac{\partial}{\partial x}\left(\delta\int_0^1 \rho u_1^2 F(\eta)^2\, d\eta\right) = \delta X_1 - \frac{a u_1^{3/2}}{\delta^{1/2}} Y \qquad (18)$$

for momentum and

$$\frac{\partial}{\partial x}\left(\delta\int_0^1 \rho u_1 F(\eta)\,d\eta\right) = a(h_w - h_\infty)\left(\frac{u_1}{\delta}\right)^{1/2} Y V_1 \quad (19)$$

for the energy equation.

These two equations can be solved simultaneously by assuming the maximum velocity and displacement thickness to be functions of x of the form

$$u_1 = C_1 x^m \quad , \quad \text{and} \quad \delta = C_2 x^n \, .$$

Substituting these functions into (18) and (19) and performing the differentiation yields

$$(2m+n) C_1^2 C_2 x^{2m+n-1} W = C_2 x^n X_1 - a C_1^{3/2} C_2^{-1/2} x^{\frac{3}{2}m - \frac{1}{2}n} Y, \quad (20)$$

and

$$(m+n) C_1 C_2 x^{m+n-1} Z = a(h_w - h_\infty) C_1^{1/2} C_2^{-1/2} x^{\frac{m}{2} - \frac{n}{2}} Y V_1 . \quad (21)$$

For these equations to be independent of x, the value of the exponent of x must be identical for each term, thus

$$2m + n - 1 = n = \frac{3}{2} m - \frac{1}{2} n$$

and

$$m + n - 1 = \frac{1}{2} m - \frac{1}{2} n \ .$$

Solution of these equations gives m and n equal to one-half, and (20) and (21) become

$$\frac{3}{2} C_1^2 C_2 W = C_2 X_1 - a C_1^{3/2} C_2^{-1/2} Y \ ,$$

and

$$C_1 C_2 Z = a (h_w - h_\infty) C_1^{1/2} C_2^{-1/2} Y V_1 \ .$$

Solving the energy equation for C_1 yields

$$C_1 = a^2 (h_w - h_\infty)^2 \left(\frac{Y V_1}{Z} \right)^2 C_2^{-3} \ ,$$

and from the momentum equation

$$C_2 = a^{2/3} \left[\frac{(h_w - h_\infty) Y V_1}{Z} \right]^{1/2} \left[\frac{\frac{3}{2} Y V_1 W (h_w - h_\infty)}{Z} + Y}{X_1} \right]^{1/6} .$$

The heat transfer coefficient is

$$h_c = \frac{q''_w}{\theta_w} = a\left(\frac{u_1}{\delta}\right)^{1/2} \frac{(h_w - h_\infty)}{\theta_w} \gamma V_1 ,$$

and is independent of x. When the functional relationships for u_1 and δ are substituted, the heat transfer coefficient becomes

$$h_c = \frac{(h_w - h_\infty)}{\theta_w} V_1 \left[a^2 \gamma^2\right]^{1/3} \left[\frac{\frac{3}{2} V_1 W (h_w - h_\infty)}{Z} + 1}{X_1}\right]^{-1/3} . \quad (22)$$

Method of Solution for Variable Properties

To numerically solve the previously developed integral relationships, assumptions were made in connection with the velocity and temperature profiles as well as the wall shear stress expression. Also the density, enthalpy, viscosity and thermal conductivity properties had to be explicitly known as a function of temperature and pressure.

The analytical solutions obtained by Fritsch (5) for the laminar free convection problem in near critical water showed that the velocity and temperature profiles were smooth functions of the same general shape as ones used to describe these parameters in a near constant property fluid. For this reason the profiles used in the constant property solution were used for the variable property turbulent problem being treated here. Specifically, $G_{(\eta)} = (1-\eta)^3$ and $F_{(\eta)} = \eta^{1/3}(1-\eta)^2$ were used. Since the wall shear stress and velocity profile are

closely related, the same shear stress expression was used with an improved value of the constant $C_{(n)}$ equal to 3.5. This yielded a value for a equal to 0.153 (See Appendix B).

The thermodynamic and transport properties for near critical water are not known nearly as well as those for ordinary water. However the experimental work available has been well analyzed and correlated. It was felt to be not worthwhile to restudy this problem but better to use the recommended results of others and proceed.

The values of specific volume were taken from Nowak (16) with a few additional values outside this range from Voukalovitch (35). Tabulated enthalpy values were taken from Touba (30) who interpolated curves developed by Nowak (15). Specific volume and enthalpy data was stated to be within 0.1 percent by Nowak. The thermal conductivity correlation developed by Vargaftik (34) was used for the difference $(k-k_o)$ between the conductivity at the desired state k and the conductivity k_o at that temperature at a pressure of one atmosphere. This correlation was suggested by Swenson (27). The value for k_o was taken from Timroth (28) and expressed numerically by Fritsch.

Viscosity was correlated in the same manner as conductivity by Vargaftik. The viscosity at atmospheric pressure was taken from Shifrin (21), and expressed in numerical form by Fritsch. The equations used in the variable property solution were

$$k - k_o = 28.63 \times 10^{-4} \rho^{1.25}$$

$$k_o = 4.0 \times 10^{-5} (t - 550) + 0.0246 \ \frac{\text{Btu.}}{\text{ft. hr. F}}$$

$$\mu - \mu_o = 60.66 \times 10^{-10} \rho^{1.48}$$

$$\mu_o = 0.04788t \times 10^{-8} + 14.79 \times 10^{-8} \quad \frac{lb.\,sec.}{ft^2} \,.$$

Multiply this value by 1.158×10^5 to obtain units of $\frac{lb.}{ft.hr.}$.

The specific heat C_p and thermal coefficient of expansion were taken from the work of Nowak. The relationship

$$C_p = 1 + \frac{\beta T}{4.81} \,,$$

with T in degrees Rankine, was developed by Nowak (16) and was used in this work to relate C_p and β. This permitted finding values where one or the other was not readily obtainable from the work of Nowak. The accuracy of specific heat was stated to be one to five percent where the variation was small to 20 percent where the property peaked. The accuracy of β was stated to be between one-half to three percent.

In an attempt to maintain accuracy of the property values, representation by high order of degree polynomials had been previously carried out. However, it was found that simple linear interpolation in a table with reasonably small intervals between points was more accurate and consistent.

The availability of a large digital computer made numerical evaluation of the integral equations possible and practical. The

numeric method used was Simpson's rule. The individual integrals, i.e., V_1, W, X_1, y, z on page 45, were divided into two parts; part A from the wall to the point of maximum velocity, and part B across the remainder of the boundary layer. To obtain a solution the integrals were evaluated for a specified bulk temperature difference by using the properties for the specified pressure. The values obtained were substituted into equation (22) determining the heat transfer coefficient. This also determined the heat flux. The numerical program is listed in Appendix D.

Preliminary trials were made to determine the number of increments necessary for convergence of the integrals. These trials indicated that satisfactory convergence would be obtained with 20 to 24 increments for part A and 40 increments for part B. All final calculations were based on 24 and 40 increments for A and B respectively.

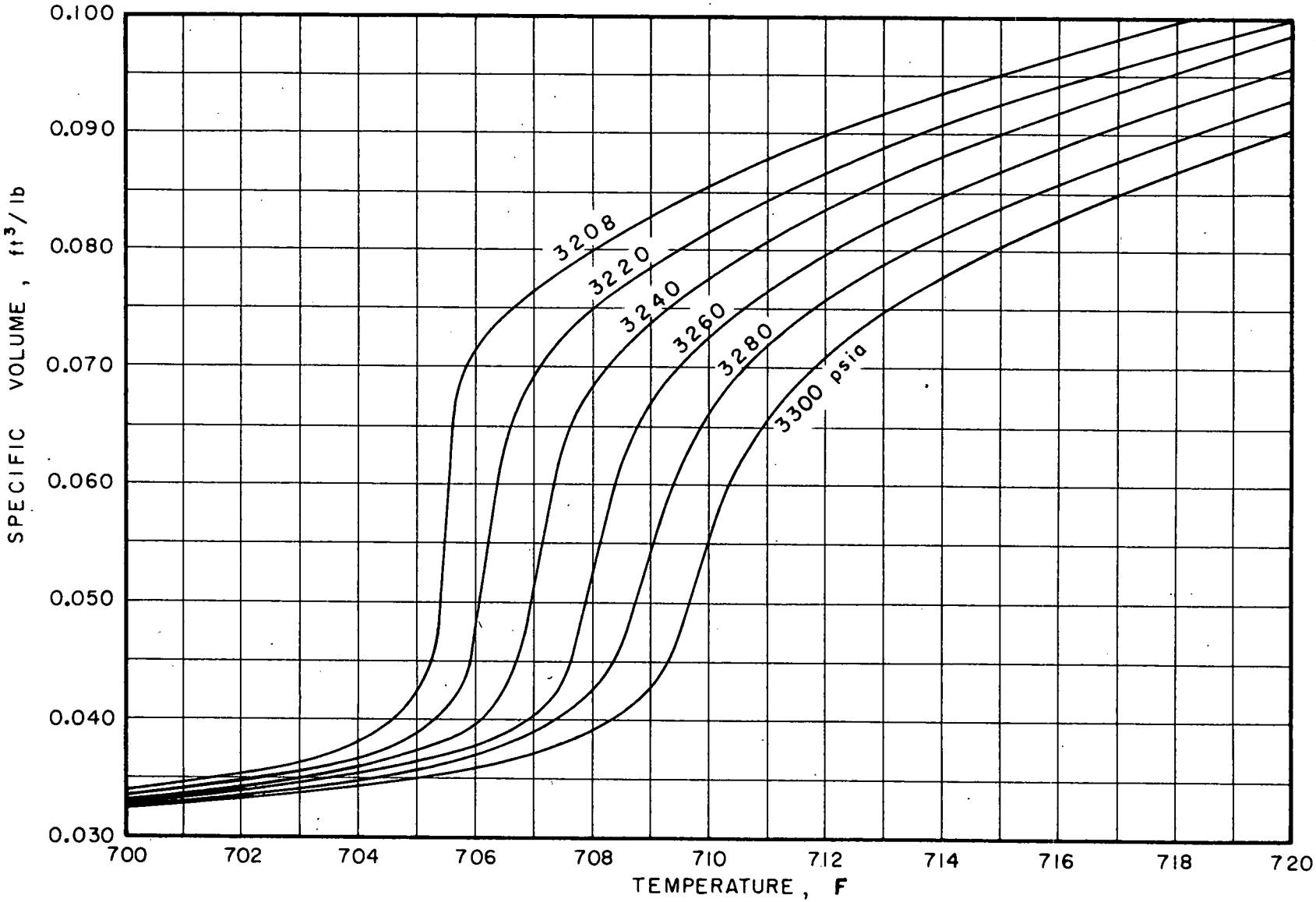

FIG. 10 SPECIFIC VOLUME FOR NEAR CRITICAL WATER

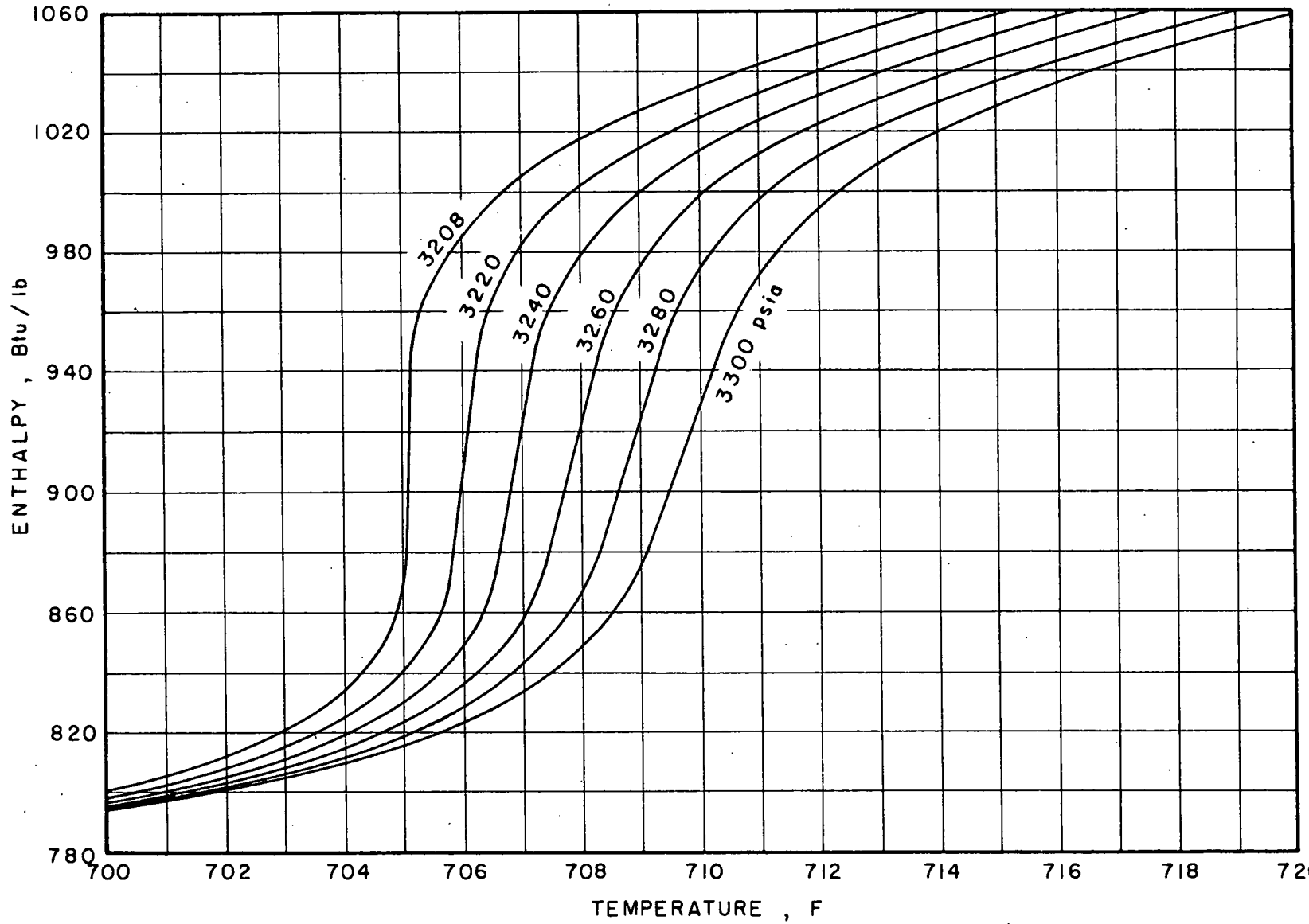

FIG. 11 ENTHALPY FOR NEAR CRITICAL WATER

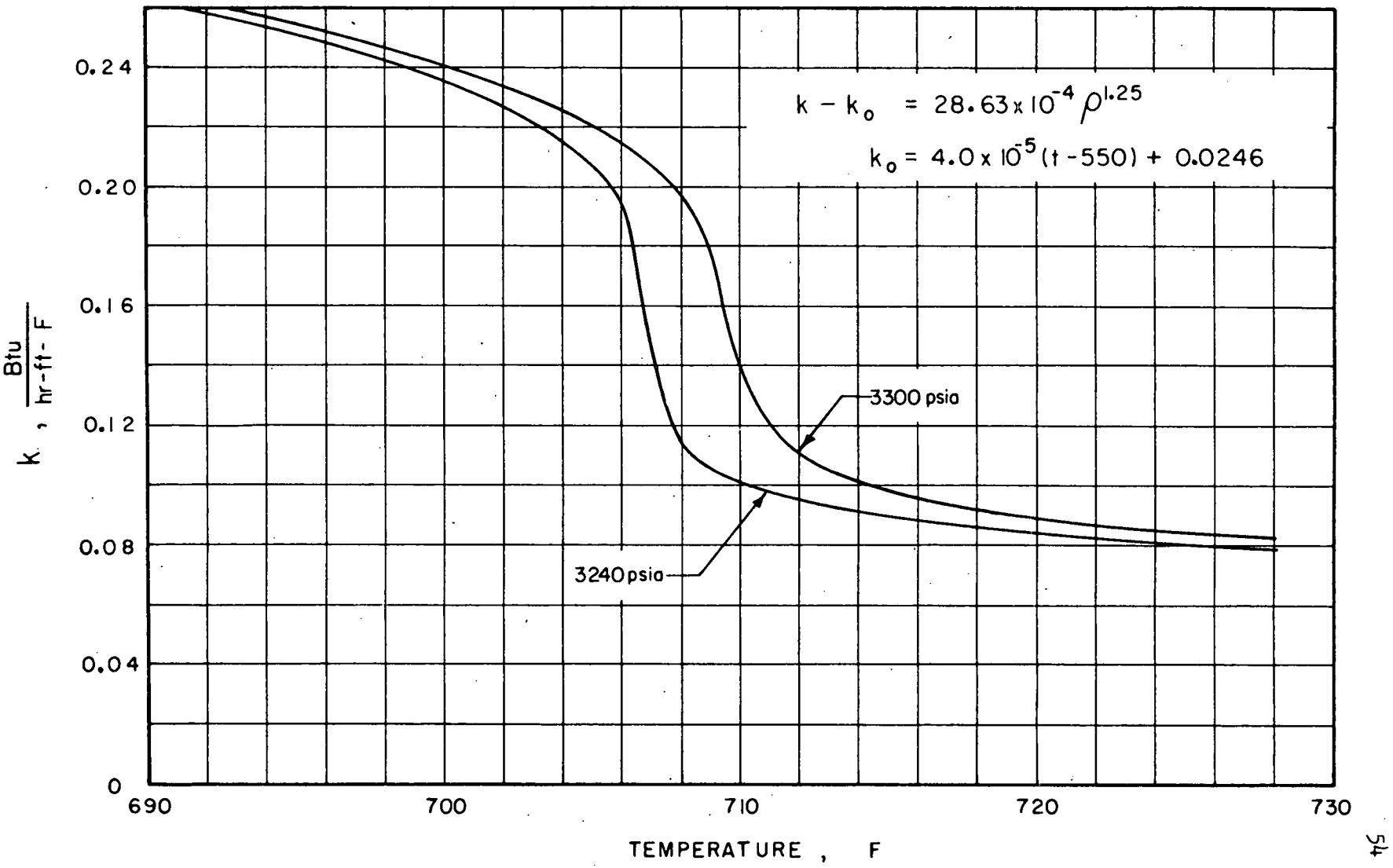

FIG. 12 THERMAL CONDUCTIVITY FOR NEAR CRITICAL WATER

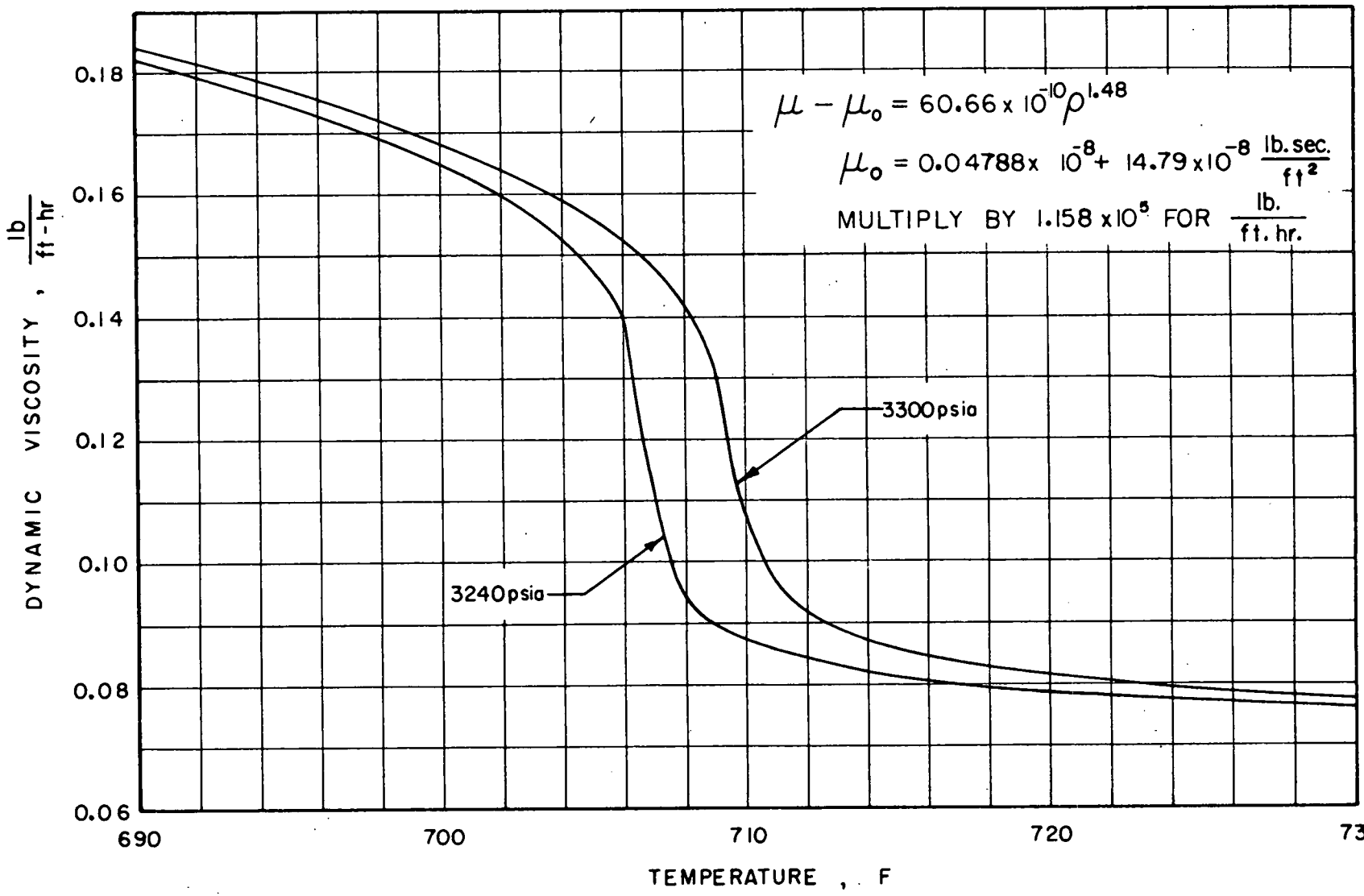

FIG. 13 DYNAMIC VISCOSITY FOR NEAR CRITICAL WATER

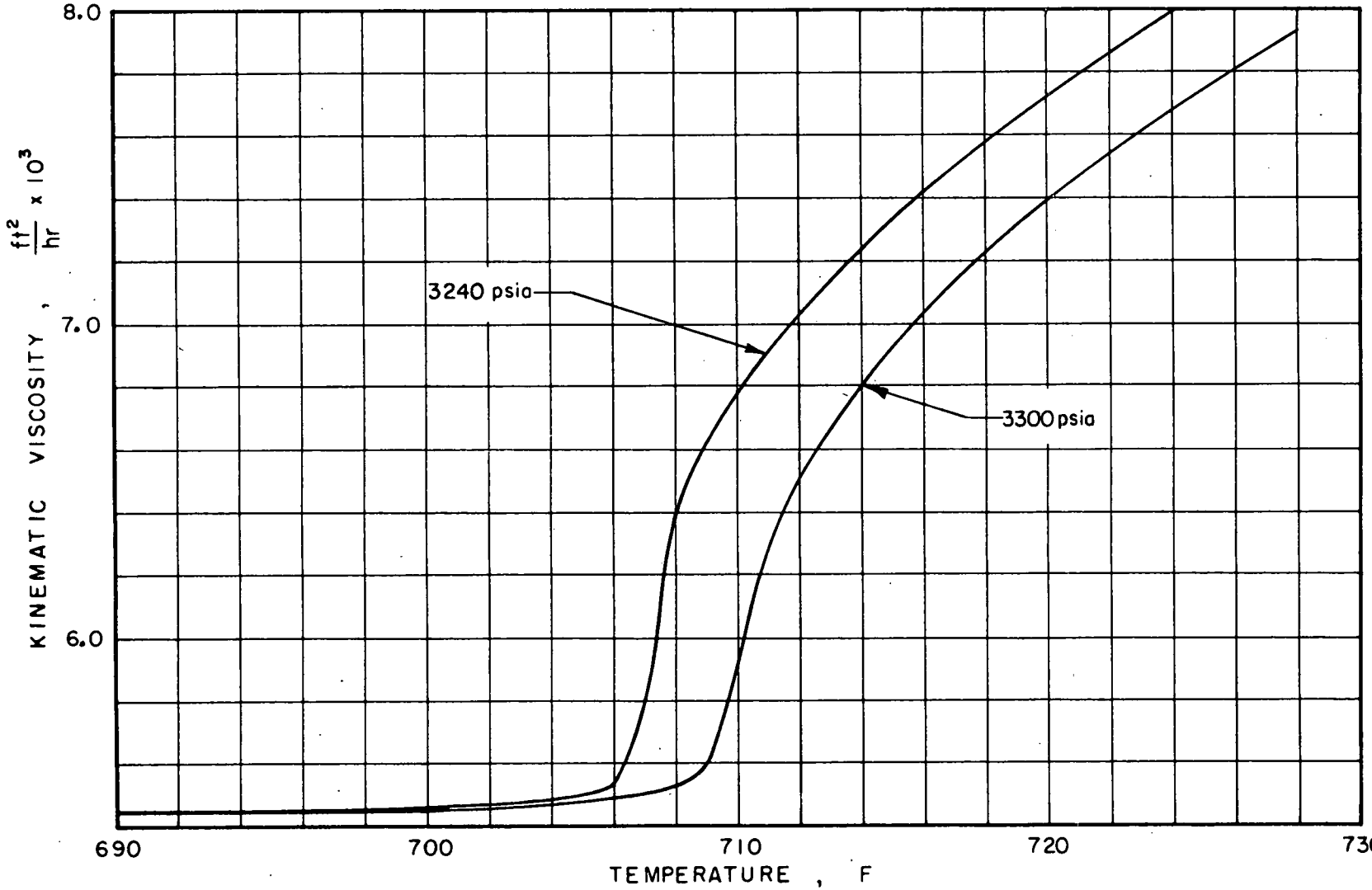

FIG. 14 KINEMATIC VISCOSITY FOR NEAR CRITICAL WATER

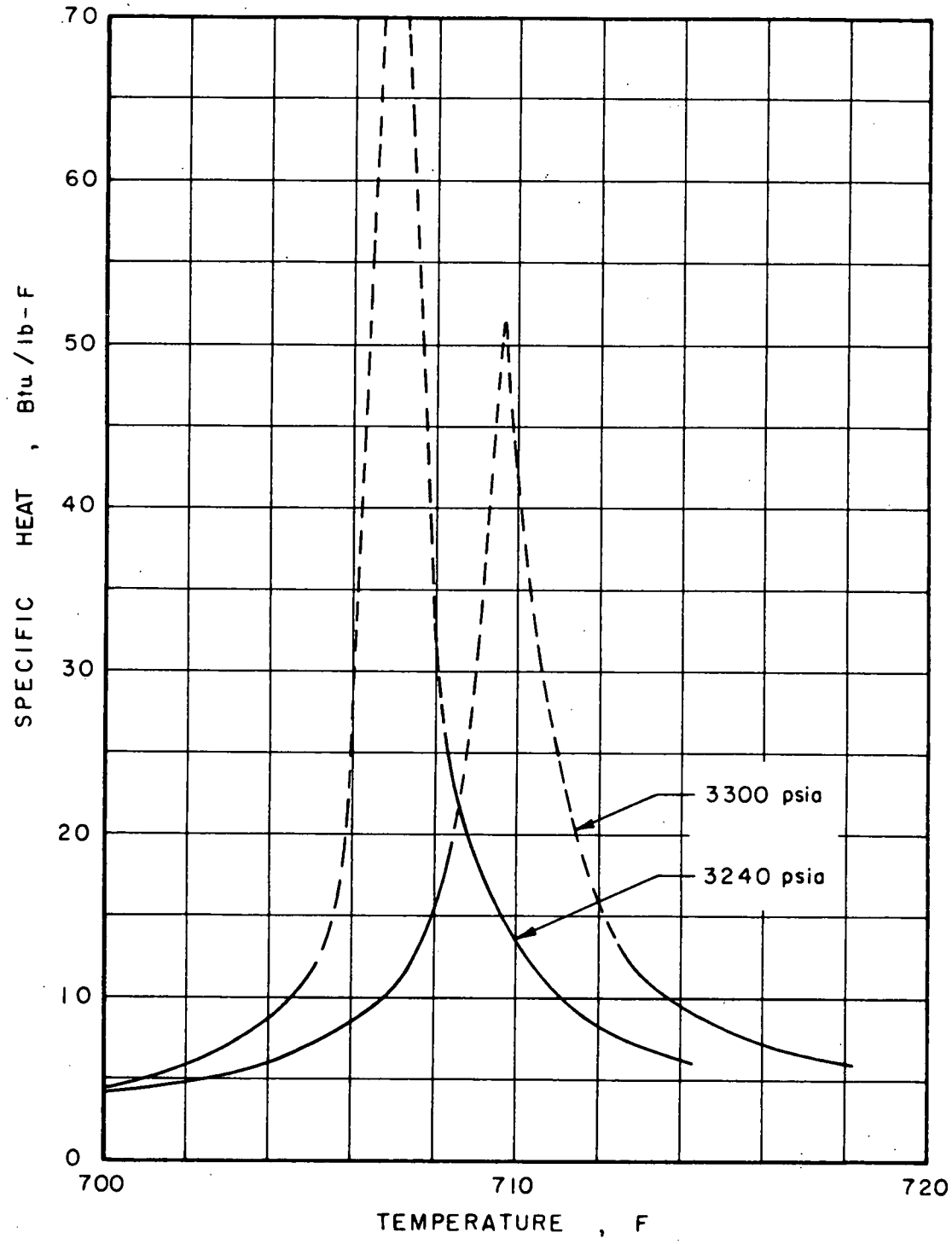

FIG. 15 SPECIFIC HEAT FOR NEAR CRITICAL WATER

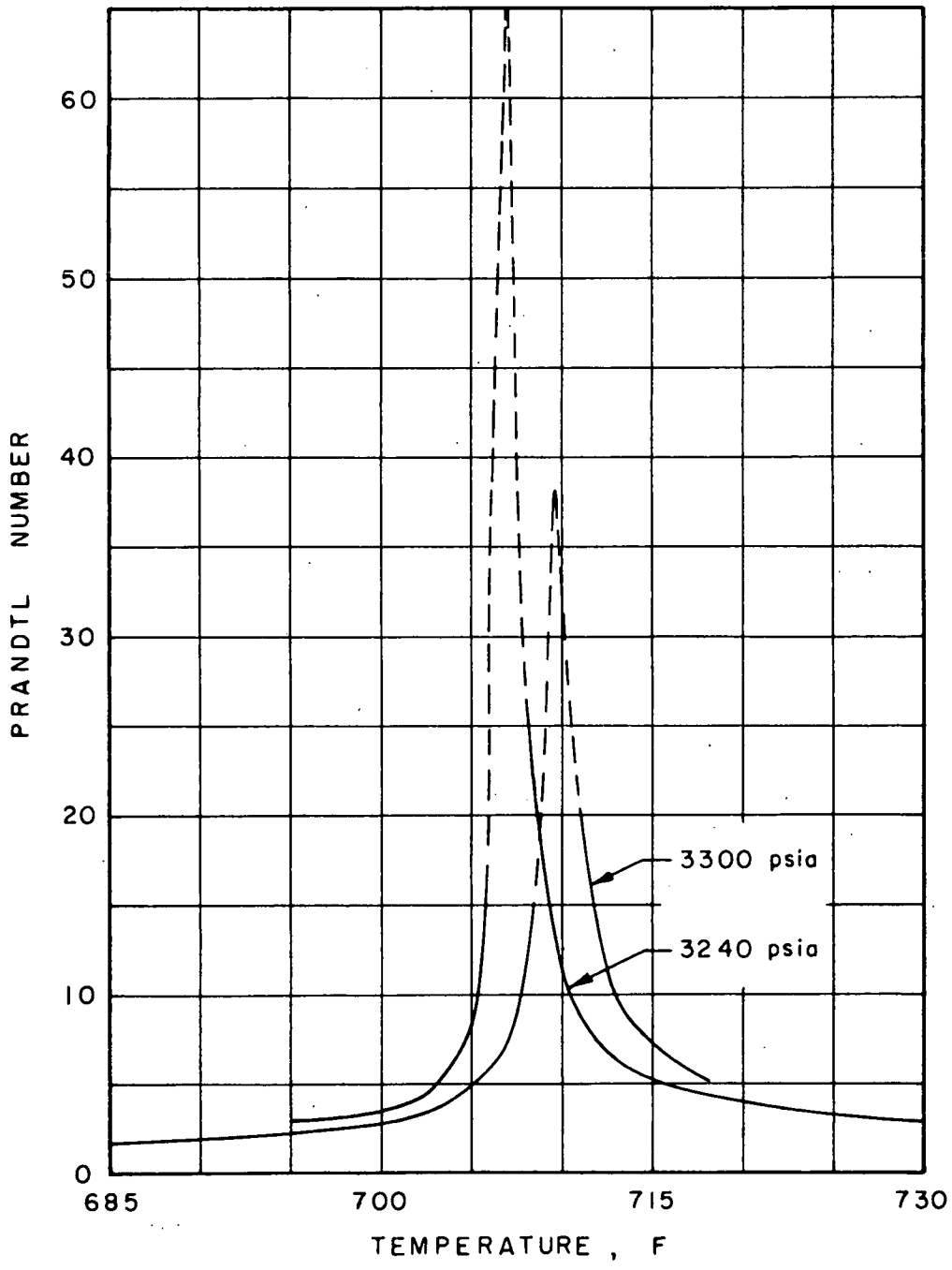

FIG. 16 PRANDTL NUMBER FOR NEAR CRITICAL WATER

ANALYTICAL RESULTS

The analytical predictions of heat flux as a function of bulk temperature and temperature difference are shown in Figure 17. The results using Reynolds analogy only between the wall and the point of the velocity maximum for the same parameters are shown in Figure 18. These curves show a very pronounced increase in heat transfer as the wall temperature increases to the value of the transposed critical temperature. This temperature is defined as the temperature where the specific heat reaches a maximum. The curves also show a decrease in heat transfer as the transposed critical temperature is exceeded. The decrease in heat transfer with an increase in wall temperature is much more pronounced for the curves in Figure 18. This effect is explained further.

The trends and magnitudes of the various parts of the analytical equation are shown in Figures 19. These curves are for a specific case but are a typical example of all cases considered. The part designated V_1 is the integral average of $Pr^{-2/3}$ and reaches a minimum near the transposed critical temperature. The integrated density difference X_1 is shown to be of large magnitude and increases monotonically with temperature difference. The integral Z, which includes the enthalpy difference, is of similar shape and importance. The integral W is of second order importance since Z is several orders of magnitude larger.

The enthalpy difference is seen to change considerably depending on the form of Reynolds analogy. The difference (h_w-h_∞) used in the analogy applied across the entire boundary layer increases monotonically. However, the difference, $(h_w-h_{u_m})$ used in the analogy applied from the wall to the maximum velocity reaches a peak and then decreases. This peaking is directly responsible for the unusual heat flux curve at 700 F bulk temperature. The effect of a steeper temperature gradient on the enthalpy difference $(h_w-h_{u_m})$ is also shown in Figure 19B. A steeper temperature gradient at the wall also increases the magnitude of the other quantities slightly but does not change the trends.

Altering the shape of the velocity profile would perhaps make significant changes in the variables. Changes would occur in the exponents of the shear stress equation (16) as a result of the generalized Blasius law equation (6). As presently postulated, a change in the velocity profile would also cause the heat transfer coefficient to be a function of the length parameter, x .

A comparison between the analytical prediction and a standard correlation with properties evaluated at the film temperature is shown in Figure 20. The agreement is seen to be very good away from the transposed critical temperature. The standard film correlation however fails in the region where the largest property variations occur. Further analytical results are given in a later section and are compared with experimental measurements.

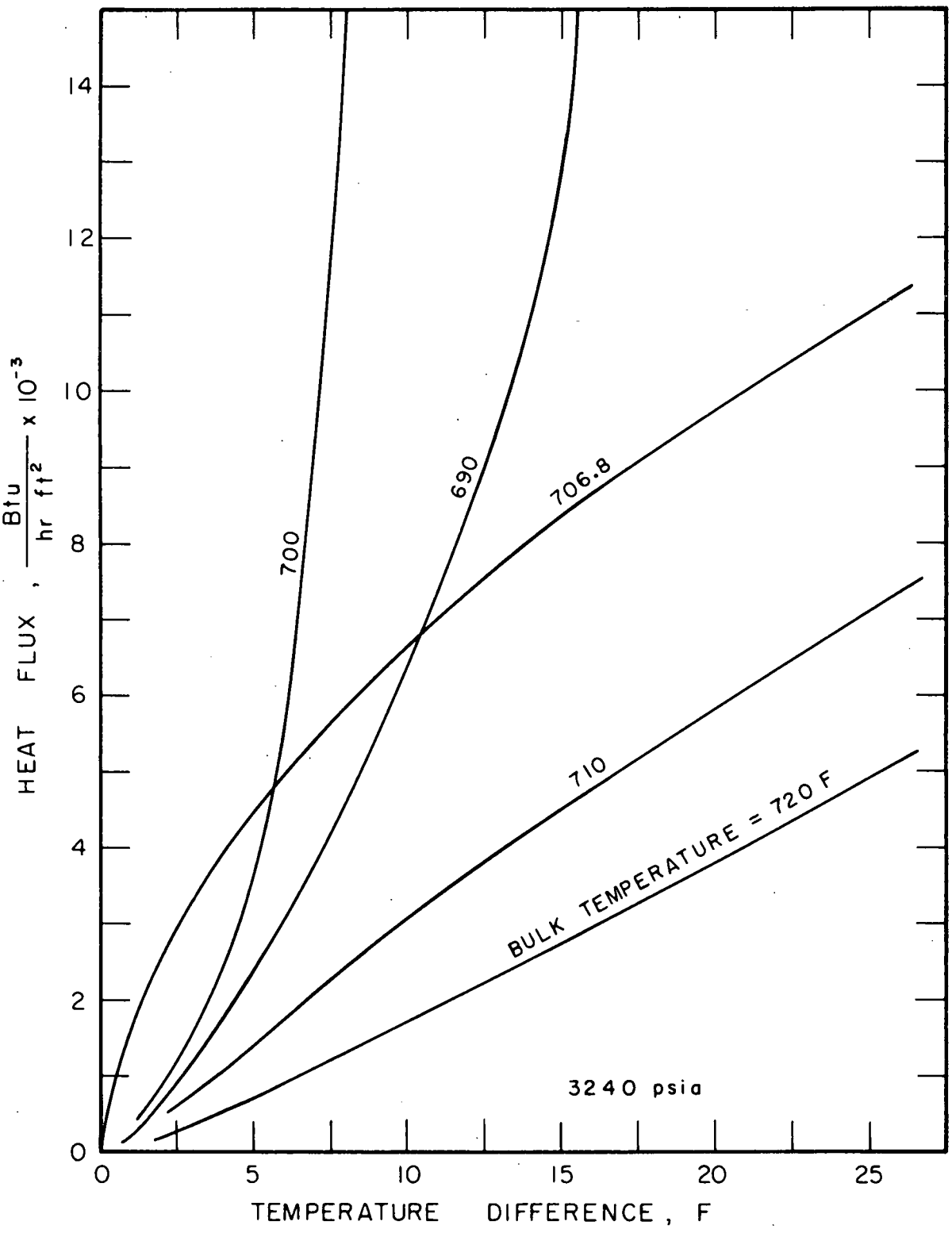

FIG. 17 ANALYTICAL PREDICTION OF HEAT FLUX (REYNOLDS ANALOGY APPLIED ACROSS ENTIRE BOUNDARY LAYER)

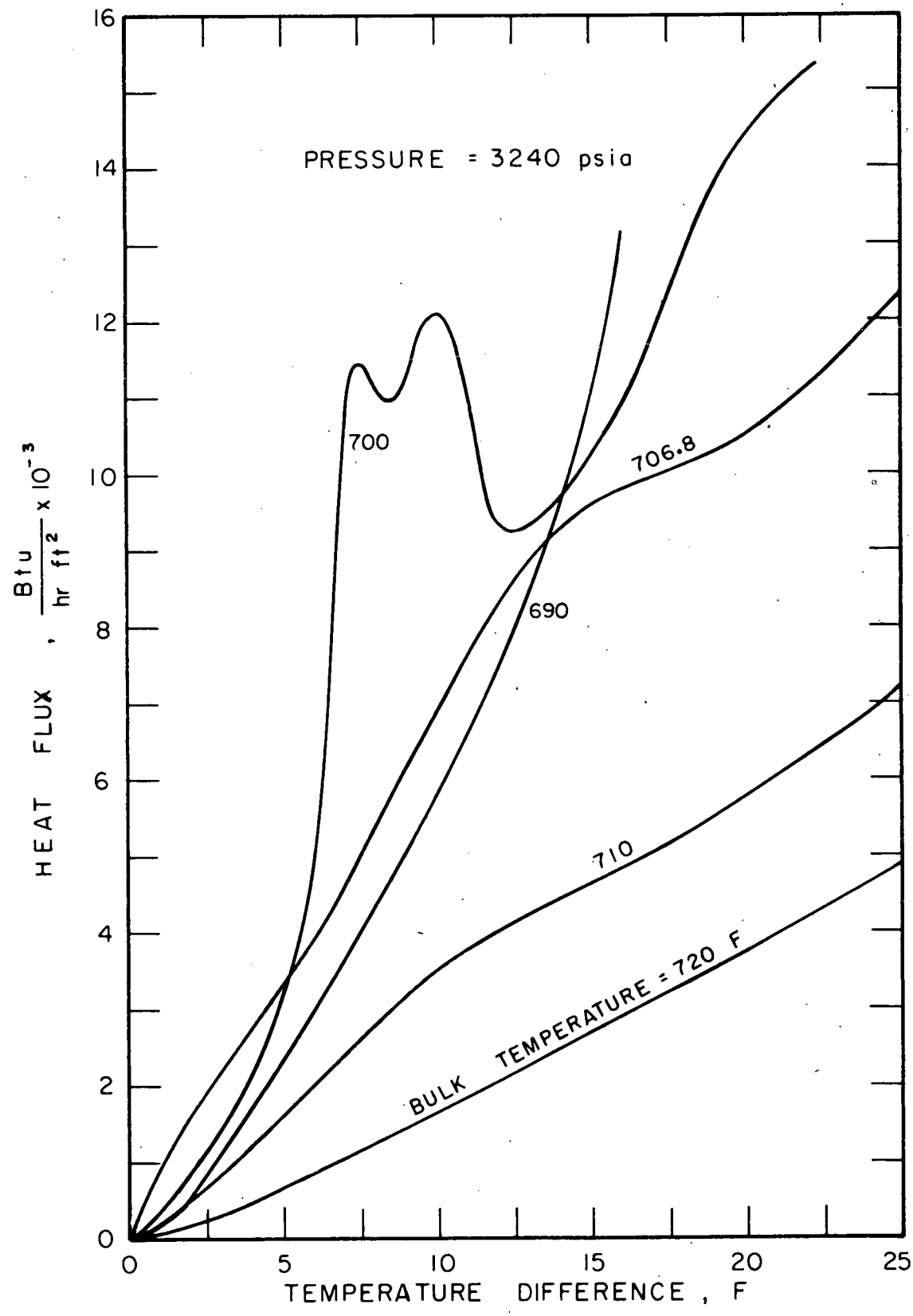

FIG. 18 ANALYTICAL PREDICTION OF HEAT FLUX (REYNOLDS ANALOGY APPLIED BETWEEN THE WALL AND VELOCITY PEAK)

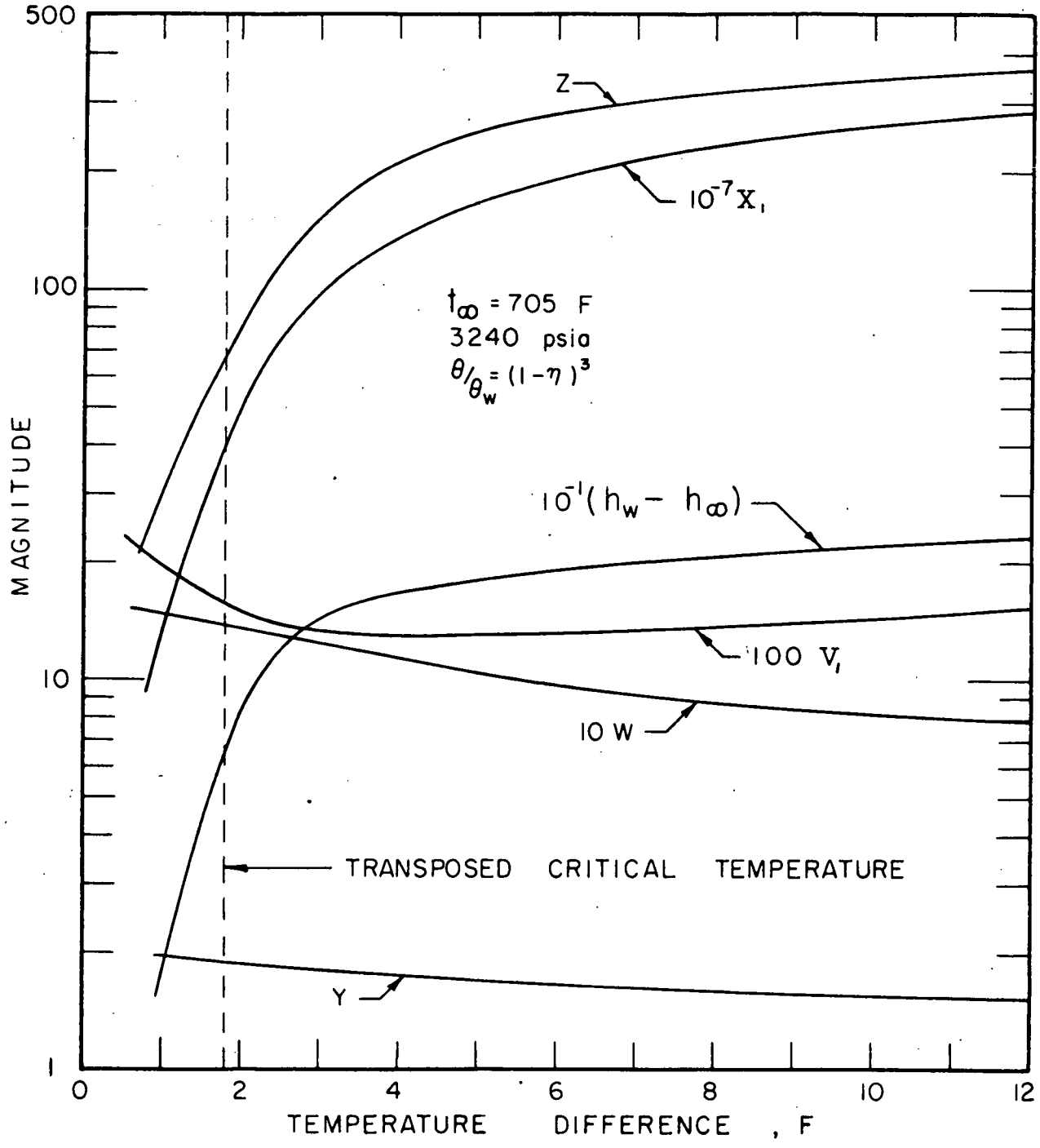

FIG. 19 A TRENDS OF ANALYTICAL EQUATION PARTS
(REYNOLDS ANALOGY APPLIED ACROSS ENTIRE BOUNDARY LAYER)

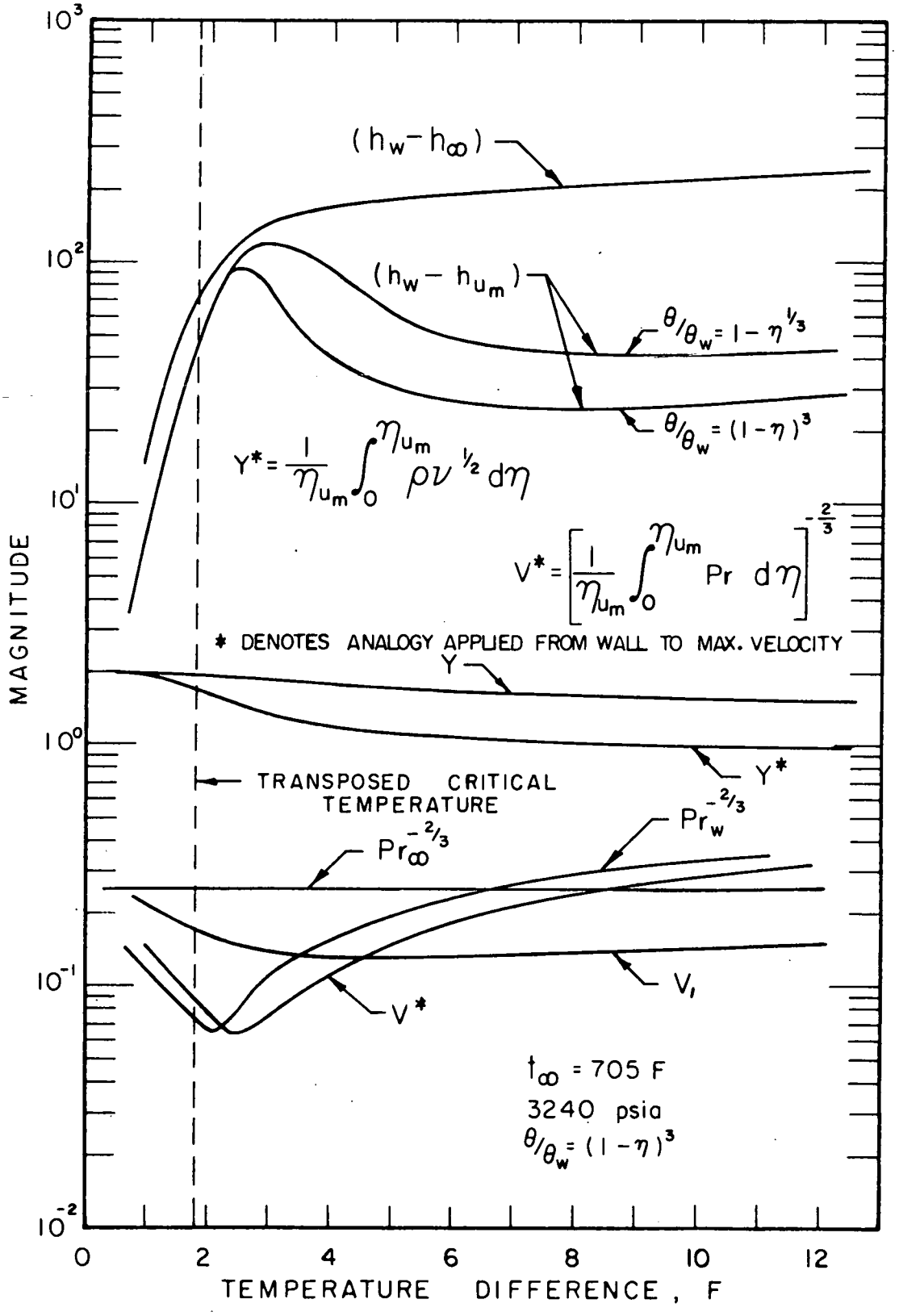

FIG. 19B TRENDS OF ANALYTICAL EQUATION PARTS

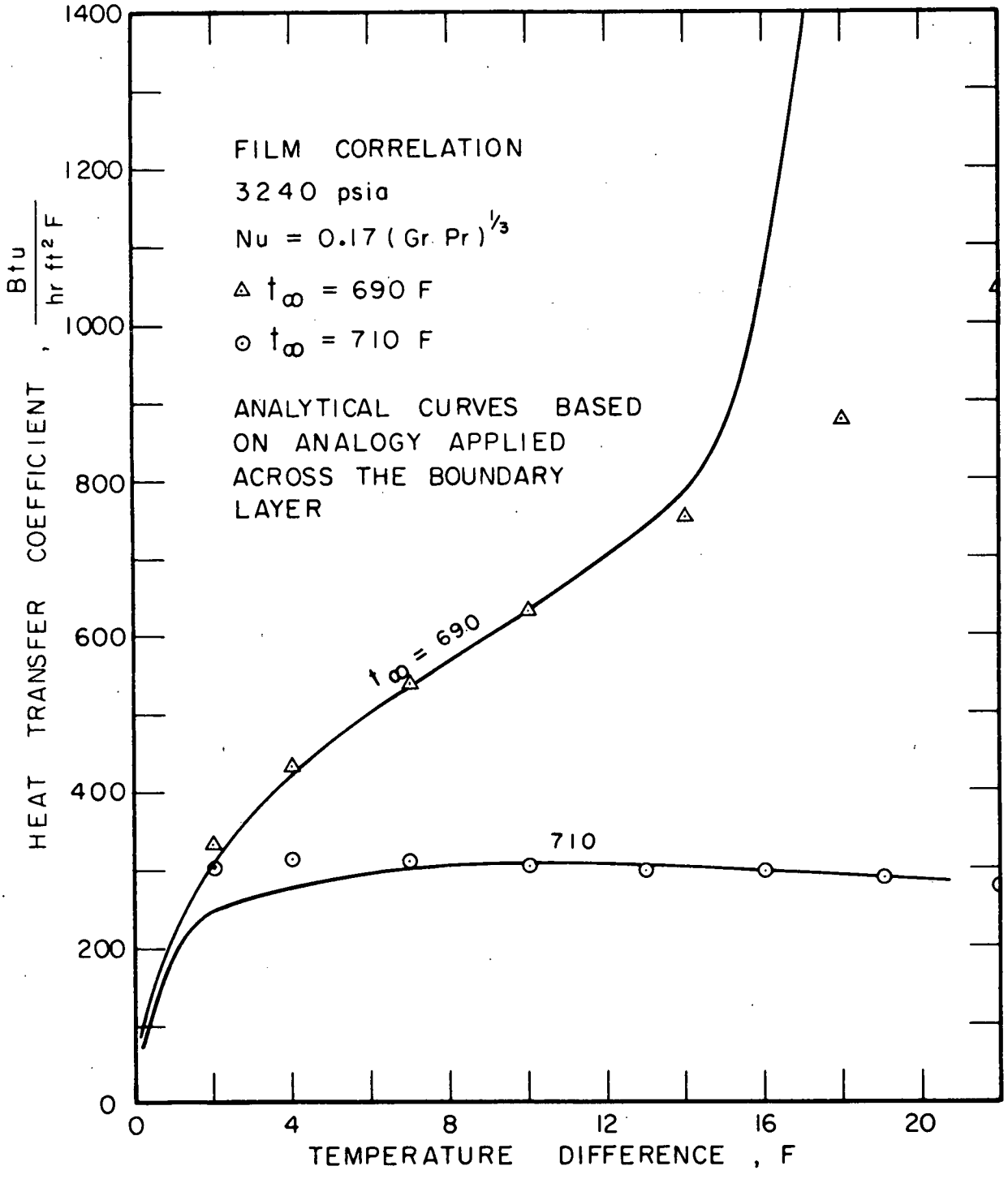

FIG. 20 COMPARISON OF ANALYTICAL PREDICTION WITH THE STANDARD FILM CORRELATION

EXPERIMENTAL APPARATUS

The objectives of the experimental program were to: (1) determine the local heat transfer coefficient in the turbulent regime along a vertical plate, (2) verify the analytical predictions over a range of temperatures and pressures, and (3) correlate the experimental results for design calculations.

To accomplish these objectives the basic apparatus built by Holt (11) and used by Fritsch (5) was again used with minor modifications to determine turbulent free convection coefficients in near critical water. A brief description of the apparatus will be given here. More detailed information may be found in the references mentioned.

General System

A schematic diagram of the system is shown in Figure 21. A picture of the control panel with the major instrumentation is shown in Figure 22. The basic piece of equipment was a stainless steel pressure vessel with inside dimensions sufficiently large to simulate an infinite medium. The vessel was externally heated by electrical resistance wiring wound around the vessel in spirial coils. The resistance wiring was divided into separate elements for better control of the vertical temperature distribution in the vessel. Outside the heating elements the apparatus was wrapped with insulation to

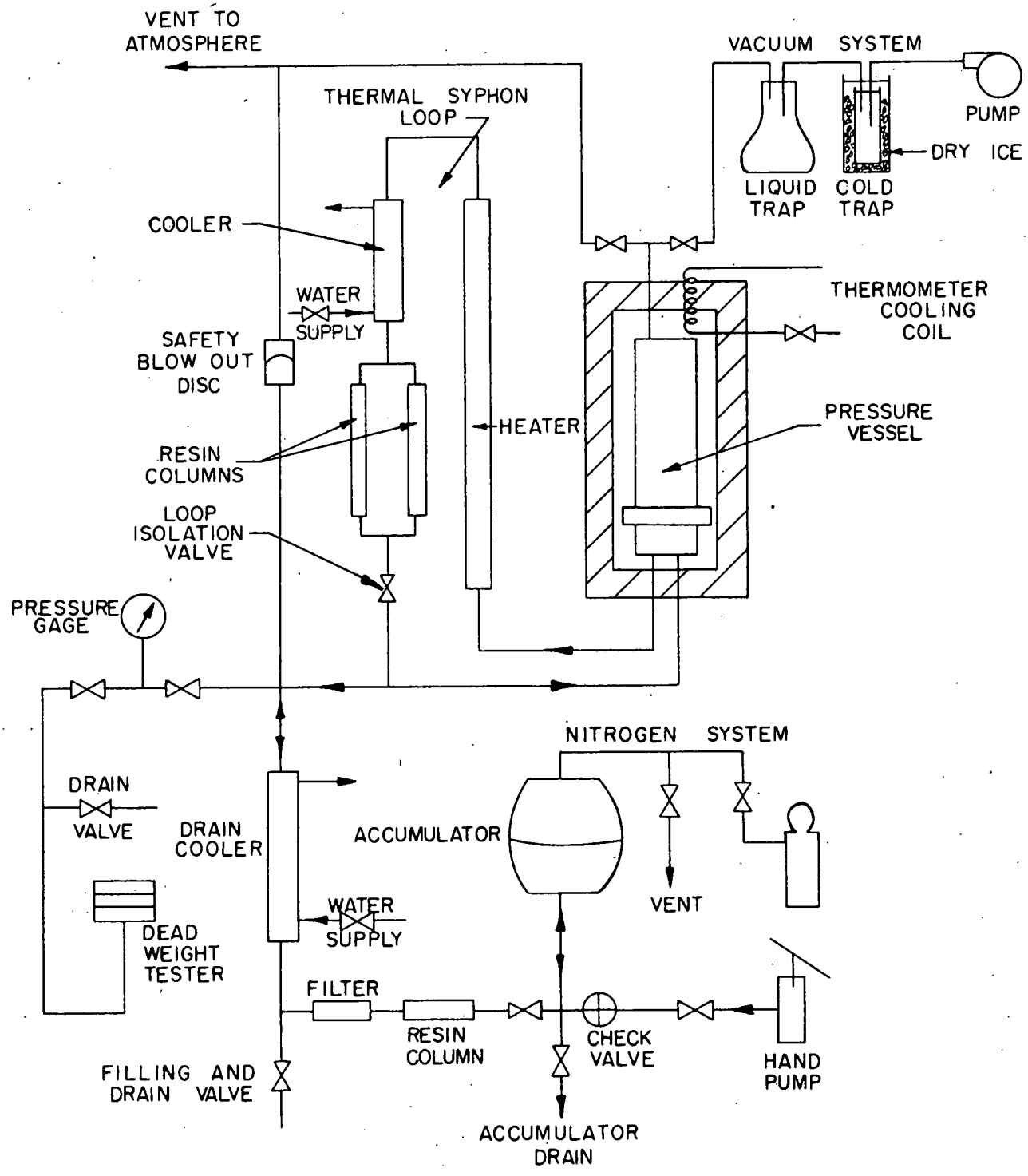

FIG. 21 SYSTEM SCHEMATIC

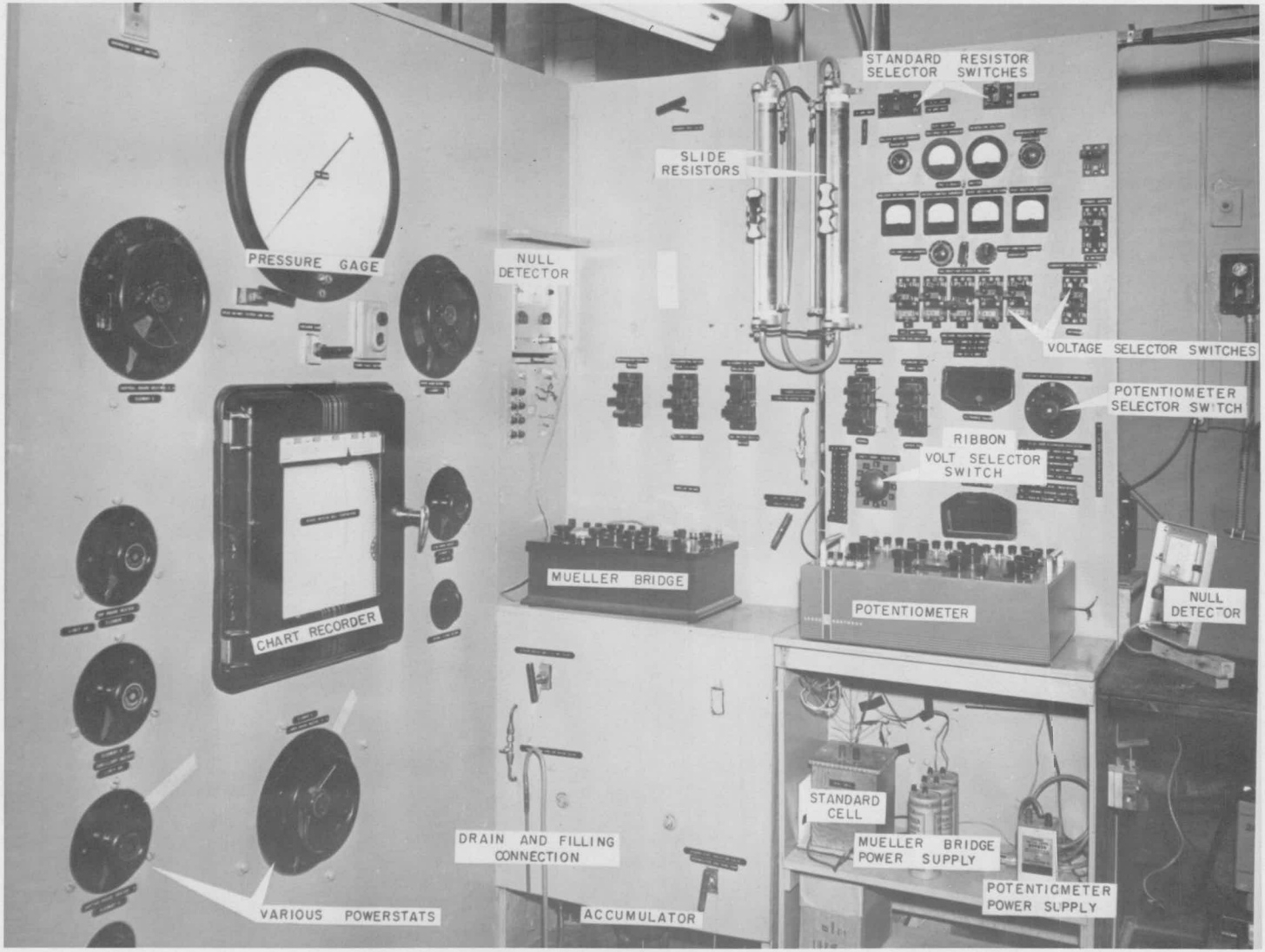

FIG. 22 CONTROL PANEL

minimize heat loss and reduce temperature variations due to changing ambient conditions.

To evacuate the test chamber of air prior to charging with water, the vessel was connected to a vacuum system consisting of a vacuum pump and a cold trap to condense the water vapor. The vacuum thus obtained was the primary method of charging the chamber with the test water. An accumulator or surge tank was also connected to minimize pressure fluctuations during operation. A connection to a high pressure hand-pump was provided for leak testing and for the addition of water during operation. All wiring leads were brought into the chamber through stainless steel tubes welded into the base of the vessel. A pressure seal was maintained at the lower end of these tubes by a fitting containing a teflon plug.

The measuring devices used to obtain the state of the bulk water in the chamber consisted of a calibrated bourdon tube pressure gage connected to the vessel and a platinum resistance thermometer enclosed in a well installed in the top of the vessel. Measurements of the test section voltage drop were made with a potentiometer.

To maintain ion free water in the vessel, a fraction of the water charge could be circulated through a column of resin by means of a thermal syphon loop, during the warm up procedure.

Test Section

To satisfy the experimental objectives, the test section had to provide a means for the measurement of local temperature and local heat generation, along the length of the plate. It was decided to use the test section as a resistance thermometer to determine temperature;

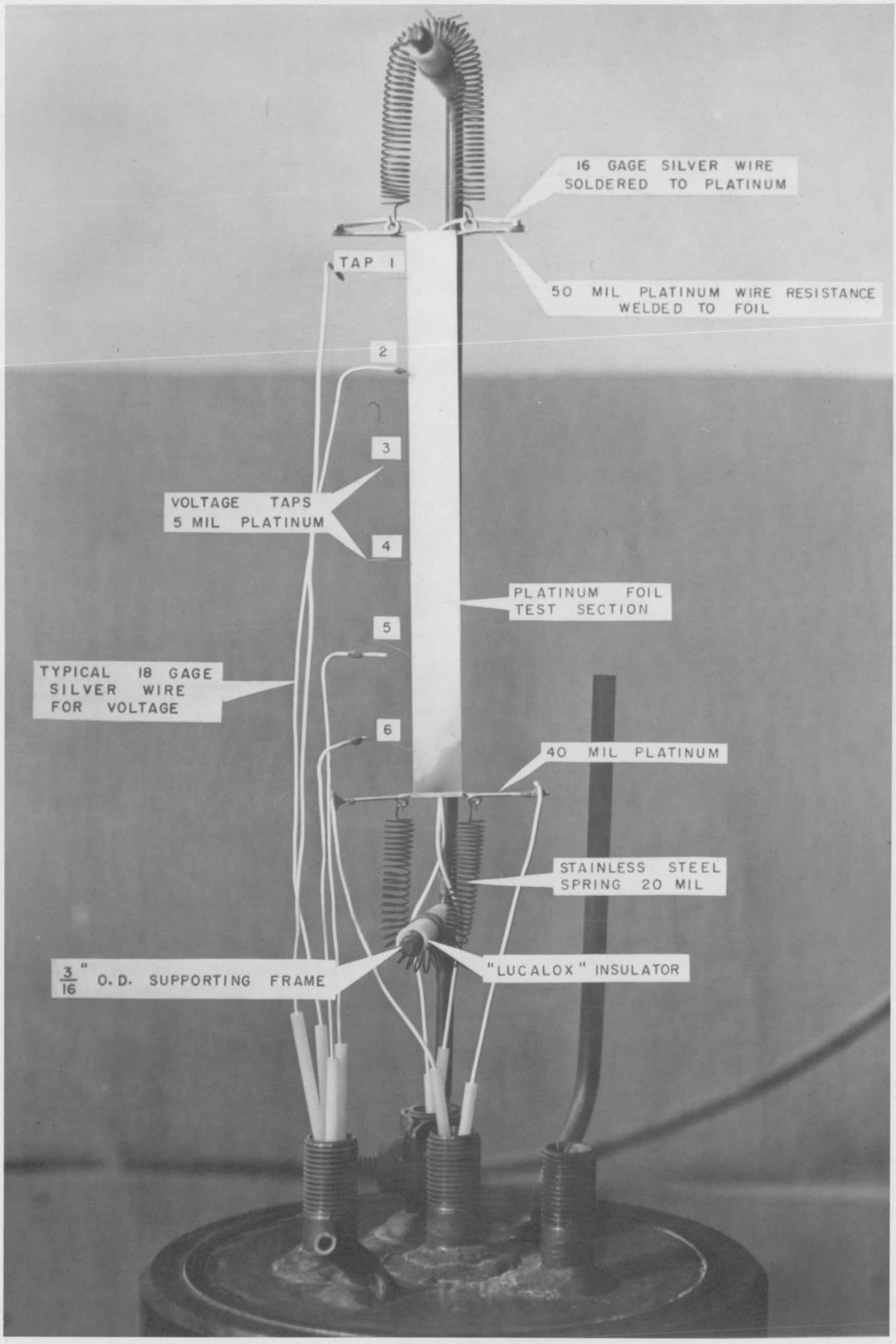

FIG. 23 TEST SECTION

thus the local heat generation could be determined from the same measurements. A typical test ribbon is shown in Figure 23.

Mechanical Design

The choice of the final test section dimensions was based upon experiment and upon the physical limitations of the equipment. The most important physical limitation was the maximum current flow. The wiring and switches were sized so that 50 amperes was an upper limit. Limitations of the direct current power supply are explained in the next section.

With the current supply set, the physical width and thickness of the test section foil was constrained. The width was sized at one-half inch to reduce edge effects since calculations indicated the boundary layer thickness would be in the order of several hundreths of an inch. Thus the plate width would be 15 or more times the disturbance thickness. Many investigators have studied free convection on a plate of width only 10 to 15 times the disturbance thickness. Calculations also indicated a plate height of about an inch would be necessary to obtain Grashof numbers of turbulent magnitude. For ease in assembly the height limit was about eight inches and six inches was more convenient.

Due to the errosive nature of high temperature-pressure water previous investigators had shown the possibility of mounting a joulean heated foil on some backing material to be impractical. Thus, the foil or plate had to be exposed to the ambient environment on both sides. This doubled the heat transfer surface and doubled the required

heat input for a specific temperature difference. Without any backing material the foil would also have an almost immediate response to environment fluctuations.

The remaining dimension was the plate thickness. Relatively thick foil, i.e., of 0.005 inches, was very easy to work with but the resistance was very small. This would cause little joulean heat to be generated and only small temperature potentials could be realized. With a heat transfer coefficient of 200 to 300 $\frac{Btu}{hr.ft^2\ F}$, a thickness of two mils seemed adequate. However, when large values of specific heat were encountered the turbulent coefficient was much larger and a foil one mil thick was required for temperature differences greater than 10 degrees Fahrenheit.

A ribbon several mils thick was also desirable from another consideration. To minimize the transfer of heat by conduction in the ribbon a poor fin characteristic was desirable. Preliminary calculations indicated that for the combination of thermal properties and thickness considered, the ribbon would act as a very poor fin. Thus heat generated locally in the ribbon could be considered to be transferred by convection to the ambient fluid and transfer by conduction would be negligible. A variation in temperature of the ribbon would only be expected if the heat transfer were a function of the length parameter. Otherwise for uniform heat generation the heat transfer coefficient and temperature of the ribbon should be constant.

Ideally, no exposed leads would carry power to the test piece as undesirable flow patterns could originate on them. However, with no backing plate possible, the leads had to be exposed to the ambient environment. Because of the current limitation and magnitude of the resistance of the platinum, the leads could not be connected along the vertical edges but only along the top and bottom.

Now the size and material of the lead wire were subject to choice. Platinum could be easily resistance welded to the foil without causing distorting stresses. Also platinum, having smaller electrical and thermal conductivities than silver, was more desirable because it reduced the fin effect of the lead wire. Other materials such as copper or aluminum were not considered since they would erode in the environment present in the pressure vessel. To simplify design the supporting structure was connected directly to the lead wires. This meant the lead wire needed to be physically strong enough to support and maintain some vertical tension in the test foil. Thus, a 40 mil wire was used on the bottom and 40 or 51 mil wire on the top. This platinum wire extended about an inch from the ribbon where it was joined to a heavy silver wire lead.

The 40 mil platinum lead wire connected at the bottom had the same cross sectional area as the 2 mil test section. Since two lead wires were connected to each end of the test section, the heat generation per unit length in the platinum wire was one-fourth that of the foil. The combined effect of a very high

heat transfer coefficient at the starting edge and the high conductivity of the heavy connecting silver lead wire removed a good part of the joulean heat generated in the platinum wire. Thus a compromise was obtained where a minimum amount of heat was conducted from the ribbon to the wire and the wire remained near the ambient temperature to minimize the possibility of undesirable turbulence.

The placement of a cylinder at the starting edge of the test section presented a need for justification. In forced flow such wires are placed downstream of the leading edge for the purpose of tripping the boundary layer to induce turbulent flow. When positioned exactly at the starting edge it should have no effect unless circulation with an approach velocity were present in the vessel. If circulation did exist the wire could be roughly considered as a cylinder in cross flow. Von Karman vortex streets occur in such cross flow at Reynolds numbers as low as 60. An approach velocity of 0.1 feet per second at the starting edge would yield a Reynolds number of several hundred thus making this phenomenon a possibility.

To make the starting flow uniform on both sides of the foil, a wire was placed on each side. These wires were slightly flattened to insure adequate electrical contact and increase physical rigidity. The width and thickness of the foil were, for practical purposes, uniform since little difference was noted after measurement with a steel rule, a magnifying glass, and a micrometer. The ribbon surface was smooth and free of

surface defects. Voltage taps of five mil diameter platinum wire were spot welded along one edge of the ribbon at one inch intervals. The top and bottom voltage taps were placed one-half inch away from the power lead connections. This spacing minimized any affect end losses would have on the temperature determination. The distances between the starting edge, top and bottom voltage taps were measured to within 0.005 inch by a cathetometer after mounting the ribbon on the framework. The power leads and voltage taps were silver wire led in through the stainless tubes.

The six inch length ribbon was positioned at the bottom by a 20 mil stainless spring connected to framework from the vessel base and hooked to the platinum lead wire. Another stainless spring attached to the lead wire at the top in similar manner kept the ribbon vertical and in tension. A near vertical position was obtained by leveling the vessel base and visually observing the angle between the ribbon and a weighted thread attached to the framework. The mating contact surface of the vessel had previously been leveled. The stainless wire was electrically insulated from the supporting framework by quartz or polycrystaline alumina tubing.

The bottom of the ribbon was located five inches above the base. This allowed about nine inches of clearance between the top of the ribbon and the vessel top.

Power and Control

Direct current power to the test section was supplied by a bank of ten six volt automotive type lead storage batteries connected in parallel with a nominal 12 volt, 50 ampere, power supply. This combination tended to minimize the random fluctuation inherent in the direct current supply and the voltage drift inherent in the battery bank. This fluctuation and drift increased proportionally with current output and became intolerable at 50 amperes. The load was split between the two power sources by adjusting the output voltage on the direct current supply. At low test section current flows, i.e., during warm up, this voltage was set to place most of the load on the direct current power supply. As higher currents were used, the battery bank supplied a larger proportion, i.e., 20 amperes maximum for a 50 ampere total load.

Current variation was provided by two electrically parallel water cooled slide rheostats. This provided a current range of 10 to 50 amperes. The current flow was obtained by measuring the voltage drop across a nominal 0.001 ohm shunt placed in series with the test section.

The power leads were 16 gauge silver wire and the voltage leads were 18 gauge silver wire. The voltage leads and internal thermocouples were connected to external wiring in an isothermal junction box located below the stainless steel lead tubes. All wiring on the water side of the teflon seal plugs was electrically insulated by quartz tubing. This tubing eroded with time at the top end.

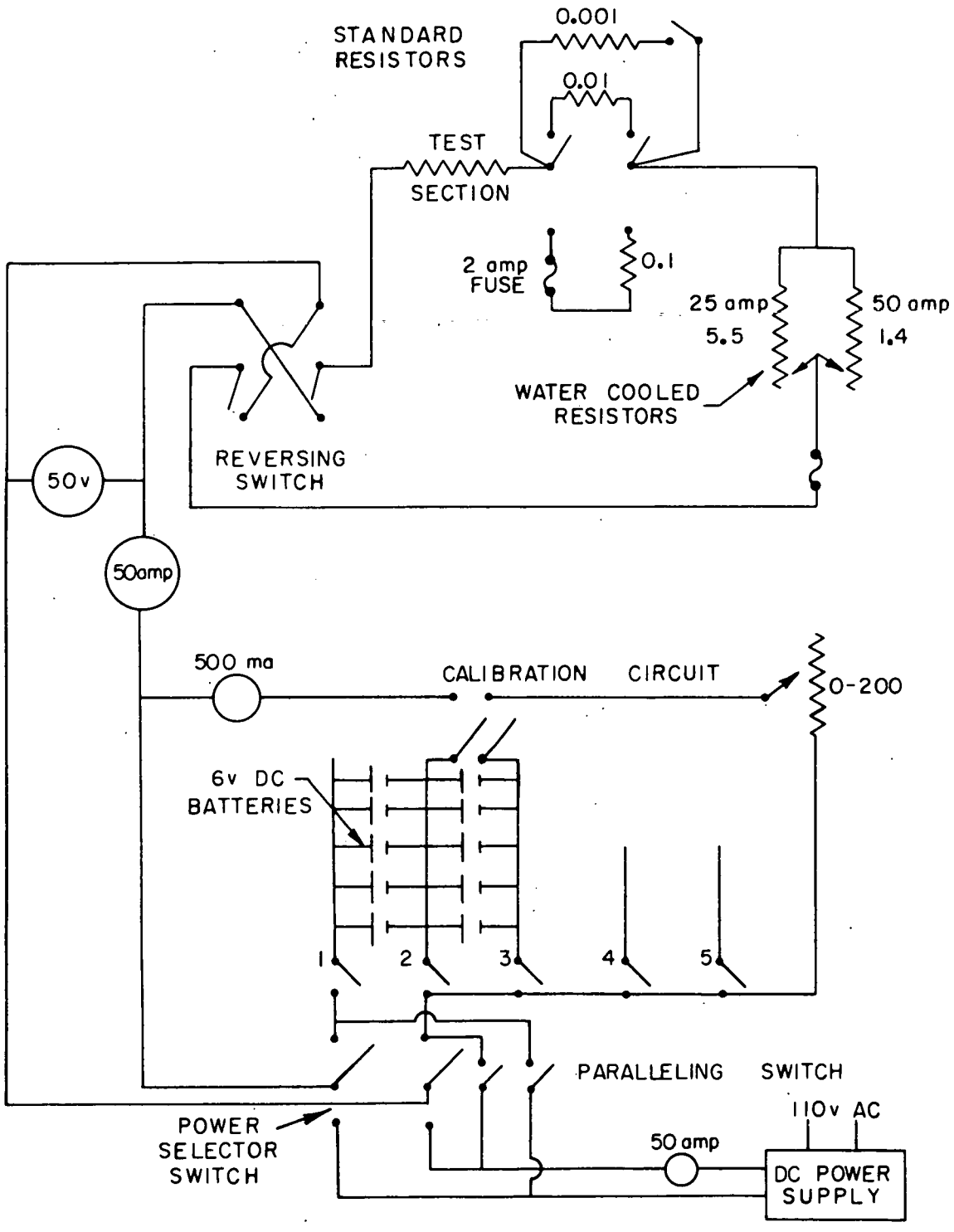

FIG. 24 TEST SECTION POWER SUPPLY

The external voltage tap wiring was brought to a multiple point selector switch. This switch was wired to provide the voltage differential between consecutive voltage taps as well as between taps placed further apart.

Measuring Equipment

The instrument used to measure the various voltage drops was a Leeds and Northrup type K-3 potentiometer in conjunction with a type 9834 electronic null detector. The working voltage was furnished by a constant current power supply. An Eppley standard cell was used as a reference and was checked by A. Clausen of the School of Mechanical Engineering. The standard resistors were of 0.10002 ohms and 0.0010002 ohms as calibrated by D. E. Lipp of the School of Electrical Engineering. A ratio box was used to facilitate measurement of voltages larger than the 1.6 maximum of the potentiometer. The ratio was 100.00 $\pm$ .01 to one and was calibrated by D. E. Lipp. The use of the ratio circuit required making a small correction to the voltage measurements to obtain the proper value of temperature.

The platinum resistance thermometer was a Leeds and Northrup type 8163 and was used with a Rubicon type 1551 Mueller bridge and another null detector. Prior to use of the thermometer, serial number 1613936, a temperature measurement check was made at the triple point of water. The ice point resistance, R_o, obtained from this check was 25.5573 ohms. This compared quite favorably with the value obtained by the National Bureau of Standards of 25.5571. The NBS number was based on measurements made at the triple point of water, the steam point, and the sulphur point. The manufacturer of the thermometer,

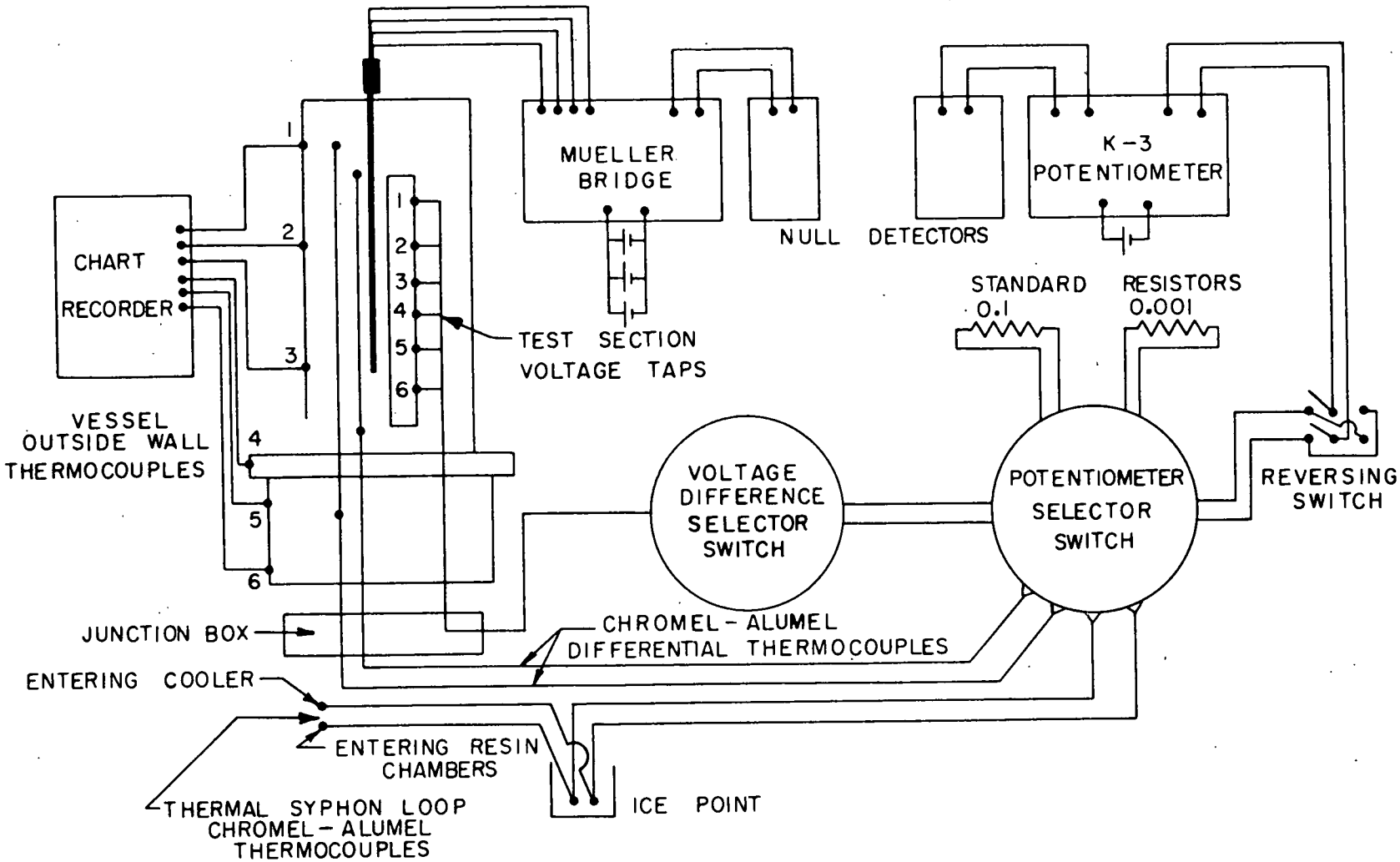

FIG. 25 SYSTEM MEASURING CIRCUITRY

Leeds and Northrup, had previously compared this thermometer to another one certified by NBS and found R_o to be 25.556 ohms. During the experimental period the thermometer was again checked at the triple point and little change was noted.

Vessel Heating and Control

The power used to heat the vessel and bulk water came from building service 110 volt and 220 volt lines. The power was regulated to the individual heating coils by controlling it through individual power transformers. During steady state operation the lower heating elements provided most of the power required. These had a provision for use of power from a constant voltage transformer rated at 2000 volt amperes output.

An approximate indication of the internal water state was given by six chromel-alumel thermocouples spot welded to the outside of the vessel. These thermocouples were located from top to bottom of the vessel at approximately equal intervals. The signal from these thermocouples was fed into a six point chart recorder to provide a visual guide for manually regulating power to the individual heating elements. An automatic device for controlling power to the individual heating elements had been previously developed but was not used in this investigation.

Because of the thermal inertia of the thick vessel wall, these thermocouples were useless for determining any vertical gradient inside the vessel. To measure this, two 28 gauge chromel-alumel thermocouples were connected to measure the vertical difference; one measured the

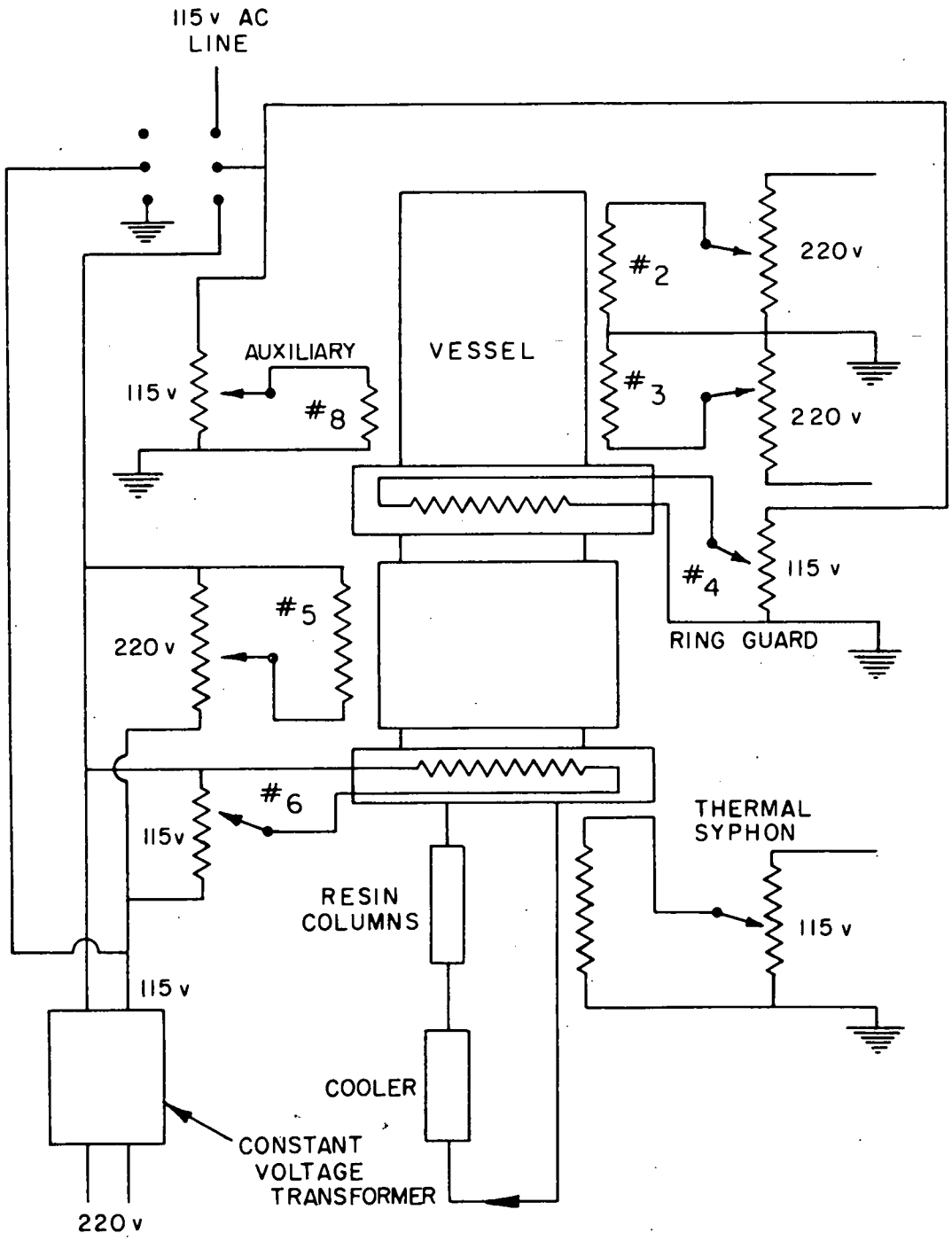

FIG. 26 VESSEL HEATING CIRCUITRY

difference from top to bottom of the vessel and the other measured the difference over the length of the test section. The long leads were made of chromel.

Achievement of a desired state was indicated by a reference resistance thermometer, certified by the National Bureau of Standards, in conjunction with the associated Mueller bridge and null detector. This thermometer was positioned vertically from the top of the pressure vessel with the middle of the sensitive element about eight or nine inches above the base. This height insured that the connecting wiring junction above the thermometer's glass seal would not be overheated. The thermometer used in previous work had been badly scorched resulting in breaking of the lead wiring.

Two additional 28 gage chromel-alumel thermocouples were used to monitor the fluid temperature in the thermal syphon loop. Because of possible resin melting and resultant contamination of the vessel, the water temperature entering the resin columns had to be kept below 140 degrees Fahrenheit when the thermal syphon loop was used.

Miscellaneous Problems

Vessel Pressure Seal

The pressure seal between the vessel and the base consisted of a tongue and groove joint. This rounded V shaped tongue had been nicked and also scored by a welding rod making it impossible to obtain a tight seal during pressure testing at room temperature. A five mil thick silver gasket was then tried and found to work. Once while operating at high temperature and pressure the gasket yielded slightly, allowing

some steam leakage until the metal apparently annealed and flowed to stop the leak.

Corrosion

During the course of equipment checkout it was necessary to rebuild the wiring, quartz tubing, and seals many times. After one disassembly it was noted that a ring of corrosion pitting had formed in all but one lead tube. This ring was located at the exact point the lead tube entered the base. To minimize the chance of material failure a fillet weld was made at this junction to obtain extra strength.

After a discussion of the problem, Dr. R. E. Grace of the Purdue School of Metallurgical Engineering recommended switching from distilled to deionized water. Also a type 316L austenitic stainless steel was recommended should replacement of the tubes ever be necessary. This type steel is less susceptible to carbon precipitation because it has a very low carbon content. Type 317 was recommended as a second choice because of high molybdenum content.

Erosion

A great deal of difficulty was experienced by erosion of the quartz tubing. A 99.9 percent pure polycrystaline alumina with the trade name "Lucalox" was tried for the top several inches of the lead wiring and around the support structure. It was found by far superior to the quartz. It is recommended that in future experiments all quartz be replaced with alumina tubing of 99 percent or better purity. Alumina slightly less pure than "Lucalox" is much cheaper and is available in longer lengths. Changing to water deionized with an Enley MB-3 resin also seemed to reduce the erosion problem.

Electrical Shorting

During the course of checking out the equipment electrical shorting of the test section wiring to ground was a common occurrence. One cause of this shorting was the design of the fitting to hold the sealant plug. This fitting was designed with two shoulders against which the insulating ceramics butted, i.e., Figure 27. At these locations there was no mechanical separation between the silver lead wires and the fitting, and the clearance between the wires and the shoulder was very small.

During operation movement occurred in the wiring due to thermal expansion and thus contact was made with the shoulder. This occurred with 16 and 18 gauge wire even though the fitting was stated to be good for 14 gauge wire. This problem was solved by inserting a small teflon cylinder through this shoulder with separate holes for the lead wires.

After this modification the electrical resistance from the test section to ground was always at least 10^4 times the resistance across the test section and was therefore satisfactory.

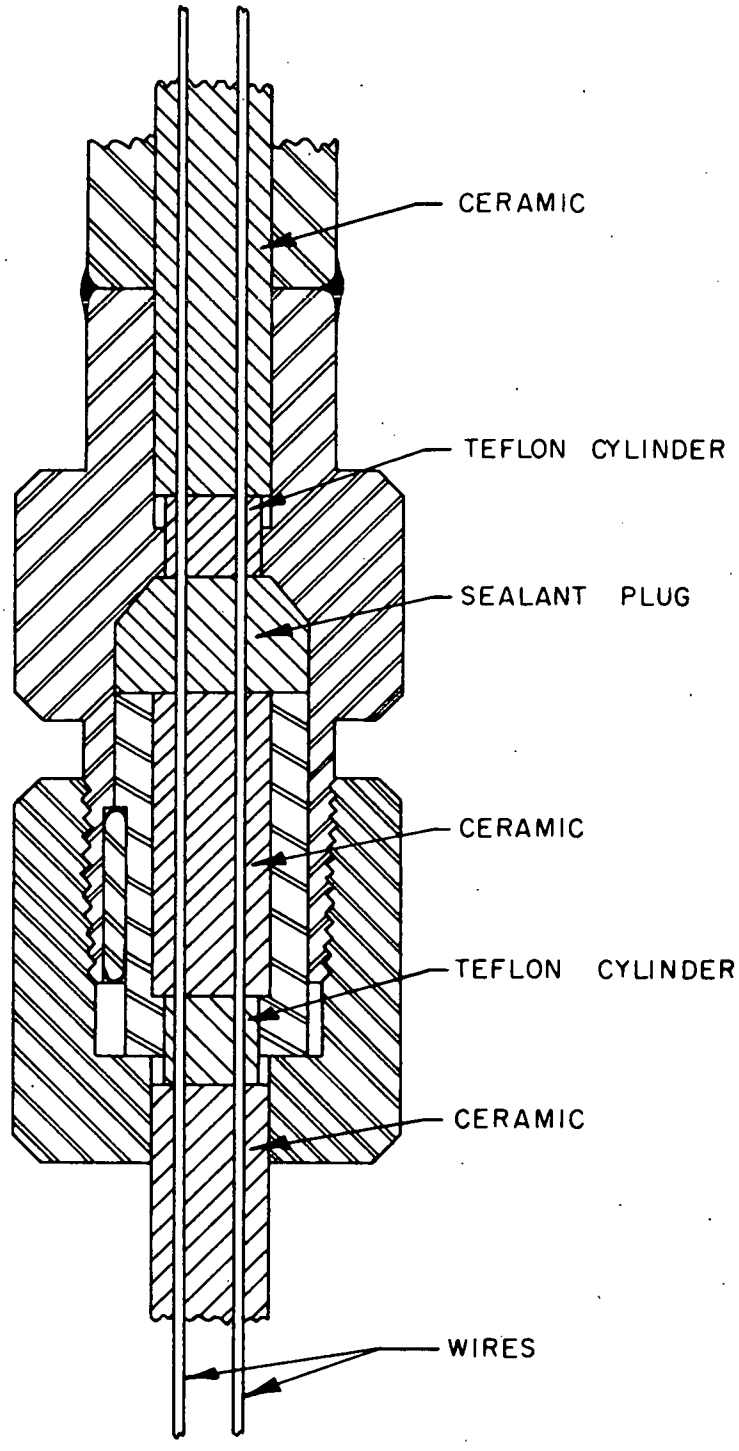

FIG. 27 SEALANT PLUG FITTING

EXPERIMENTAL PROCEDURE

Temperature Measurement

The correct measurement of temperature was the most critical experimental technique required in the conduct of the investigation. This was because the temperature difference between the test section and the infinite bulk fluid determined the value of the heat transfer coefficient once the heat flux was established. Also, in terms of analytical substantiation of experimental results, the thermodynamic and transport property values of water change much more rapidly with temperature than with pressure.

Two methods of obtaining test section temperature were used in previous investigations with the present basic apparatus. These methods were resistance thermometry and the thermoelectricity. The use of platinum as a test section material allowed resistance thermometry to be used because it is inert and stable at the temperature of near critical water. By use of the calibrated platinum resistance thermometer the reference bulk fluid temperature was accurately known.

Holt (11) used the test section as a resistance thermometer by assuming it had the same temperature-resistance relationship as the calibrated platinum thermometer. This required knowledge of the test section resistance at zero degrees centigrade, R_{x_o}, which was obtained by direct measurement in flaked ice or by measurement at other temperatures with comparison to the calibrated thermometers resistance

ratio at that temperature, viz.,

$$\frac{R_{x_o}}{R_x} = \left(\frac{R_t}{R_o}\right)^{-1}$$

where R_x was the test section resistance at a specified temperature and R_t/R_o was the resistance ratio of the calibrated thermometer at temperature t and where R_o was its ice point resistance.

The two methods of computing R_{x_o} did not agree, thus Holt used the R_{x_o} obtained by comparison. This discrepancy was probably due to several reasons: (1) the platinum of the test section had a different resistance-temperature relationship because of different purity, and (2) the instrument used to measure voltages, i.e., a Leeds and Northrup K-2 type potentiometer, was not of sufficient accuracy to assure measurements within one-half degree Fahrenheit. An exact knowledge of R_{x_o} was necessary since at 350 Centigrade a 1 percent error in R_x/R_{x_o} could cause an error of 6 degrees Centigrade.

Fritsch (5) attempted to use this technique but discarded it because of inconsistency at small temperature differences. He then used fine wire thermocouples connected to his test section with the reference junction located next to the sensitive element of the thermometer. Three wires were needed to correct for voltage drop across the couple. He attempted to correct for the fin effect of his thermocouple by using a relationship for a wire attached to a semi-infinite wall. Based on this relationship, his experimental results were consistently 15-22 percent higher than the analytical prediction.

An analysis given in Appendix G showed that the fin effect error for a finite thin foil of thickness used in this investigation was much larger than for a semi-infinite solid not considering internal heat generation and heat loss from the body to the ambient environment. The solution for the temperature error considering these effects was beyond the scope of this work. Thus, it was decided that thermocouples attached like fins would not produce a satisfactory way to measure temperature.

The method used in this work was a modification of Holt's procedure. The test section resistance was determined by direct measurement in the temperature range of interest. This was done by passing a small calibration current through the ribbon and measuring the resultant voltage drop once steady state had been achieved. The resistance of the certified thermometer was used as the standard for comparison.

Assembly and Operation

Prior to assembly of the test section and supporting framework all component parts of the vessel in contact with the water were thoroughly cleaned by a procedure developed by Holt (11) as follows: (1) vessel parts were cleaned with detergent solution in water and rinsed with distilled water, and (2) vessel parts were cleaned with carbon tetrachloride, ethylene trichloride, acetone, and ether in that order to remove residual oil.

Next, the thermocouple silver lead wiring was threaded through the quartz insulating tube and positioned in the base lead tubes. The

teflon pressure seal plug was threaded on the wiring and the pressure fitting tightened to hold the wiring in place.

The test section was constructed from platinum ribbon foil. The lead wiring was welded to the foil which was then cleaned to remove finger prints. The section was then supported by the stainless steel wire springs. The platinum leads were then silver soldered to the silver lead wires. By use of a weighted thread the section was visually adjusted to a very near vertical position. Care had to be taken in positioning the section and lead wiring to leave room for the thermometer well which protected the resistance thermometer. The power leads were connected and enough current was passed through the ribbon to bring it to a red color to anneal it for about two hours.

The base was then lifted into place with a wide silver gasket positioned across the tongue of the base. The base cap was threaded on the vessel and compression bolts tightened. The lower two heating elements were positioned around the base cap and connected. Thermocouples were resistance welded to the cap. Finally, insulation was positioned around the base.

After connecting the deionizing loop piping, the system was evacuated for several hours and then charged with about two gallons of deionized boiling water. The water was cooled on its way to the vessel by the drain line cooler. The water connection to the accumulator was disconnected and blanked off. This reduced the amount of water and work needed to pressurize the system. A test pressure was obtained by use of the hand-pump and all fittings were checked for water drops.

After the accumulator was installed no more leak tests were made even though the base was disassembled several times to remodel or rebuild the test section. Calibration runs made with the accumulator isolated from the vessel indicated that the system pressure remained constant and thus no leaks were present.

To accurately determine the distance between voltage taps, current of several hundred milliamperes was passed through the section after the vessel interior had reached a uniform temperature. The voltage drop between the individual taps and across the end taps allowed calculation of the distances between taps. When these measurements were made, the vertical temperature difference across the test section was less than one-fourth degree Fahrenheit as measured by one of the differential thermocouples.

The first run made on a test section was for calibration. The system was heated to several desired temperatures and measurements taken. After one day of operation additional water was charged into the vessel. All water charged into the vessel had a resistivity of two to four million ohm-centimeters.

During the heating process the vessel was vented after the water reached saturation to help eject any air remaining or leaking into the vessel. Excess water was stored in the accumulator until the desired pressure was obtained. Additional water was drained from the system. Water makeup was supplied through the hand-pump if needed. Occasionally during heating the thermal syphon loop was operated to help maintain water purity.

During the heating period considerable water had to be bled from the vessel. To keep this water from flashing into steam an annular heat exchanger was inserted around the tube between the vessel and drain valve. This cooler also prevented hot water from entering the accumulator and damaging the rubber bladder.

Also during the warming up period the Mueller bridge ratio and zero adjustments were checked. The ratio adjustment did not vary significantly during the period of the tests. The zero adjustment varied considerably and sometimes varied beyond the scale adjustment, although the error introduced was very small. The pressure gauge was checked atainst a dead weight tester at a pressure near the desired operational one.

The power supply for the potentiometer was turned on about a day previous to actual taking of measurements. A two volt battery and small direct current power supply were both used at different times for this purpose. The null detectors were also turned on well ahead of time or left in operation.

Data Taking

The heating period took nearly three hours. The test section was energized after a pressure of about 150 pounds was obtained. This initial current was set at either 12 or 18 amps and maintained until the first set of data was taken.

Since very stable conditions existed after obtaining steady state, readings were taken of all voltage positions across the test section. After these initial readings were taken power was increased in intervals. After each increase in power, the current was monitored

until it appeared to have stabilized, then readings were taken and the current was checked again to ensure against drift. At higher current flows fewer readings were taken because of current drift and bulk fluid temperature drift upward.

The addition of more current to the test section tended to increase the pressure and bulk fluid temperature. The pressure was monitored and water was continuously bled from the system to maintain the desired value. The power input to the external heating elements was slightly reduced to counteract the temperature increase but a slow increase was practically inevitable.

Readings were taken at six or seven current settings over about a twenty minute period. Two people were required to obtain readings; one monitored the potentiometer and the other monitored the Mueller bridge, vessel pressure and vessel heating elements.

Calibration Procedure

Prior to taking test data the resistance of the test section was determined as a function of temperature. This was done by heating the vessel to several steady state temperatures and then passing a current of about one-fourth ampere through the section. The voltage drop between the end taps was measured and compared to the voltage drop across the standard 0.1 ohm resistor with a resistance value known to four significant figures. The resultant data was fitted by the curve

$$R = A + B(t - 670.0) \quad ,$$

where $\bar{R}$ was the resistance in ohms, and A and B were constants. After the constants A and B were determined, the temperature, t, was recalculated for the measured resistance and compared to the measured value. The largest error was found to be less than 0.2 degree Fahrenheit.

After installation of the one mil thick test section it was noted that the calibration was not consistent each day. This required checking at several points each day in addition to taking data. Thus the constants of the calibration curve were adjusted each day to obtain consistent results. Closer inspection of the quartz tubing indicated it was badly eroded. This lowered the test section resistance to the vessel making possible small short circuits. These paths through the vessel did not significantly change the heat generation in the test section but did alter the temperature calibration by a noticeable amount. After reinsulating with new quartz tubing the consistency of calibration improved.

The pressure maintained during the calibration procedure was around 3300-3400 psia. At this pressure the system could be stabilized in a much shorter time than it would take at 2500 to 2800 psia. The vertical temperature difference over the test section was less than one-fourth degree Fahrenheit during the calibration runs.

The actual distance between adjacent voltage taps was determined by voltage ratio measurements taken while the vessel was essentially at uniform temperature. While the calibration current was passed through the section, several readings were taken to insure that no current drift occurred. This was also checked during the calibration runs at high temperatures.

EXPERIMENTAL RESULTS AND ANALYTICAL COMPARISON

The experimental data for two families of heat flux curves are shown in Figures 28 and 29. The data in Figure 28 was taken with the two mil thick ribbon at a bulk pressure of 3240 psia while the data in Figure 29 was taken with the one mil thick ribbon at 3300 psia. The experimental measurements relating to the individual data points may be found in Appendix F. The designated experimental runs were taken with the bulk fluid at a near constant temperature and pressure. Individual points of the run were obtained with different values of current passing through the ribbon.

The curves indicate that the heat transfer rate was a maximum for the data runs where the bulk fluid temperature was very near the point of maximum specific heat. When this transposed critical temperature was exceeded the heat transfer rate became less in proportion to the difference between the bulk fluid and transposed critical temperature. This is shown by the near linear curves of decreasing slope. For bulk fluid temperatures less than the transposed critical temperatures the heat transfer rate increased as the ribbon temperature approached the transposed critical temperature. The smooth trends shown indicated that the data was consistent and reproducible.

The data for the two mil ribbon are compared to the analytical predictions in Figure 30 A to F. The analytical curves represent the

case where Reynolds analogy was applied from the wall to the point of maximum velocity in the boundary layer as well as completely across the boundary layer. Limiting cases are also shown by dotted lines where the Prandtl number was evaluated at the wall or in the bulk fluid.

The numbering system is as follows; (1) the analogy applied from the wall to the point of maximum velocity, (2) the analogy applied across the entire boundary layer as done in the analytical development, (3) the analogy applied across the boundary layer but with the Prandtl number evaluated as in (1), (4) Prandtl number evaluated in the bulk fluid, and (5) the Prandtl number evaluated at the wall. The difference between case (1) and (3) comes from the equation (16) in the evaluation of the integral Y. For case (1) Y is evaluated as an integrated average between the wall and maximum velocity while for case (3) Y is evaluated across the entire boundary layer.

These plots indicated that most of the experimental data fell between the limiting cases. This would be expected wherever all physical properties were changing monotonically, i.e., on either side of the specific heat peak (Figure 15), as is the case for the data compared in Figure 30A, B, E and F. Lack of agreement for this data would mean either the analytical model or data were in error.

Figures 30A and B indicate that the Prandtl number evaluated in the model was too small making the prediction high, i.e., curve (2). This follows from equation (22) since the heat transfer coefficient is nearly proportional to V_1, which in turn is inversely proportional to $Pr^{2/3}$. A Prandtl number evaluated closer to the wall, i.e., at a higher temperature corresponding closer to the specific heat peak, would give better agreement.

Figure 30E indicates that the Prandtl number used was too large and better agreement could be obtained if a number corresponding closer to the wall temperature were used. The comparison to run 36 shown on Figure 30F indicates good agreement but the comparison to run 37 shown on the same figure is not as good. The cases (2) and (3) are not shown for run 37 since they do not differ significantly from the limiting cases.

For the data runs where the specific heat peak was straddled by the bulk fluid and wall temperatures, i.e., Figures 30C and D, the limiting cases were of little value. Better agreement would be obtained if the magnitude of the Prandtl number were taken closer to the magnitude of the peak.

Figure 30D clearly shows the failure of the analytical model based on Reynolds analogy applied from the wall to the point of maximum velocity, i.e., curve (1). When the transposed critical temperature is exceeded the enthalpy difference $(h_w - h_{u_m})$ peaks causing a similar peaking effect in the heat transfer coefficient and the heat flux. The steeper temperature profile, i.e., $\theta/\theta_w = 1 - \eta^{1/3}$, only causes a change in magnitude but not in trend.

A correlation of some 77 data points representing a range of bulk fluid temperatures and temperature differences at both 3240 and 3300 psia was attempted by a least squares procedure on a digital computer. The best fit was obtained by

$$Nu = 0.0872\, Gr'^{1/3}\, Pr^{0.247} \left(\frac{t_\infty}{t_w - t_\infty}\right)^{0.137}$$

where all properties not specified were evaluated in the bulk fluid. The exponent of one-third for the Grashof number was assumed to eliminate any dependence on a length parameter. The other three numbers were obtained by the algebraic procedure. The average error of this correlation was 15 percent with some individual error of up to 40 percent.

Several different methods of evaluating the specific heat as well as the remaining properties were attempted but a better correlation was not found. No consistent deviation between the data and correlation was noted except the correlation prediction was low for data with a bulk temperature slightly less than the transposed critical temperature.

An indication of the local ribbon-bulk fluid temperature difference as a function of height is shown in Figure 31. Because of the difficulty of maintaining a constant current through the ribbon, local measurements were made only on a few early runs. The current drift experienced limited the accuracy of temperature determination for the data taken. The practice of taking local measurements also lengthened the time required to take data which allowed a larger change in bulk temperature to occur.

Since these results indicated that the local temperature difference, and thus the heat transfer coefficient, was independent of the length parameter, the practice of taking local data was discontinued to obtain more accurate and consistent results as shown in the previous figures.

The data taken at a bulk temperature of 709.08 F and 709.17 F are in the near vicinity of the transposed critical temperature of 709.7 F at 3300 psia. The scattering of data for the small temperature difference case is representative of the possible percentage error at small differences in temperature.

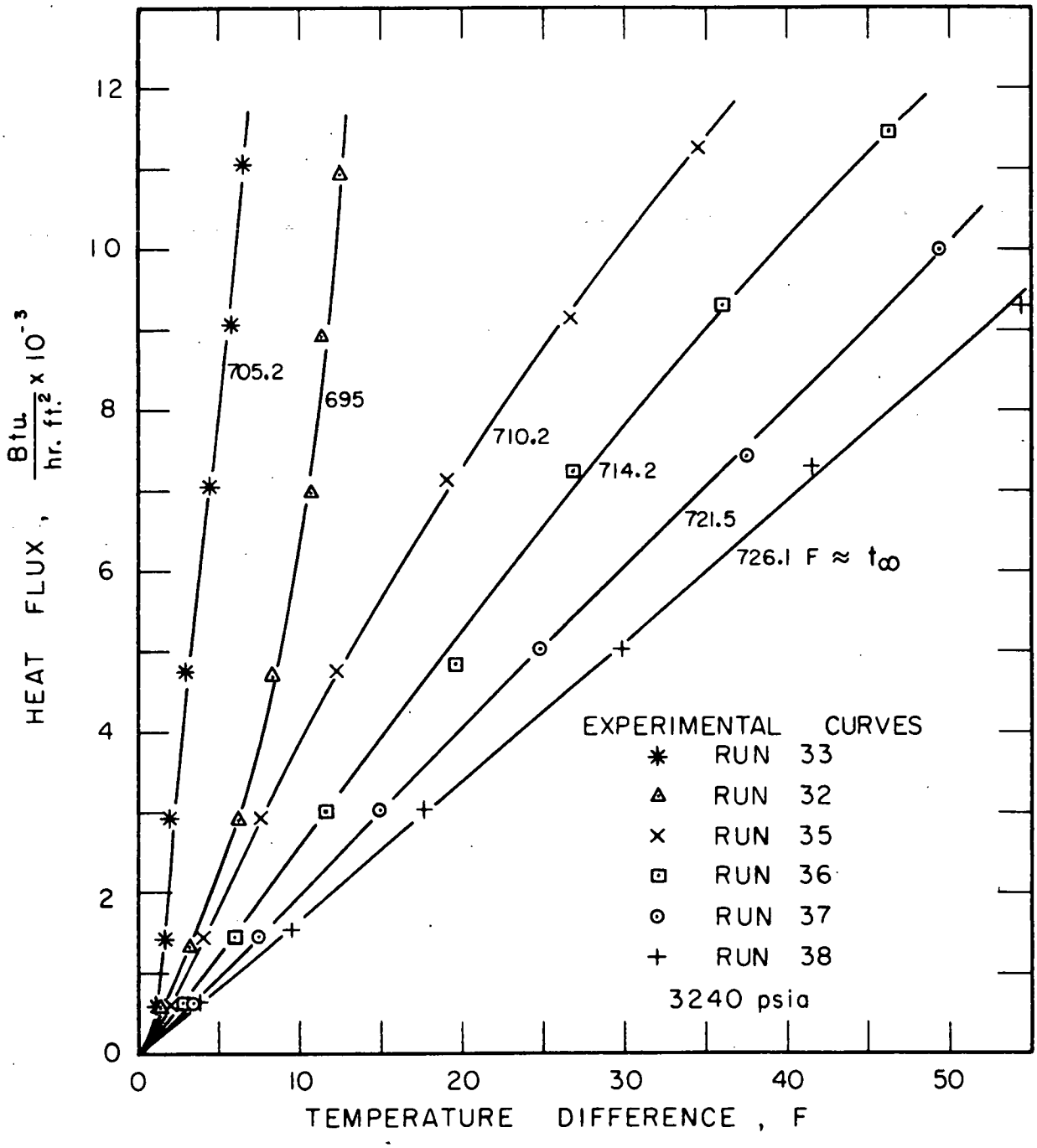

FIG. 28 EXPERIMENTAL HEAT FLUX CURVES FOR 3240 psia

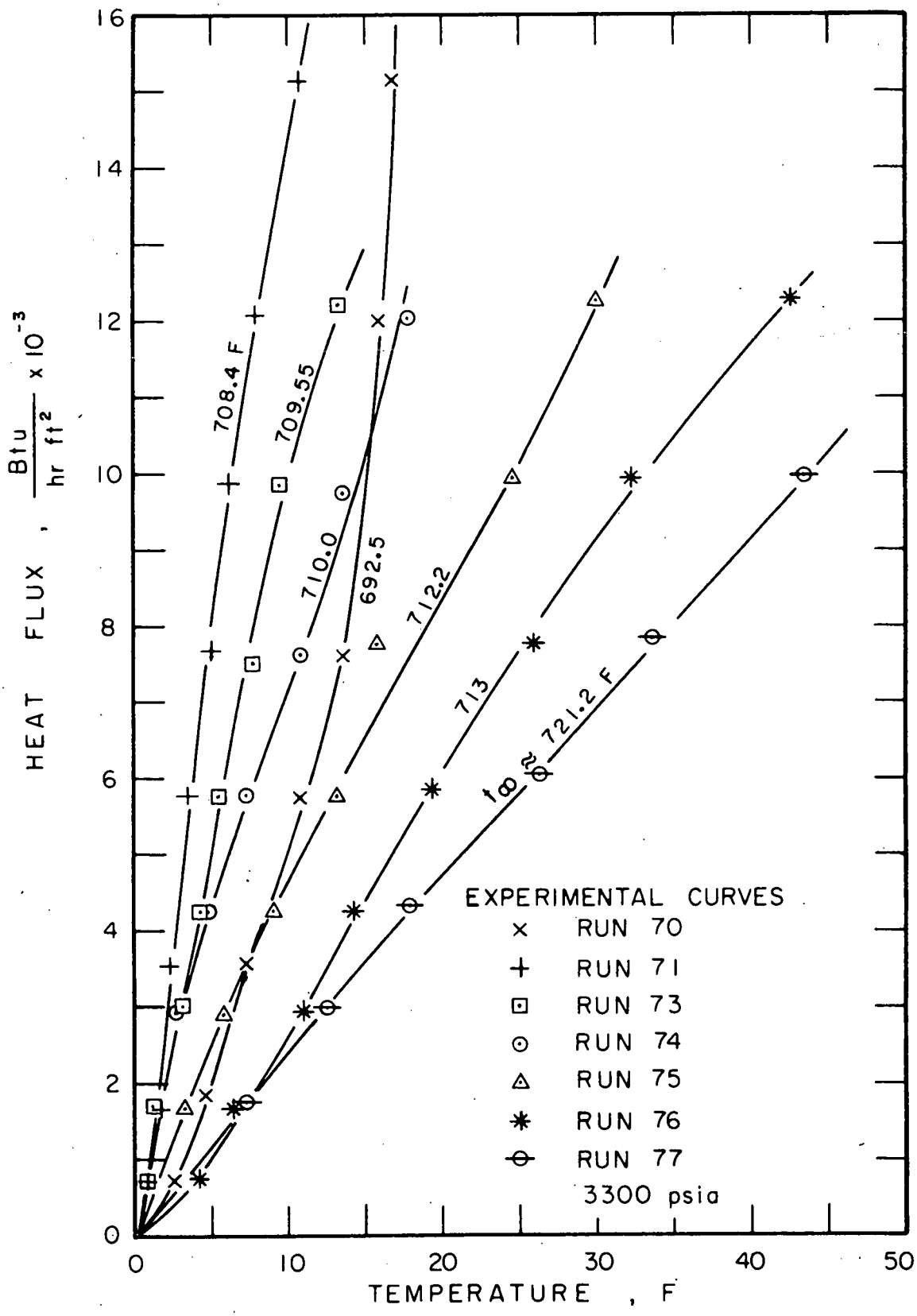

FIG. 29 EXPERIMENTAL HEAT FLUX CURVES FOR 3300 psia

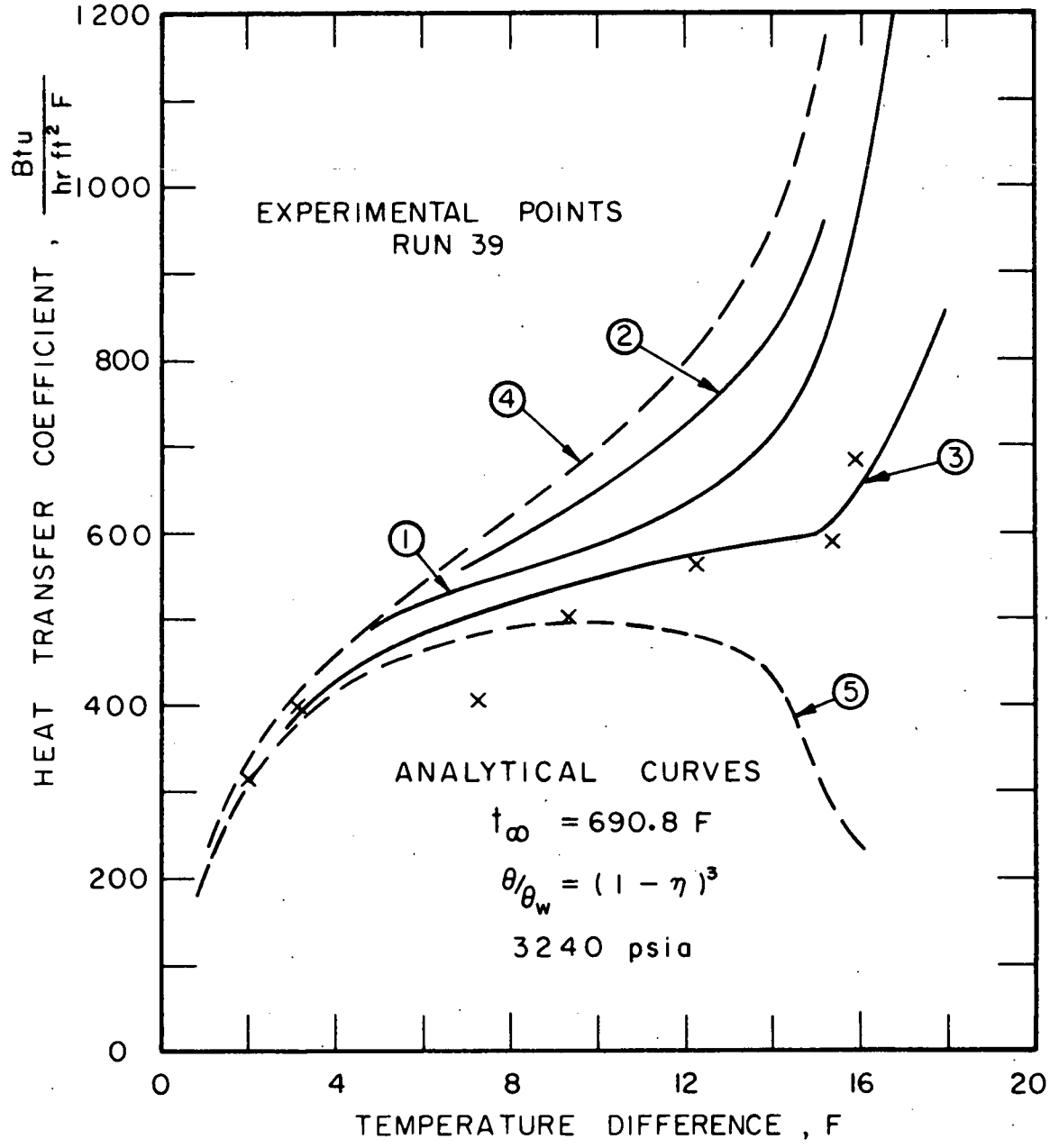

FIG. 30-A EXPERIMENTAL RESULTS COMPARED TO ANALYTICAL PREDICTION

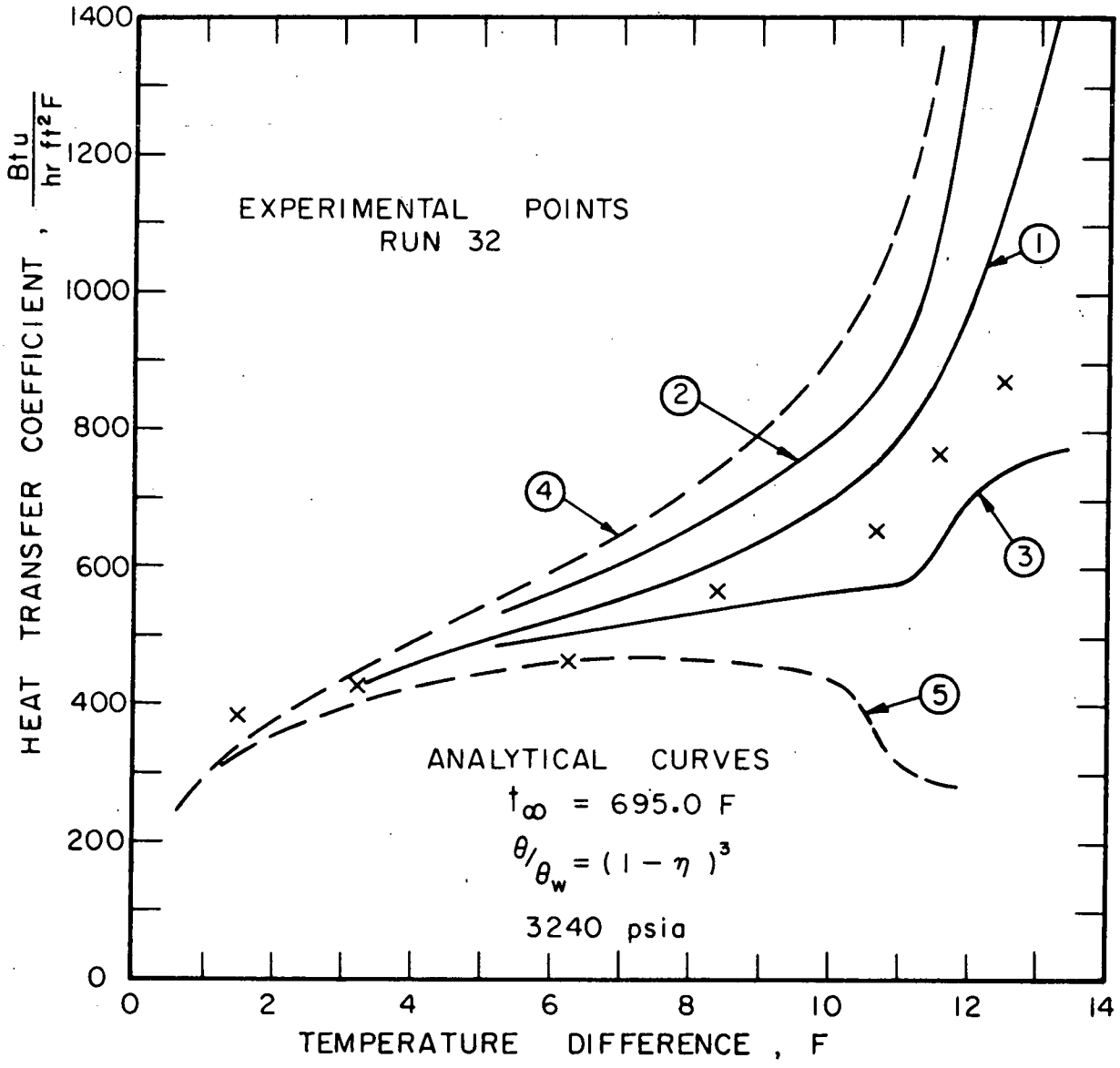

FIG. 30-B EXPERIMENTAL RESULTS COMPARED TO ANALYTICAL PREDICTION

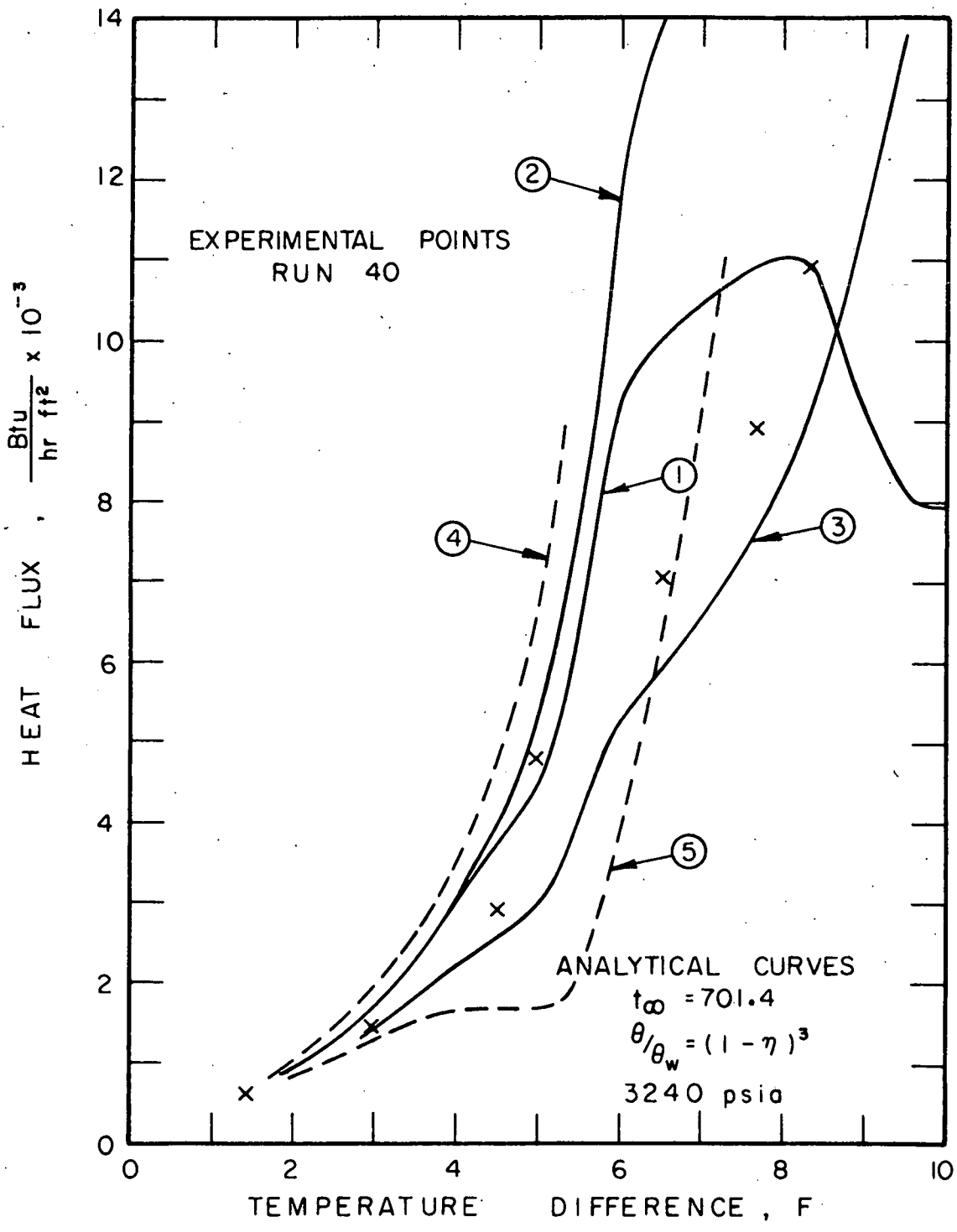

FIG. 30-C EXPERIMENTAL RESULTS COMPARED TO ANALYTICAL PREDICTION

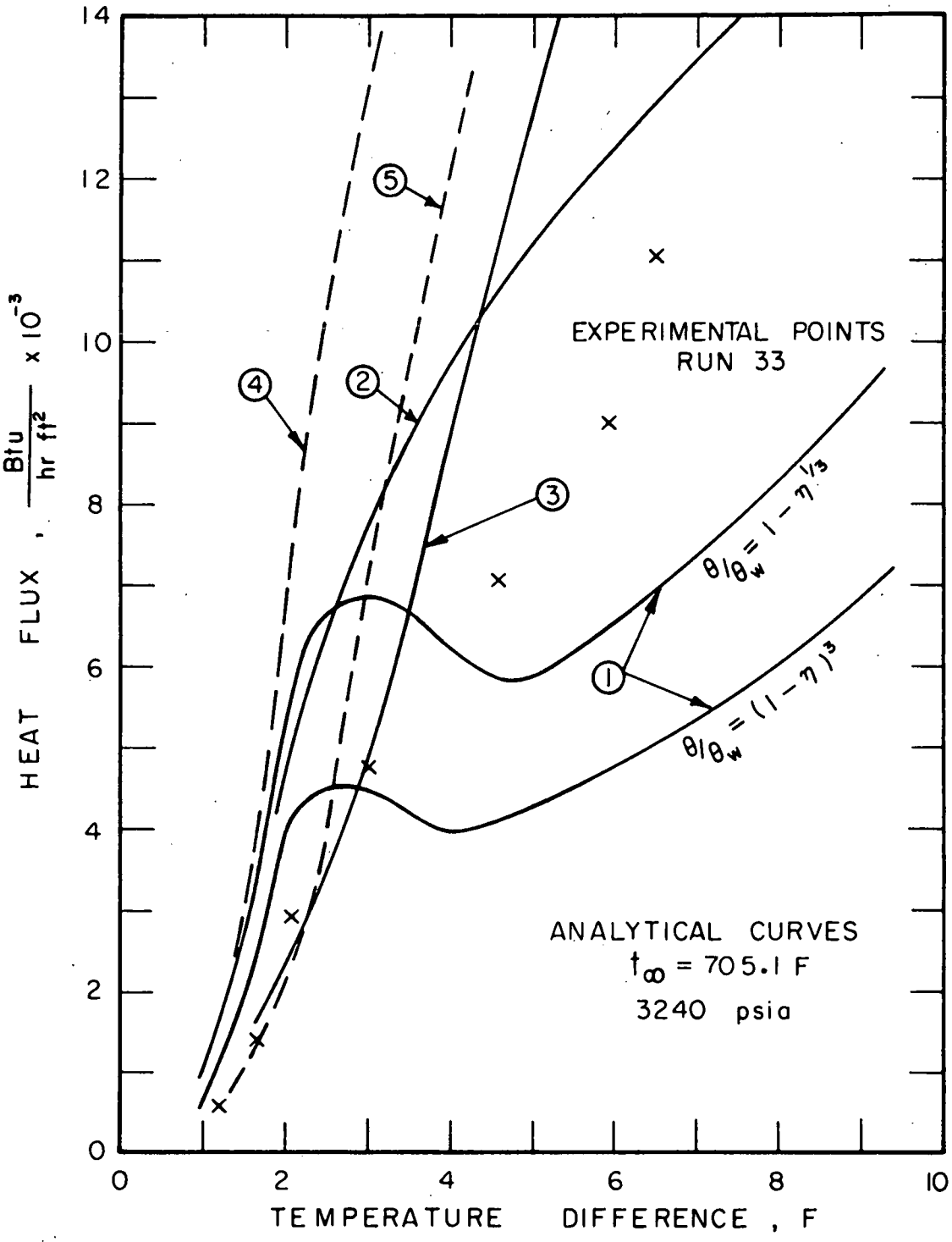

FIG. 30 - D EXPERIMENTAL RESULTS COMPARED TO ANALYTICAL PREDICTION

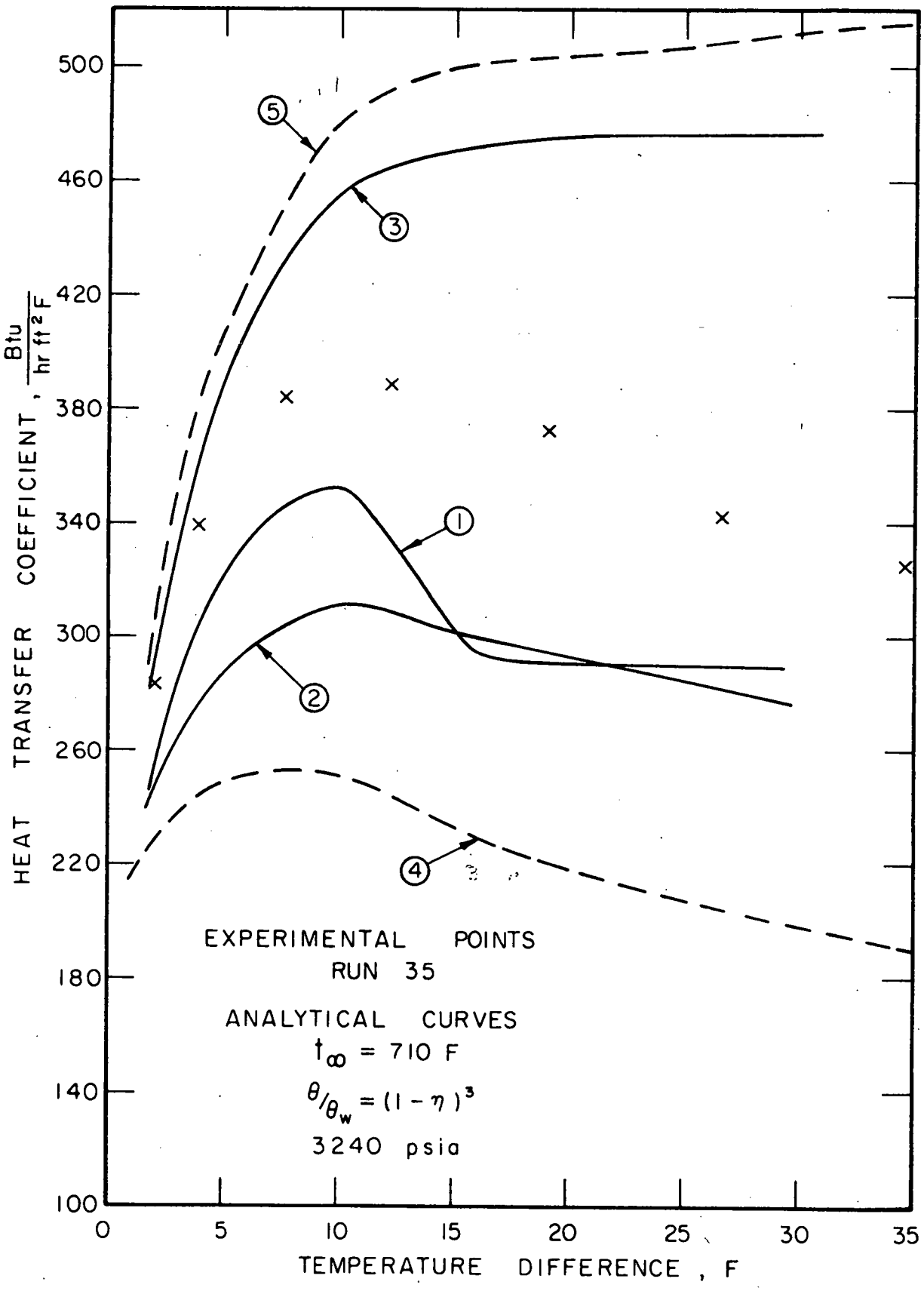

FIG. 30-E EXPERIMENTAL RESULTS COMPARED TO ANALYTICAL PREDICTION

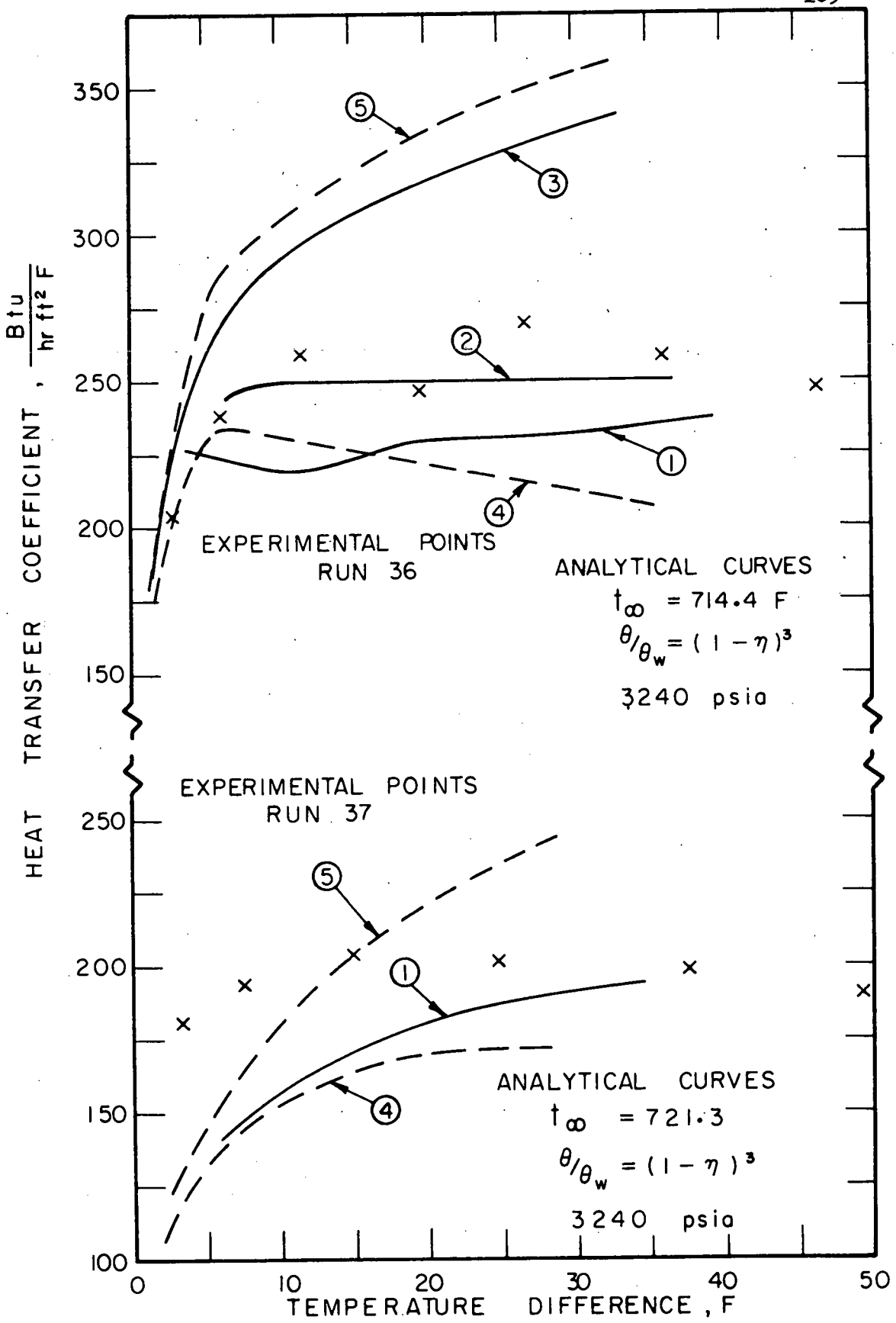

FIG. 30-F EXPERIMENTAL RESULTS COMPARED TO ANALYTICAL PREDICTION

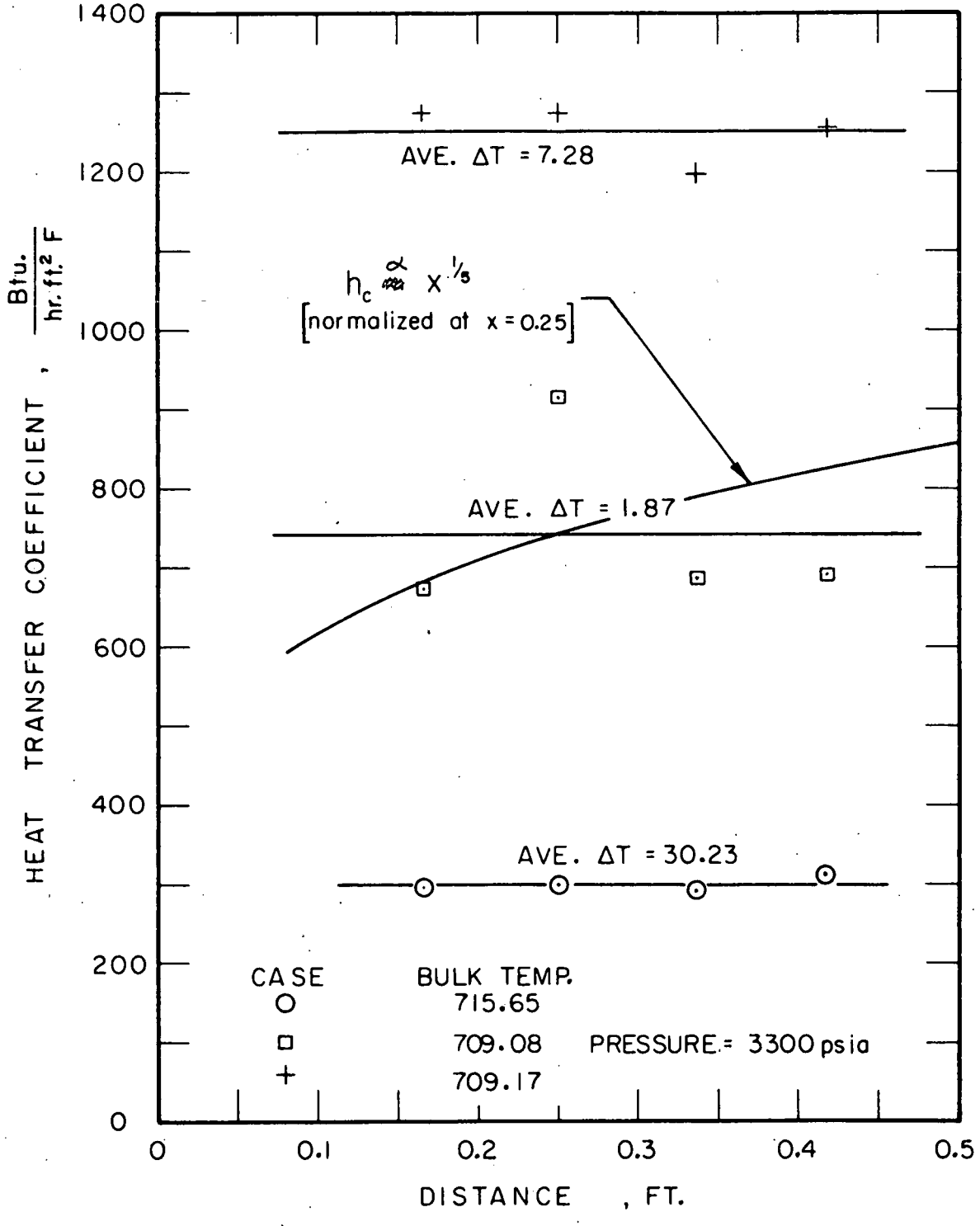

FIG. 31 LOCAL HEAT TRANSFER COEFFICIENT AS A FUNCTION OF DISTANCE ALONG THE PLATE

CONCLUSIONS AND RECOMMENDATIONS

The technique of integrating the boundary layer equations across a prescribed velocity and temperature profile including the effects of property variation yielded a simple mathematical model. The predictions of this model gave reasonably good agreement with experimental data for turbulent free convection in near critical water from a vertical surface with relatively small temperature differences. A basic assumption was that the heat transfer coefficient was independent of length along the heated element. This assumption was experimentally upheld within the limits of experimental error even in the vicinity of the maximum thermal coefficient of expansion.

The general agreement between the experimental data and the relatively simple model gives further strength to the postulate that heat transfer in the near critical region may be adequately described by conventional methods by taking into consideration the property changes which occur. No unusual trend or phenomenon was observed which would indicate another mechanism by which heat is transferred in the near vicinity of the thermodynamic critical point.

Better agreement between the analytical prediction and the experimental results would occur if the Prandtl number correction factor were properly calculated for each specific condition. The comparison between the model and data indicate that for heat transfer very near the transposed critical points the Prandtl number should be adjusted to

a value higher than the average and near the maximum. An educated guess based on study of Figures 30A-F whould allow computation correct within 15 percent. An exact functional relationship for evaluation of the Prandtl number might be obtained by trial and error but it is likely to be complex.

The experimental data was fairly well correlated by a modification of a conventional correlation. Scatter did occur partly because of experimental error and partly because the correlation failed to account completely for the large variation in property values. The standard film correlation would correlate the experimental data very well for bulk fluid and wall temperatures several degrees below the transposed critical temperature. This is shown indirectly by the comparison of the film correlation to the analytical model in Figure 20 and the comparison to data in Figure 30A.

It is recommended that more experimental data be obtained in both laminar and turbulent flow. To proceed with the resistance thermometry technique employed with this investigation, a power supply with precise self regulation would be necessary to obtain better accuracy. The present Mueller bridge should be calibrated or a better one obtained for more precise measurement of the bulk temperature. Local measurements would prove conclusively whether the heat transfer coefficient is a function of the length parameter in the turbulent regime.

Data taken on plates at various heights and small temperature differences could be used to obtain a measure of the transition point.

An exact solution for the laminar case in terms of specific heat has been obtained (5). This solution failed in the vicinity of the

specific heat peak due to a lack of knowledge of this property. A new solution of this problem in terms of enthalpy might allow investigation over the complete range of property variation.

LIST OF REFERENCES

LIST OF REFERENCES

1. Bayley, F. J., "An Analysis of Turbulent Free Convection Heat Transfer," Proceedings of the Institution of Mechanical Engineers, Vol. 169, No. 20, 1955.

2. Bonilla, C. F., and Sigel, L. A., "High Intensity Natural Convection Heat Transfer Near the Critical Point," Chemical Engineering Progress Symposium Series, Vol. 57, No. 32, 1961.

3. Doughty, D. L., and Drake, R. M., Jr., "Free Convection Heat Transfer from a Horizontal Right Circular Cylinder to Freon 12 Near the Critical State," ASME Transactions, Vol. 78, p. 1843, Nov. 1956.

4. Eckert, E. R. G., and Jackson, T. W., "Analysis of Turbulent Free-Convection Boundary Layer on Flat Plate," NACA Technical Report, 1015, 1951.

5. Fritsch, C. A., "Free Convective Heat Transfer to a Super-Critical Fluid; An Analytical and Experimental Study," Ph.D. Thesis, Purdue University, January 1962.

6. Fujii, T., "Experimental Studies of Free Convection Heat Transfer," Bulletin of Japan Society of Mechanical Engineers, Vol. 2, No. 8, p. 551, November 1959.

7. Fujii, T., "Analysis of Turbulent Free Convection," Bulletin of Japan Society of Mechanical Engineers, Vol. 2, No. 8, p. 559, November 1959.

8. Griffith, J. D., and Sabersky, R. H., "Convection in a Fluid at Supercritical Pressures," American Rocket Society Journal, Vol. 30, pp. 289-291, March 1960.

9. Griffiths, E., and Davis, A. H., The Transmission of Heat by Radiation and Convection, Special Report No. 9, Food Investigation Board, British Department of Scientific and Industrial Research, 1922.

10. Holman, J. P., and Boggs, J. H., "Heat Transfer to Freon 12 Near the Critical State in a Natural Circulation Loop," ASME Transactions, Series C, Journal of Heat Transfer, Vol. 82, p. 221, 1960.

11. Holt, V. E., "An Experimental Investigation of High-Flux Free Convection Heat Transfer up to Near-Critical Condition," Ph.D. Thesis, Purdue University, June 1961.

12. Jakob, M., Heat Transfer, Volume I, John Wiley & Sons, Inc., 1949.

13. Kreith, F., Principles of Heat Transfer, International Text Book Co., 1958.

14. McAdams, W. H., Heat Transmission, 3rd Edition, McGraw-Hill Book Co., 1954.

15. Nowak, E. S., "An Equation of State and Certain Thermodynamic Properties for Water and Water Vapor in the Critical Region," Ph.D. Thesis, Purdue University, June 1962.

16. Nowak, E. S., Grosh, R. J., and Liley, P. E., "Smoothed Pressure - Volume - Temperature Data for Water in the Critical Region Derived from Experimental Measurements," ASME Transactions, Series C, Journal of Heat Transfer, Vol. 83, pp. 14-27, 1961.

17. Ostrach, S., "An Analysis of Laminar Free-Convection Flow and Heat Transfer about a Flat Plate Parallel to the Direction of the Generating Body Force," NACA Technical Report 1111, 1953.

18. Rohsenow, W. M., and Choi, H. Y., Heat, Mass and Momentum Transfer, Prentice-Hall, Inc., p. 169, 1961.

19. Schlichting, H., Boundary Layer Theory, 4th Edition, McGraw-Hill Book Co., p. 507, 1960.

20. Schmidt, E., Eckert, E., and Grigull, U., Heat Transfer by Liquids Near the Critical State, AAF Translation No. 527, Air Material Command, Wright Field, Dayton, Ohio, 1946.

21. Shifrin, A. S., "The Viscosity of Water Under Atmospheric Pressure," Teploenergetika, No. 9, p. 22-27, September 1959. Translated at Purdue University.

22. Saunders, O. A., "The Effect of Pressure upon Natural Convection in Air," Proceedings of the Royal Society of London, Series A, Vol. 157, pp. 278-291, 1936.

23. Saunders, O. A., "Natural Convection in Liquids," Proceedings of the Royal Society of London, Series A, Vol. 172, pp. 55-71, 1939.

24. Saunders, O. A., and Fishenden, M., An Introduction to Heat Transfer, Oxford University Press, London, p. 97, 1950.

25. Siegel, R., Analysis of Laminar and Turbulent Free Convection from a Smooth Vertical Plate with Uniform Heat Dissipation per Unit Surface Area, General Electric Report No. R 54 GL 89, April 7, 1954.

APPENDICES

26. Simon, H. A., "An Interferometric Investigation of Laminar Free Convection in Carbon Dioxide near Its Critical Point," Ph.D. Thesis, University of Minnesota, January 1962.

27. Swenson, H. S., Research Center, Babcock & Wilcox, Co., Personal communication.

28. Timroth, D. L., Tables of Thermodynamic Properties of Water and Water Vapor, First Edition, Moscow 1952 Leningrad. Translated by Westinghouse Electric Corporation, Land Turbine Engineering Division, South Philadelphia Works, November 1959.

29. Touba, R. F., "Heat Transfer to Critical Water Flowing Through a Heated Vertical Tube Under the Effects of Combined Forced and Free Convection," M. S. Thesis, Purdue University, June 1962.

30. Touloukian, Y. S., Hawkins, G. A., and Jakob, M., "Heat Transfer by Free Convection from Heated Vertical Surfaces to Liquids," ASME Transactions, Vol. 70, p. 13, 1948.

31. Tuan, Y., "Heat Transfer in Natural Convection Flow of Water," M. S. Thesis, University of Washington, 1959.

32. Van Dyke, M. S., "Boundary Layer Temperature in Natural Convection Flow of Water," M. S. Thesis, University of Washington, 1960.

33. Van Putte, D. A., "Heat Transfer to Water in the Near Critical Region," M. S. Thesis, Purdue University, January 1961.

34. Vargaftik, N. B., and Tarzhizanov, A. A., "An Experimental Investigation into Heat Conduction of Water Steam of High Parameters," Telploenergetiku, No. 9, pp. 15-22, September 1959. Translated into English, Purdue University.

35. Voukalovitch, M. P., Enthalpy, Entropy, and Specific Volume of Water and Superheated Steam as a Function of Pressure and Temperature, Translation by Theoretical Physics and Mathematics Section, Babcock & Wilcox Company, Atomic Energy Division, March 1963.

36. Waibler, P. J., "Natural Convection Heat Transfer with Water at High Grashof Numbers," Ph.D. Thesis, University of Illinois, 1958.

APPENDIX A

NOMENCLATURE

a = constant in Blasius expression

a_1 = constant for platinum resistance thermometer

A = constant for ribbon calibration

b = dimension of control volume perpendicular to vertical wall, ft.

B = constant for ribbon calibration

C_1, C_2, C' = constants

C, C'' = heat transfer parameters

$C_{(n)}$ = constant corresponding to n

C_p = specific heat at constant pressure, $\frac{\text{Btu.}}{\text{lb. F}}$

g = acceleration of gravity, $(3600)^2 \times 32.17 \frac{\text{ft.}}{\text{hr}^2}$

h = enthalpy, $\frac{\text{Btu.}}{\text{lb.}}$

h_c = local heat transfer coefficient, $\frac{\text{Btu.}}{\text{hr.ft}^2\text{ F}}$

I = internal energy, $\frac{\text{Btu.}}{\text{lb.}}$

F = degrees Fahrenheit

$F(\eta)$ = velocity profile function

$G(\eta)$ = temperature profile function

H = enthalpy difference with the bulk fluid as the reference, $h - h_\infty$, $\frac{\text{Btu.}}{\text{lb.}}$

J = Joules constant, Btu. = 778.16 ft.lb.

k = thermal conductivity, $\frac{\text{Btu.}}{\text{hr.ft. F}}$

k_o = thermal conductivity at atmospheric pressure

k' = constant

l = constant

L = plate length, ft.

m, n = exponents

p = pressure, $\frac{lb.}{ft.^2}$

q'' = heat flux per unit area, $\frac{Btu.}{hr.ft.^2}$

q = heat transferred, $\frac{Btu.}{hr.}$

r = radius, ft.

R_o = ice point resistance of platinum thermometer, ohms

R_t = resistance of platinum thermometer at temperature, t, ohms

R_x = resistance of test ribbon, ohms

R_{x_o} = resistance of test ribbon at ice point, ohms

t = temperature, F.

T = absolute temperature

u = velocity component of boundary layer in the x direction, $\frac{ft.}{hr.}$

u_m = maximum value of velocity component in boundary layer in the x direction, $\frac{ft.}{hr.}$

u_1 = reference steam velocity obtained as if velocity profile maintained shape as in forced convection

v = velocity in y direction, $\frac{ft.}{hr.}$

v' = specific volume, $\frac{ft.^3}{lb.}$

V = voltage measurement

v^* = $(\frac{g\tau_w}{\rho})^{\frac{1}{2}}$ = friction velocity, $\frac{ft.}{hr.}$

V_1 = integral function, defined by equation p. 45

w = velocity in z direction $\frac{ft.}{hr.}$

W = integral function, defined by equation p. 45

X = body force in x direction, $\frac{lb.}{ft.^3}$

X_1 = integral function, defined by equation p. 45

x = coordinate in direction parallel to the wall, ft.

y = coordinate in direction perpendicular to the wall, ft.

Y = integral function, defined by equation p. 45

Z = integral function defined by equation p. 45

Subscripts

C = property evaluated at critical point

u_m = quantity evaluated at maximum velocity

w = property evaluated at the wall

x = dimensionless number based on a local value of x

∞ = property evaluated in bulk fluid

2-5 = quantity measured between voltage tap 2 and 5 of ribbon

1-6 = quantity measured between voltage taps 1 and 6 of ribbon

Greek Letters

$\beta = \frac{1}{v'}\frac{\partial v'}{\partial t}$ = volumetric coefficient of expansion, $\frac{1}{F.}$

δ = boundary layer thickness, ft.

Δ = a difference

ϵ_M = eddy diffusivity for momentum, $\frac{ft.^2}{hr.}$

ϵ_H = eddy diffusivity for heat transfer, $\frac{ft.^2}{hr.}$

μ = dynamic viscosity, $\frac{lb.}{hr.ft.}$

μ_o = dynamic viscosity at atmospheric pressure

$\mu\Phi$ = viscous dissipation term

ν = kinematic viscosity, $\frac{ft.^2}{hr.}$

$\rho = \frac{1}{v'}$ = mass density, $\frac{lb.}{ft.^3}$

τ = shear stress, $\frac{lb.}{ft.^2}$

$\eta = \frac{y}{\delta}$, dimensionless distance parameter

η_{u_m} = dimensionless distance parameter evaluated at maximum velocity

λ = dimensionless friction coefficient

θ = temperature difference based on bulk temperature, $t - t_\infty$, F.

θ_1 = time, hr.

lb. force = lb. mass at $g = 32.17 \frac{ft.}{sec^2}$

Dimensionless Numbers

$Gr = \frac{g\beta\rho^2 x^3 \Delta t}{\mu^2}$, Grashof number

$Gr' = \frac{g(\rho_\infty - \rho)\rho_\infty x^3}{\mu^2}$, Grashof number based on density difference

$N_u = \frac{h_c x}{k}$, Nusselt number

$Pr = \frac{\mu c_p}{k}$, Prandtl number

$Ra = GrPr$, Rayleigh number

$Ra' = Gr'Pr$, Rayleigh number based on density difference

APPENDIX B

CONSTANT PROPERTY SOLUTION

Reynolds Analogy Applied across the Boundary Layer

The problem of turbulent free convection in a near constant property fluid was solved by using an integral form of the momentum and energy equations as done by Eckert (4) and Siegel (24). The following development is similar to previous work except for the following assumptions.

Velocity Profile

The velocity profile across the boundary layer is

$$u = u_1 \eta^{1/3} (1-\eta)^2.$$

Temperature Profile

The temperature profile across the boundary layer is taken as

$$t - t_\infty = (t_w - t_\infty)(1-\eta)^3.$$

Wall Shear Stress

From the general relationship for the wall shear stress (6) with n equal three and C(n) equal 5.1, the shear stress is

$$\tau_w = 0.087 \frac{\rho u_1^2}{g} \left(\frac{\nu}{u_1 y}\right)^{1/2},$$

with the stream velocity, u_1, as a reference.

Reynolds Analogy

The form of Reynolds analogy used is

$$q''_w = g\,\tau_w C_p \frac{(t_w - t_\infty)}{u_1}\, Pr^{-2/3}.$$

The momentum and energy equations presented earlier are

$$\rho \frac{\partial}{\partial x}\left(\delta \int_0^1 u^2 d\eta\right) = g\rho\beta\delta \int_0^1 \theta\, d\eta - g\,\tau_w ,$$

and

$$q''_w = \rho C_p \frac{\partial}{\partial x}\left(\delta \int_0^1 u\,\theta\, d\eta\right).$$

Substituting the shear stress expression, and Reynolds analogy into the equations yields

$$0.054\rho \frac{d}{dx}(\delta u_1^2) = \frac{2.87 g\beta\delta^{3/2} q''_w}{C_p u_1^{1/2} \nu^{1/2} Pr^{-2/3}} - \frac{0.087\rho u_1^{3/2}\nu^{1/2}}{\delta^{1/2}} ,$$

and

$$1.1\, Pr^{-2/3}\nu^{1/2} = \frac{d}{dx}\left(\delta^{3/2} u_1^{1/2}\right).$$

These two equations are solved simultaneously by assuming only u_1 and δ are functions of the x direction. This functional relationship is assumed to be

$$u_1 = C_1 x^m , \text{ and } \quad \delta = C_2 x^n .$$

Substituting these relations in the above equations and taking the derivative as indicated yields

$$0.054\rho C_1^2 C_2 (2m+n) X^{2m+n-1} = \frac{2.87 g\beta q''_w C_1^{-\frac{1}{2}} C_2^{\frac{3}{2}} X^{\frac{3n}{2}-\frac{1}{2}m}}{C_p \nu^{1/2} P_r^{-2/3}} - 0.087\rho\nu^{1/2} C_1^{\frac{3}{2}} C_2^{-\frac{1}{2}} X^{\frac{3}{2}m-\frac{n}{2}},$$

and

$$1.1 P_r^{-2/3} \nu^{1/2} = C_1^{1/2} C_2^{3/2} \left(\frac{3}{2}m + \frac{1}{2}n\right) X^{\frac{3}{2}m+\frac{1}{2}n-1}.$$

Equating coefficients of x for each term of the equations yields relationships which could be satisfied only if m and n equal one-half. Substituting these values back into the equations and solving for C_1 and C_2 results in the values, viz.,

$$C_1 = \left(\frac{1.1\nu^{1/2}}{P_r^{2/3}}\right)^2 C_2^{-3},$$

and

$$C_2 = \left\{ \left[0.081\rho\left(\frac{1.1\nu^{1/2}}{P_r^{2/3}}\right) + 0.087\rho\nu^{1/2} \right] \left(\frac{1.1\nu^{1/2}}{P_r^{2/3}}\right)^4 \left(\frac{\nu^{1/2} C_p P_r^{-2/3}}{2.87 g \beta q''_w}\right) \right\}^{1/8}.$$

The definition of the heat transfer coefficient is used to evaluate it explicitly as

$$h_c = \frac{q''_w}{\theta_w} = 0.087\rho C_p \left(\frac{u_1 \nu}{\delta}\right)^{1/2} P_r^{-2/3}.$$

Substituting initially for u_1 and δ, then for C_1 and C_2, multiplying by $\frac{x}{k}$ and rearranging yields

$$Nu = 0.121 \left[\frac{Gr}{1 + 0.976\, Pr^{-2/3}} \right]^{1/3} Pr^{5/9}.$$

This expression indicates that heat transfer is not a function of x. For a value of C(n) equal 3.5 in the wall shear stress expression, the non-dimensional relationship corresponded better to accepted correlations and is

$$Nu = 0.178 \left[\frac{Gr}{1 + 0.978\, Pr^{-2/3}} \right]^{1/3} Pr^{5/9}.$$

For this value of C(n), the constant a equals 0.153.

Reynolds Analogy from the Wall to the Velocity Peak

For the case where Reynolds analogy was used from the wall to the point of maximum velocity, the following changes are made.

Velocity Profile

The velocity profile is defined as

$$u = l\, u_m\, \eta^{1/3} (1-\eta)^2$$

where the constant, l, corrects for the proper magnitude of the velocity and is numerically equal to the inverse of $\eta^{1/3}(1-\eta)^2$ evaluated at η_{u_m}. The peak velocity occurs at $\eta = 0.143$ and thus l equals 2.6.

Temperature Profile

From the profile, $\theta = \theta_w (1-\eta)^3$, the value of the temperature at the point η_{u_m} is found to be $t_{\eta_{u_m}} - t_\infty = \theta_{\eta_{u_m}} = 0.629\,\theta_w$.

Wall Shear Stress

Since the reference velocity is u_m, the corresponding distance is

$$y_{u_m} = \eta_{u_m} \delta = 0.143 \delta.$$

The shear stress equation is then

$$\tau_w = 0.23 \frac{\rho}{g} u_m^2 \left(\frac{\nu}{u_m \delta}\right)^{1/2}.$$

Reynolds Analogy

Reynolds analogy is changed to be

$$q_w'' = g \tau_w C_p \frac{(t_w - t_{\eta_{u_m}})}{u_m} P_r^{-2/3}.$$

This temperature difference is related to the wall, bulk fluid temperature difference yielding

$$q_w'' = 0.371 g \tau_w \frac{C_p \theta_w}{u_m} P_r^{-2/3}.$$

The final result is

$$Nu = 0.086 \left[\frac{Gr}{1 + 0.987 P_r^{-2/3}}\right]^{1/3} P_r^{5/9},$$

which is somewhat lower value than the previous calculation. To obtain better agreement a value of C(n) equalling 2.5 would be necessary.

APPENDIX C

ENERGY EQUATION

Derivation

A common form of the general energy equation in terms of the property of internal energy can be derived as

$$\rho \frac{DI}{D\theta_1} = \nabla \cdot k \nabla t + q''' + \mu \Phi - P \nabla \cdot \overline{U} \ ,$$

where I is the internal energy, $\mu \Phi$ is the viscous dissipation, and $\overline{U}$ is the velocity vector. This equation is developed by Rohsenow (18) with slightly different nomenclature. Using the definition of enthalpy, $h = I + PV'$, the left side becomes

$$\rho \left[\frac{Dh}{Dt} - P \frac{DV'}{Dt} - V' \frac{DP}{Dt} \right].$$

For fluids with variable density, the equation of continuity may be used to show

$$\rho \frac{DV'}{D\theta_1} = -\frac{1}{\rho} \frac{D\rho}{D\theta_1} = -\frac{1}{\rho} \left(\frac{\partial \rho}{\partial \theta_1} + u \frac{\partial \rho}{\partial x} + v \frac{\partial \rho}{\partial y} + w \frac{\partial \rho}{\partial z} \right) =$$

$$\left(\frac{\partial u}{\partial x} + \frac{\partial v}{\partial y} + \frac{\partial w}{\partial z} \right) = \nabla \cdot \overline{U}.$$

Thus the energy equation in terms of enthalpy is

$$\rho \frac{Dh}{D\theta_1} = \nabla \cdot k \nabla t + q''' + \mu \Phi + \frac{DP}{D\theta_1} .$$

Neglecting viscous dissipation, energy generation, and pressure gradients in the y direction, a two dimensional boundary layer equation may be written as

$$\rho\left(u \frac{\partial h}{\partial x} + v \frac{\partial h}{\partial y}\right) = \frac{\partial}{\partial y}\left(k \frac{\partial t}{\partial y}\right) + \frac{u}{J} \frac{dP}{dx} .$$

An approximate order of magnitude analysis may be made to compare the pressure gradient term to the left hand side of the equation. If, $x \simeq L$, and $y \simeq \delta$, from the continuity equation

$$v \simeq \frac{u\delta}{L} . \qquad \text{Also, } \frac{dP}{dx} \text{ is proportional to } \rho.$$

Substituting these proportionalities in the equation yields

$$\rho\left(u \frac{\Delta h}{L} + \frac{u\delta}{L} \frac{\Delta h}{\delta}\right) \simeq \frac{u\rho}{J} + \text{heat flux},$$

and after simplifying

$$\Delta h \simeq \frac{L}{J} + \text{heat flux}\left(\frac{L}{u\rho}\right).$$

As Δh is in the order of several Btu and L is in the order of feet, it is obvious that

$$\Delta h \gg \frac{L}{J} .$$

This approximate analysis indicates that the work done against gravity is small compared to the energy transferred by convection and conduction and may be neglected from the energy equation. If either this term or the viscous dissipation term, $\mu\left(\frac{\partial u}{\partial y}\right)^2$, were significant the method of analysis used would not work.

Pressure Gradient

The effect of the vertical hydrostatic pressure gradient on enthalpy is shown by the following order of magnitude argument. At a pressure of 3240 psia and 707 Fahrenheit, the enthalpy change of water per pound pressure is around three Btu. The vertical distance across the test ribbon is about one-half foot. As the density of water at these conditions is about 20 $\frac{\text{lb.}}{\text{ft}^3}$, the pressure difference across the test ribbon is

$$\text{height X density} = 0.07 \text{ psi.}$$

Thus the enthalpy variation along the length of the ribbon is about 0.2 Btu. In comparison, a one degree Fahrenheit change at this state point would cause an enthalpy difference of about 60 Btu. Thus the enthalpy pressure dependence caused by a vertical pressure gradient is of secondary importance compared to temperature dependence in the horizontal plane, across the boundary layer.

APPENDIX D

VARIABLE PROPERTY PROGRAM

Nomenclature

ABLE = constant a, pp.

CLIST = tabulated values of specific heat

COND (A or B) = thermal conductivity, k

CONSTL = ℓ, p. 120

CP (A or B) = specific heat, Cp

DENS (A or B) = density, ρ

DLIST = tabulated values of specific volume

ELIST = tabulated values of enthalpy

ENTH (A or B) = enthalpy, h

ENTINF = enthalpy, of bulk fluid

ENTUM = enthalpy, at maximum velocity

ENTWAL = enthalpy, at the wall

EVEN = even numbered calculations in Simpson's rule

FRACT (A or B) = fraction of dimensionless boundary layer

FLUX (A,B,AV,WA) = heat flux corresponding to HCP (A,BU,AV,WAL)

HCP (A,AV,BU,WAL) = heat transfer coefficient for PRCP, PRCPAV, PRCPBU, PRWALL

MAX (A or B) = number of intervals in integration by Simpson's rule

ODD = odd numbered claculations in Simpson's rule

PIF3D = third order interpolation function for specific volume

PIF1C = first order interpolation function for enthalpy and specific heat.

PR(A or B) = Prandtl number

PRCP = integrated average Prandtl number from wall to maximum velocity

PRCPAV = average integrated Prandtl number in boundary layer

PRCPBU = Prandtl number in the bulk fluid

PRWALL = Prandtl number at the wall

SPVOL (A or B) = specific volume, v'

VCPA = $PRCP^{-2/3}$

VCPAVG = V_1, p. 45

VCPBUL = $PRCPBU^{-2/3}$

VWALL = $PRWALL^{-2/3}$

VELP (A or B) = $F(\eta)$ evaluated at

VISCO (A or B) = dynamic viscosity, μ

VNNUM = η at maximum velocity

TEMDIF = temperature difference, θ_w

TEMP (A or B) = temperature, t

TEMUM = temperature at maximum velocity

TLIST (C,E, or D) = tabulated temperature corresponding to enthalpy or specific volume

WAK = W p. 45

XRAY = X_1 p. 45

YOK = Y p. 45

ZUL = Z p. 45

Special Endings

A = property or function evaluated at a point between wall and maximum velocity

B = property or function evaluated at a point between maximum velocity and edge of boundary layer

```
C  MAIN  PROGRAM  (MOD 11)
 55    DIMENSION TEMPA(50), TEMPB(100),DENSA(50),DENSB(100),CONDA(50),
      1       CONDB(100),ENTHA(50),ENTHB(100),VISCOA(50),VISCOB(100),
      2       VELPA(50),VELPB(100),DLIST(100),ELIST(100),TLISTD(100),
      3       TLISTE(100),SPVOLA(50),SPVOLB(100),CLIST(100),TLISTC(100)
      4 ,          FRACTA(50)          ,          FRACTB(100) ,CPA(50),CPB(100)
      5 ,PRA(50),PRB(100)
   10 READ INPUT TAPE 5,51,TEMWAL,TEMINF,REPEAT,PRESS,NCASE
      IF (REPEAT-1.) 15,15,16
   15 READ INPUT TAPE 5,61,ND,(TLISTD(N),N=1,ND)
      READ INPUT TAPE 5,62,    (DLIST(N),N=1,ND)
      READ INPUT TAPE 5,61,NE,(TLISTE(N),N=1,NE)
      READ INPUT TAPE 5,62,    (ELIST(N),N=1,NE)
   17 READ INPUT TAPE 5,61, NC,(TLISTC(N), N=1,NC)
      READ INPUT TAPE 5,62, (CLIST(N), N=1,NC)
      READ INPUT TAPE 5,51, SKIPCP,PRINT, ABLE,VNNUM,MAXA,MAXB
   16 MAXXA=MAXA+1
      MAXXB=MAXB+1
      LESSA=MAXA-1
      LESSB=MAXB-1
      CMAXA=MAXA
      CMAXB=MAXB
      STEPA=(VNNUM/CMAXA)/3.
      STEPB=((1.-VNNUM)/CMAXB)/3.
      TEMDIF=TEMWAL-TEMINF
      DO 101 I=1,MAXXA
      X=I-1
      IF(X) 11,12,12
   11 X=0.
   12 FRACTA(I)=VNNUM*( X )/CMAXA
      TEMPA(I)=TEMDIF*(1.-FRACTA(I))**3.  +TEMINF
  101 VELPA(I)=(FRACTA(I)**(1./3.))*(1.-FRACTA(I))**2.
      DO 102 I=1,MAXXB
      X=I-1
      IF(X) 13,14,14
   13 X=0.
   14 FRACTB(I)= VNNUM+(1.-VNNUM)*( X ) /CMAXB
      TEMPB(I)=TEMDIF*(1.-FRACTB(I))**3.  +TEMINF
  102 VELPB(I)=(FRACTB(I)**(1./3.))*(1.-FRACTB(I))**2.
      ME=0
      MD=0
      DO 202 J=1,MAXXB
      I=MAXXB-J+1
      TEMP=TEMPB(I)
      SPVOLB(I) =PIF3D(TEMP,TLISTD,ND,DLIST,MD)
      DENSB(I)=1./SPVOLB(I)
  202 ENTHB(I)=       PIF1C(TEMP,TLISTE,NE,ELIST,ME)
      DO 201 J=1,MAXXA
      I=MAXXA-J+1
      TEMP=TEMPA(I)
      SPVOLA(I)= PIF3D(TEMP,TLISTD,ND,DLIST,MD)
      DENSA(I)=1./SPVOLA(I)
  201 ENTHA(I)=       PIF1C(TEMP,TLISTE,NE, ELIST,ME)
      DO 203 I=1,MAXXA
      VISCOA(I)=32.17*(0.04788*TEMPA(I)+14.79+.6066*DENSA(I)**1.48)*(
     1      10.**(-8))*3600.0
  203 CONDA(I)=0.0246+(.4*(TEMPA(I)-550.0)+28.83*DENSA(I)**1.25)*10.**
     1       (-4)
      DO 204 I=1,MAXXB
      VISCOB(I)=32.17*(0.04788*TEMPB(I)+14.79+.6066*DENSB(I)**1.48)*(
     1      10.**(-8))*3600.0
  204 CONDB(I)=0.0246+(.4*(TEMPB(I)-550.0)+28.83*DENSB(I)**1.25)*10.**
     1       (-4)
      ENTWAL=ENTHA(1)
      ENTUM=ENTHA(MAXXA)
      ENTINF=ENTHB(MAXXB)
      TEMUM=TEMPA(MAXXA)
C     CALCULATE  CP  FROM TABLE
  259 MC=0
      DO  260  J=1,MAXXB
      I=MAXXB-J+1
      TEMP=TEMPB(I)
  260 CPB(I)= PIF1C(TEMP,TLISTC,NC,CLIST,MC)
      DO 261 J=1,MAXXA
      I=MAXXA-J+1
      TEMP=TEMPA(I)
  261 CPA(I)= PIF1C(TEMP,TLISTC,NC,CLIST,MC)
C       CALCULATE V  BASED ON CP TABLE
      DO 264 I=1,MAXXA
  264 PRA(I)=VISCOA(I)*CPA(I)/CONDA(I)
      DO 266 I=1,MAXXB
  266 PRB(I)=VISCOB(I)*CPB(I)/CONDB(I)
      EVEN=0.
      ODD=0.
      DO 270  I=2,MAXA,2
```

```
      270 EVEN=EVEN+PRA(I)
          DO 271 I=3,LESSA,2
      271 ODD=ODD+PRA(I)
          PRCP=STEPA*(PRA(1)+4.*EVEN+2.*ODD+PRA(MAXXA))/VNNUM
          VCPA=PRCP**(-2./3.)
C           CALCULATE  V  AVERAGE BASED ON CP TABLE
          EVEN=0.
          ODD=0.
          DO 275 I=2,MAXB,2
      275 EVEN=EVEN+PRB(I)
          DO 276 I=3,LESSB,2
      276 ODD=ODD+PRB(I)
          PBPART=STEPB*(PRB(1)+4.*EVEN+2.*ODD+PRB(MAXXB))
          VBCP=PBPART**(-2./3.)
          PRCPAV=PRCP*VNNUM+PBPART
          VCPAVG=PRCPAV**(-2./3.)
C           CALCULATE BULK PRANDTL NO. BASED ON CP TABLED
          VCPBUL=(VISCOB(MAXXB)*CPB(MAXXB)/CONDB(MAXXB))**(-2./3.)
          PRCPBU=VCPBUL**(-3./2.)
C     CALCULATE  V  AT  THE WALL
          VWALL=(VISCOA(1)*CPA(1)/CONDA(1))**(-2./3.)
          PRWALL=VWALL**(-3./2.)
C                       YOKA
      310 EVEN=0.
          ODD=0.
          DO 311 I=2,MAXA,2
      311 EVEN=EVEN+(DENSA(I)*VISCOA(I))**.5
          DO 312 I=3,LESSA,2
      312 ODD=ODD+(DENSA(I)*VISCOA(I))**.5
          YOKA=STEPA*((DENSA(1)*VISCOA(1))**.5+4.0*EVEN+2.* ODD+
         1(DENSA(MAXXA)*VISCOA(MAXXA))**.5)/VNNUM
C     YOKB          (B  PART, NOT AVERAGE)
          ODD=0.
          EVEN=0.
          DO 315 I=2,MAXB,2
      315 EVEN=EVEN+(DENSB(I)*VISCOB(I))**.5
          DO 316 I=3,LESSB,2
      316 ODD=ODD+(DENSB(I)*VISCOB(I))**.5
          YOKB=STEPB*((DENSB(1)*VISCOB(1))**.5+4.0*EVEN+2.* ODD+
         1(DENSB(MAXXB)*VISCOB(MAXXB))**.5)
          YOK=VNNUM*YOKA+YOKB
C                         WAK
          EVEN=0.
          ODD=0.
          DO 321 I=2,MAXA,2
      321 EVEN=EVEN+DENSA(I)*VELPA(I)**2
          DO 322 I=3,LESSA,2
      322 ODD=ODD+DENSA(I)*VELPA(I)**2
          WAKA=STEPA*(DENSA(1)*VELPA(1)**2+4.*EVEN+2.*ODD+DENSA(MAXXA)
         1  *VELPA(MAXXA)**2)
          ODD=0.
          EVEN=0.
          DO 331 I=2,MAXB,2
      331 EVEN=EVEN+DENSB(I)*VELPB(I)**2
          DO 332 I=3,LESSB,2
      332 ODD=ODD+DENSB(I)*VELPB(I)**2
          WAKB=STEPB*(DENSB(1)*VELPB(1)**2+4.*EVEN+2.*ODD+DENSB(MAXXB)*
         1   VELPB(MAXXB)**2)
          WAK=WAKA+WAKB
C                                   XRAY
          EVEN=0.
          ODD=0.
          DO 341 I=2,MAXA,2
      341 EVEN=EVEN+DENSA(I)
          DO 342 I=3,LESSA,2
      342 ODD=ODD+DENSA(I)
          XRAYA=STEPA*(DENSA(1)+4.*EVEN+2.*ODD+DENSA(MAXXA))
          EVEN=0.
          ODD=0.
          DO 351 I=2,MAXB,2
      351 EVEN=EVEN+DENSB(I)
          DO 352 I=3,LESSB,2
      352 ODD=ODD+DENSB(I)
          XRAYB=STEPB*(DENSB(1)+4.*EVEN+2.*ODD+DENSB(MAXXB))
          XRAY=32.17*(DENSB(MAXXB)-XRAYA-XRAYB) *3600.**2.
C                               ZUL
          ODD=0.
          EVEN=0.
          DO 361 I=2,MAXA,2
      361 EVEN=EVEN+DENSA(I)*VELPA(I)*(ENTHA(I)-ENTINF)
          DO 362 I=3,LESSA,2
      362 ODD=ODD+DENSA(I)*VELPA(I)*(ENTHA(I)-ENTINF)
          ZULA=STEPA*(DENSA(1)*VELPA(1)*(ENTHA(1)-ENTINF)+4.*EVEN+2.*ODD
         1       +DENSA(MAXXA)*VELPA(MAXXA)*(ENTHA(MAXXA)-ENTINF))
          ODD=0.
```

```
      EVEN=0.
      DO 391 I=2,MAXB,2
  391 EVEN=EVEN+DENSB(I)*VELPB(I)*(ENTHB(I)-ENTINF)
      DO 372 I=3,LESSB,2
  372 ODD=ODD+DENSB(I)*VELPB(I)*(ENTHB(I)-ENTINF)
      ZULB=STEPB*(DENSB(1)*VELPB(1)*(ENTHB(1)-ENTINF)+4.*EVEN
     1          +2.*ODD+DENSB(MAXXB)*VELPB(MAXXB)*(ENTHA(MAXXB)-ENTINF))
      ZUL=ZULA+ZULB
C                HEAT COEF
      CONSTL=1.
      VN=1.
      DH=ENTWAL-ENTINF
      PART =((YOK *ABLE)**2.*1./(VN    *CONSTL))**(1./3.)*DH
      XCPART=((1.5*VCPA*WAK*DH/ZUL+1./CONSTL)/XRAY)**(-1./3.)
      HCPA =VCPA/TEMDIF*PART*XCPART
      HCPAVG=VCPAVG/TEMDIF*PART*((1.5*VCPAVG*WAK*DH/ZUL+1./CONSTL)
     1 /XRAY)**(-1./3.)
      HCPBUL=VCPBUL/TEMDIF*PART*((1.5*VCPBUL*WAK*DH/ZUL+1./CONSTL)
     1 /XRAY)**(-1./3.)
      HCPWAL= VWALL/TEMDIF*PART*((1.5*VWALL *WAK*DH/ZUL+1./CONSTL)
     1 /XRAY)**(-1./3.)
      FLUXWA=TEMDIF*HCPWAL
C   CALCULATE  HEAT  FLUXES
      FLUXA =TEMDIF*HCPA
      FLUXAV =TEMDIF*HCPAVG
      FLUXBU =TEMDIF*HCPBUL
      WRITE OUTPUT TAPE 6,106,NCASE,PRESS,TEMWAL,TEMINF,TEMDIF
      IF (PRINT-1.0)  399,399,401
  401 WRITE OUTPUT TAPE 6,108
      WRITE OUTPUT TAPE 6,53
      DO 500 I=1,MAXXA
  500 WRITE OUTPUT TAPE 6,110,FRACTA(I),VELPA(I),TEMPA(I),SPVOLA(I),
     1         ENTHA(I)
      WRITE OUTPUT TAPE 6,108
      WRITE OUTPUT TAPE 6,54
      DO 501 I=1,MAXXB
  501 WRITE OUTPUT TAPE 6,110,FRACTB(I),VELPB(I),TEMPB(I),SPVOLB(I),
     1           ENTHB(I)
      WRITE OUTPUT TAPE 6,108
      WRITE OUTPUT TAPE 6,550
      DO 510  I=1,MAXXA
  510 WRITE OUTPUT TAPE 6,110, TEMPA(I),CONDA(I),VISCOA(I),CPA(I)
      WRITE OUTPUT TAPE 6,108
      WRITE OUTPUT TAPE 6,56
      DO 511  I=1,MAXXB
  511 WRITE OUTPUT TAPE 6,110, TEMPB(I),CONDB(I),VISCOB(I),CPB(I)
  399 WRITE OUTPUT TAPE 6,108
      WRITE OUTPUT TAPE 6,400,TLISTD(1),DLIST(1),ELIST(1),TLISTE(1),
     1 VNNUM,ABLE,MAXA,MAXB,ZULA,ZULB,ZUL
      WRITE OUTPUT TAPE 6,57 , ENTWAL,ENTUM,ENTINF,TEMDIF
      WRITE OUTPUT TAPE 6,58 ,WAKA,WAKB,WAK,PART,XCPART
      WRITE OUTPUT TAPE 6,59 ,XRAYA,XRAYB, XRAY,YOKA,YOKB,YOK
      WRITE OUTPUT TAPE 6,60,VCPA,VBCP,VCPAVG,VCPBUL
      WRITE OUTPUT TAPE 6,108
      WRITE OUTPUT TAPE 6,403                  ,HCPA,FLUXA,PRCP,HCPAVG ,
     1 FLUXAV,PRCPAV,HCPBUL,FLUXBU,PRCPBU,HCPWAL,FLUXWA,PRWALL
      GO TO 10
   51 FORMAT(2F10.2,2F10.5,2I10,2F10.5)
   52 FORMAT(2F10.2,2F10.5,4I10)
   53 FORMAT(1H0,6X,6HFRACTA,14X,5HVELPA,15X,5HTEMPA,15X,
     1          6HSPVOLA,14X,5HENTHA/)
   54 FORMAT(1H0,6X,6HFRACTB,14X,5HVELPB,15X,5HTEMPB,15X,
     1          6HSPVOLB,14X,5HENTHB/)
  550 FORMAT(1H0,6X,5HTEMPA,15X,5HCONDA,15X,6HVISCOA,14X,3HCPA)
   56 FORMAT(1H0,6X,5HTEMPB,15X,5HCONDB,15X,6HVISCOB,14X,3HCPB)
   57 FORMAT  (//,5X,7HENTWAL=F10.2,5X,6HENTUM=F10.2,5X,7HENTINF=F10.2,
     1 5X,7HTEMDIF=F10.3)
   58 FORMAT(//,5X,5HWAKA=F14.8,4X,5HWAKB=F14.8,4X,4HWAK=F14.8,4X,5HPART
     1=F14.8,4X,7HXCPART=F14.8//)
   59 FORMAT  (5X,6HXRAYA=F14.8,5X,6HXRAYB=F14.8,5X,5HXRAY=E14.6,
     1 //,5X,5HYOKA=F14.8,5X,5HYOKB=F14.8,5X,5HYOK =F14.8//)
   60 FORMAT (5X,5HVCPA=F14.8,5X,5HVBCP=F14.8,5X,7HVCPAVG=F14.8,5X,
     1 7HVCPBUL=F14.8,//)
   61 FORMAT(I5/(6F10.3))
   62 FORMAT (6F10.3)
  106 FORMAT (1H1,10X,8HCASE NO.,I4,5X,9HPRESSURE=,F6.0, 5X,12HWALL TEMP
     1, =F8.2,5X,12HBULK TEMP, =F8.2,5X,13HTEMP, DIFF, =F5.2//)
  107 FORMAT(4E20.8)
  108 FORMAT(1H0)
  109 FORMAT(1H1)
  110 FORMAT(5E20.8)
  400 FORMAT(18HOTABLE TEST VALUES,5X,10HTLISTD(1)=,F8.2,5X,9HDLIST(1)=,
     1  F8.5,5X,9HELIST(1)=,F8.2,5X,10HTLISTE(1)=,F8.2//5X,6HVNNUM=F8.6,
     2 3X,5HABLE=F8.3,3X,5HMAXA=I3,3X,5HMAXB=I3,3X,5HZULA=F12.8,3X,5HZUL
     3B=F12.8,3X,4HZUL=F12.8)
```

```
  403 FORMAT(
     1       8X,21HHEAT TRANS. COEFF. IS,F8.2,3X,12HHEAT FLUX IS,F9.2,3X,
     2 21H(CLOSE PRANDTL NO. OF,F8.3,3X,20HBASED ON TABLED CP.)//8X,21HH
     3EAT TRANS. COEFF. IS,F8.2,3X,12HHEAT FLUX IS,F9.2,3X,21H(AVE.  PRA
     4NDTL NO. OF,F8.3,3X,20HBASED ON TABLED CP.)//8X,21HHEAT TRANS. COE
     5FF. IS,F8.2,3X,12HHEAT FLUX IS,F9.2,3X,21H(BULK  PRANDTL NO. OF,
     6  F8.3,3X,20HBASED ON TABLED CP.)//8X,21HHEAT TRANS. COEFF. IS,
     7  F8.2,3X,12HHEAT FLUX IS,F9.2,3X,21H(WALL PRANDTL NO. OF,F8.3,3X,
     8 20HBASED ON TABLED CP.))
       END


CPIF1C
       FUNCTION PIF1C(TEMP,TLISTC,NC,CLIST,MC)
       DIMENSION TLISTC(100),CLIST(100)
       BLIF(P,Q,R,S,T)=((Q-P)*(S-T)/(R-Q)+S)
       IF(TEMP-TLISTC(NC)) 2,1,1
     1 I=NC-1
       GO TO 15
     2 IF(TEMP-TLISTC(1)) 3,3,4
     3 I=1
       GO TO 15
     4 IF(MC) 7,5,7
     5 I=1
       GO TO 8
     7 I=MC
     8 IF(TEMP-TLISTC(I)) 10,10,9
     9 I=I+1
       GO TO 8
    10 MC=I
       I=I-1
    15 PIF1C=BLIF(TEMP,TLISTC(I),TLISTC(I+1),CLIST(I),CLIST(I+1))
       RETURN
       END


CPIF3D
       FUNCTION PIF3D(TEMP,TLISTD,ND,DLIST,MD)
       DIMENSION TLISTD(100), DLIST(100)
       BLIF (P,Q,R,S,T) =((Q-P)*(S-T)/(R-Q)+S)
       IF  (TEMP-TLISTD(ND)) 2,1,1
     1 I=ND-1
       K=1
       GO TO 30
     2 IF (TEMP-TLISTD(1)) 4,4,3
     4 I=1
       K=1
       GO TO 30
     3 IF (MD) 41,40,41
    40 I=1
       GO TO 42
    41 I=MD
    42 IF (TEMP-TLISTD(I)) 44,44,43
    43 I=I+1
       GO TO 42
    44 MD=I
     7 I=I-1
       IF((I+1)-ND) 11,5,11
    11 IF (I-1) 30,5,24
     5 K = 2
       GO TO 30
    24 K=3
    30 BLIF1 = BLIF(TEMP,TLISTD(I),TLISTD(I+1),DLIST(I),DLIST(I+1))
    10 IF(K-1) 23,23,12
    23 PIF3D=BLIF1
       RETURN
    12 IF((I+2)-ND) 13,13,16
    13 IF((I-1)-1) 14,15,15
    14 L=I+2
       GO TO 17
    15 L=I+2
       GO TO 17
    16 L=I-1
    17 BLIF2 = BLIF(TEMP,TLISTD(I),TLISTD(L),DLIST(I),DLIST(L))
       BLIF3 = BLIF(TEMP,TLISTD(I+1),TLISTD(L),BLIF1,BLIF2)
       IF (K-2) 19,19,27
    19 PIF3D= BLIF3
       RETURN
    27 L=I-1
    37 BLIF4 =BLIF  (TEMP,TLISTD(I),TLISTD(L),DLIST(I),DLIST(L))
       BLIF5=BLIF(TEMP,TLISTD(I+1),TLISTD(L),BLIF1,BLIF4)
    21 PIF3D=BLIF(TEMP,TLISTD(I+2),TLISTD(L),BLIF3,BLIF5)
       RETURN
       END
```

APPENDIX E

TABULATED PROPERTY VALUES

Table 1. Specific Heat Versus Temperature and Pressure

Temperature	Psia.		Temperature	Psia.	
F	3240	3300	F	3240	3300
680	2.25	2.20	715	5.77	8.22
681	2.27	2.22	716	5.40	7.25
682	2.31	2.25	717	5.06	6.37
683	2.34	2.27	718	4.84	5.93
684	2.37	2.32	719	4.58	5.52
685	2.42	2.36	720	4.37	5.15
686	2.48	2.40	721	4.17	4.87
687	2.53	2.45	722	3.99	4.60
688	2.61	2.52	723	3.82	4.39
689	2.70	2.58	724	3.68	4.19
690	2.79	2.64	725	3.55	4.03
691	2.87	2.73	726	3.45	3.90
692	2.98	2.82	727	3.36	3.77
693	3.08	2.92	728	3.26	3.65
694	3.23	3.03	729	3.16	3.54
695	3.36	3.14	730	3.09	3.43
696	3.54	3.28	731	3.01	3.33
697	3.74	3.42	732	2.94	3.24
698	3.97	3.62	733	2.87	3.15
699	4.25	3.82	734	2.79	3.07
700	4.63	4.04	735	2.74	2.98
701	5.10	4.33	736	2.68	2.91
702	5.68	4.66	737	2.63	2.85
703	7.00	5.13	738	2.57	2.78
704	8.90	5.95	739	2.52	2.73
705	11.25	7.07	740	2.47	2.67
706	27.5	8.6	741	2.43	2.62
707	85.	13.0	742	2.39	2.56
708	31.5	15.5	743	2.34	2.51
709	19.0	29.5	744	2.30	2.46
709.7	--	51.3	745	2.26	2.42
710	13.5	42.4	746	2.23	2.37
711	10.25	25.0	747	2.19	2.34
712	8.35	17.5	748	2.15	2.30
713	7.00	11.5	749	2.12	2.26
714	6.20	9.55	750	2.09	2.22

Table 2. Enthalpy Versus Temperature and Pressure

Btu/lb.	Psia. 3240	Psia. 3300
730.0	676.85F	677.45F
735.0	679.35	680.00
740.0	681.75	682.40
745.0	683.25	684.40
750.0	685.35	686.50
755.0	687.80	688.55
760.0	689.75	690.55
765.0	691.55	692.35
770.0	693.10	693.95
775.0	694.40	695.20
780.0	695.80	696.60
785.0	697.10	698.00
790.0	698.35	699.35
795.0	699.50	700.60
800.0	700.65	701.80
805.0	701.60	702.90
810.0	702.50	703.90
815.0	703.30	704.80
820.0	704.00	705.55
825.0	704.60	706.25
830.0	705.00	706.73
835.0	705.33	707.15
840.0	705.63	707.55
845.0	705.90	707.85
850.0	706.10	708.05
855.0	706.30	708.32
860.0	706.40	708.50
865.0	706.50	708.70
870.0	706.55	708.85
875.0	706.60	709.00
880.0	706.65	709.10
885.0	706.70	709.20
890.0	706.75	709.30
895.0	706.80	709.40
900.0	706.83	709.45
905.0	706.88	709.55
910.0	706.92	709.65
915.0	706.98	709.75
920.0	707.02	709.85
925.0	707.08	709.95
930.0	707.13	710.00
935.0	707.18	710.08
940.0	707.23	710.17
945.0	707.27	710.26
950.0	707.30	710.35
955.0	707.41	710.50
960.0	707.50	710.62
965.0	707.62	710.75
970.0	707.75	710.90
975.0	707.90	711.10
980.0	708.06	711.27
985.0	708.27	711.50
990.0	708.48	711.73
995.0	708.72	712.00
1000.0	709.00	712.35
1005.0	709.36	712.75
1010.0	709.75	713.15
1015.0	710.18	713.65
1020.0	710.70	714.15
1025.0	711.25	714.70
1030.0	711.90	715.40
1035.0	712.55	716.05
1040.0	713.25	716.80
1045.0	714.00	717.55
1050.0	714.75	718.40
1055.0	715.60	719.25
1060.0	716.40	720.10
1065.0	717.28	721.00
1070.0	718.15	722.00
1075.0	719.00	722.85
1080.0	720.10	724.00
1085.0	721.30	725.25
1090.0	722.60	726.50
1095.0	724.00	728.00
1100.0	725.50	729.40
1105.0	727.0	730.90
1110.0	728.55	732.50
1115.0	730.20	734.20
1120.0	731.90	735.80
1125.0	733.50	737.40
1130.0	735.50	739.20
1135.0	737.20	741.10
1140.0	739.00	743.11
1145.0	740.90	745.10
1150.0	743.00	747.10
1155.0	745.00	749.10
1160.0	747.10	751.20

Table 3. Specific Volume Versus Temperature and Pressure

F	Psia. 3240	Psia. 3300	F	Psia. 3240	Psia. 3300
	$\frac{ft^3}{lb.}$	$\frac{ft^3}{lb.}$		$\frac{ft^3}{lb.}$	$\frac{ft^3}{lb.}$
680.00	0.02801	0.02785	710.00	0.07758	0.05500
692.00	0.03036	0.03002	710.50	0.07930	0.06020
693.00	0.03063	0.03027	711.00	0.08064	0.06515
694.00	0.03093	0.03053	711.50	0.08210	0.06820
695.00	0.03120	0.03079	712.00	0.08338	0.07055
696.00	0.03155	0.03111	712.50	0.08460	0.07260
697.00	0.03178	0.03142	713.00	0.08570	0.07440
698.00	0.03223	0.03168	713.50	0.08680	0.07610
699.00	0.03264	0.03202	714.00	0.08773	0.07770
700.00	0.03310	0.03240	715.00	0.08975	0.08045
701.00	0.03358	0.03280	716.00	0.09160	0.08278
702.00	0.03420	0.03326	717.00	0.09327	0.08495
702.50	0.03460	0.03345	718.00	0.09492	0.08692
703.00	0.03495	0.03378	719.00	0.09635	0.08880
703.50	0.03540	0.03400	720.00	0.09783	0.09052
704.00	0.03587	0.03436	722.00	0.10062	0.09370
704.50	0.03650	---	724.00	0.10295	0.09635
705.00	0.03724	---	726.00	0.10525	0.09883
705.50	0.03820	0.03550	728.00	0.10760	0.10135
706.00	0.03948	0.03602	730.00	0.10968	0.10363
706.50	0.04580	0.03660	732.00	0.11160	0.10565
707.00	0.05220	0.03722	734.00	0.11400	0.10775
707.50	0.06100	0.03810	736.00	0.11590	0.10979
708.00	0.06835	0.03900	740.00	0.11960	0.11360
708.50	0.07160	0.04030	745.00	0.12350	0.11800
709.00	0.07375	0.04265	752.00	0.12820	0.12310
709.50	0.07570	0.04900			

APPENDIX F

Experimental Data

The experimental data obtained and used in correlation is shown in the following tables. Table 4 gives the measurements taken and Table 5 gives the computed values of the various parameters.

The run number, i.e., 32, corresponds to a series of data points taken with nearly constant bulk temperature and pressure. The points of the run were taken at different test section current settings. The asterisk means the data presented was taken over voltage taps 1-6 instead of taps 2-5.

Table 4. Measured Experimental Data

2 Mil Test Section

Run	Pressure Psia.	Mueller Bridge ohms	Standard Resistor Volts	Ribbon Volts
32-1	3240	61.02767	0.011747	0.3072
2		61.02897	0.017831	0.46696
3		61.03105	0.025988	0.68229
4		61.03537	0.033313	1.4563
5		61.0456	0.040242	1.06064
6		61.05245	0.045467	1.19936
7		61.07245	0.050296	1.32814
33-1	3240	61.55065	0.011783	0.31069
2		61.55165	0.018006	0.4750
3		61.55232	0.026099	0.68871
4		61.55387	0.033189	0.87644
5		61.55632	0.040356	1.06711
6		61.55965	0.045737	1.21079
7		61.5685	0.050476	1.33709
35-1	3240	61.78615	0.01167	0.30911
2		61.78702	0.018128	0.4810
3		61.7885	0.026033	0.6927
4		61.79307	0.033061	0.88304
5		61.79855	0.04038	1.08462
6		61.8070	0.045446	1.22819
7		61.8220	0.050318	1.36876
37-1*	3240	62.35642	0.011741	0.52214
2*		62.3571	0.018088	0.80704
3*		62.3629	0.026269	1.1792
4*		62.3754	0.033558	1.51859
5		62.37925	0.040654	1.11814
6		62.3962	0.045492	1.2630
38-1	3240	62.58235	0.011817	0.31742
2		62.5843	0.018584	0.50155
3		62.5874	0.026138	0.7000
4		62.5964	0.033495	0.91884
5		62.60887	0.040166	1.1121
6		62.62162	0.045098	1.26142
39-1	3240	60.8205	0.01288	0.31517
2		60.8178	0.018352	0.4907
3		60.81925	9.026312	0.68904
4		60.82707	0.033086	0.86801
5		60.83768	0.04008	1.05419
6		60.8478	0.04536	1.19594
7		60.8578	0.050233	1.32559
40-1	3240	61.35767	0.011788	0.30991
2		61.35735	0.018086	0.80042
3		61.35905	0.02608	0.68741
4		61.36367	0.033295	0.8780
5		61.36845	0.040255	1.06291
6		61.37562	0.045459	1.20165
7		61.3826	0.05024	1.32883

1 Mil Test Section

Run	Pressure Psia.	Mueller Bridge ohms	Standard Resistor Volts	Ribbon Volts
70-2	3300	60.9085	0.016053	0.71674
3		60.9100	0.022157	0.99124
4		60.9150	0.028145	1.2627
5		60.9230	0.032357	1.4551
7		60.9435	0.040656	1.8312
8		60.9520	0.045625	2.058
71-1	3300	61.7117	0.010024	0.45173
3		61.7128	0.022076	0.99615
4		61.7125	0.028165	1.2721
5		61.7144	0.032413	1.46583
6		61.7175	0.036681	1.6604
7		61.7193	0.040610	1.8407
8		61.723	0.045405	2.0627
73-1	3300			
2		61.7739	0.015127	0.68272
3		61.7754	0.020295	0.91731
4		61.7746	0.024108	1.0905
5		61.7766	0.028062	1.2707
6		61.776	0.03202	1.4524
7		61.776	0.036595	1.6622
8		61.7785	0.040736	1.8559
74-3	3300	61.7972	0.02002	0.90545
4		61.7978	0.024104	1.0919
5		61.7987	0.028075	1.2740
6		61.79885	0.032136	1.4624
7		61.8021	0.036403	1.6604
8		61.8035	0.040326	1.8452
76-1	3300	61.93795	0.010075	0.45706
2		61.9405	0.01505	0.68414
3		61.9435	0.02012	0.91784
4		61.9463	0.024036	1.0992
5		61.9505	0.028038	1.2875
6		61.9525	0.032249	1.4882
7		61.9600	0.036298	1.6835
8		61.9675	0.040357	1.8862
77-2	3300	62.359	0.015047	0.68874
3		62.364	0.020061	0.92214
4		62.363	0.024038	1.1094
5		62.372	0.028392	1.3189

Table 5. Computed Experimental Data

2 Mil Test Section

Run	h_c $\frac{Btu}{hr.ft^2.F}$	q" $\frac{Btu}{hr.ft^2}$	t_w F	t_∞ F	$G_r'_\infty$	P_{r_∞}	N_{u_∞}	$R_a'_\infty$
32-1	387.7	590.	696.25	694.73	1.12×10^{10}	2.32	579.3	2.61×10^{10}
2	424.8	1361.	697.96	694.75	2.48	2.32	634.9	5.75
3	465.3	2899.	701.03	694.8	5.40	2.32	695.7	12.5
4	565.8	4772.	703.32	694.88	7.50	2.33	922.7	17.5
5	651.7	6978.	705.79	695.08	14.67	2.35	977.3	34.5
6	768.4	8915.	706.82	695.22	27.67	2.37	1154.	65.6
7	873.9	10921.	708.12	695.62	40.36	2.42	1318.	97.8
33-1	496.5	599.	706.31	705.10	9.97×10^{10}	9.26	904.2	92.3×10^{10}
2	792.	1398.	706.89	705.12	18.9	9.49	1444.	180.
3	1376.	2939.	707.27	705.14	24.8	9.65	2510.	239.
4	1587.	4756.	708.17	705.17	33.2	10.0	2900.	333.
5	1540.	7041.	709.79	705.21	36.8	10.6	2823.	390.
6	1529.	9054.	711.2	705.28	38.7	11.3	2812.	439.
7	1691.	11030.	711.98	705.46	39.2	13.4	3140.	525.
35-1	283.0	590.	711.87	709.78	3.64×10^{10}	12.6	1036.	45.9×10^{10}
2	339.1	1426.	714.0	709.8	5.99	12.5	1243.	75.1
3	384.8	2948.	717.49	709.83	8.77	12.4	1412.	108.
4	389.2	4773.	722.18	709.92	11.19	12.0	1434.	134.
5	373.5	7160.	729.2	710.03	13.65	11.6	1382.	158.
6	342.1	9125.	736.87	710.2	15.59	11.1	1274.	173.
7	325.4	11260.	745.1	710.5	16.74	10.3	1225.	173.

Run	h_c $\frac{Btu}{hr.ft^2.F}$	q'' $\frac{Btu}{hr.ft^2}$	t_w F	t_∞ F	$G_{r'_\infty}$	P_{r_∞}	N_{u_∞}	$R_{a'_\infty}$
36-1	204.2	611.	717.28	714.29	2.41×10^{10}	5.48	840.	13.2×10^{10}
2	238.0	1437.	720.36	714.32	4.20	5.48	980.	23.0
3	258.9	3007.	726.0	714.39	6.60	5.45	1068.	36.0
4	247.9	4842.	734.0	714.47	9.20	5.43	1024.	49.9
5	269.7	7223.	741.39	714.61	10.85	5.38	1117.	58.3
6	257.8	9288.	750.98	714.95	12.14	5.26	1074.	63.9
7	247.5	11460.	761.62	715.32	13.34	5.15	1038.	68.7
37-1 *	180.7	603.	724.47	721.13	2.60×10^{10}	3.92	890.	10.1×10^{10}
2 *	193.9	1436.	728.55	721.14	5.33	3.92	1069.	20.9
3 *	204.5	3047.	736.16	721.26	9.33	3.90	1129.	36.4
4 *	202.0	5013.	746.32	721.51	12.87	3.86	1118.	49.7
5	198.0	7432.	759.12	721.58	8.85	3.85	897.	34.1
6	190.7	9394.	771.18	721.92	10.2	3.80	867.	38.8
38-1	169.6	613.	729.25	725.63	1.25×10^{10}	3.36	795.	4.22×10^{10}
2	160.7	1524.	735.15	725.67	2.98	3.36	753.	10.0
3	172.7	3035.	743.3	725.73	4.73	3.36	810.	15.9
4	168.4	5032.	755.79	725.91	6.54	3.34	791.	21.9
5	175.9	7303.	767.67	726.16	7.99	3.32	828.	26.5
6	170.9	9301.	780.83	726.41	9.40	3.30	806.	31.1
39-1	317.7	623.	692.59	690.63	1.03×10^{10}	1.97	458.	2.05×10^{10}
2*	399.7	1438.	694.17	690.57	3.91	1.97	704.	7.72
3	405.9	2964.	697.7	690.6	4.83	1.97	584.	9.53
4	501.4	4695.	700.12	690.76	6.79	1.98	723.	13.5
5	562.6	6908.	703.24	690.96	10.55	1.99	812.	21.0
6	590.3	8869.	706.19	691.17	20.69	2.00	853.	41.5
7	684.3	10890.	707.28	691.37	34.8	2.02	991.	70.4

Run	h_c $\frac{Btu}{hr.ft^2.F}$	q'' $\frac{Btu}{hr.ft^2}$	t_w F	t_∞ F	$G_r'_\infty$	P_{r_∞}	N_{u_∞}	$R_a'_\infty$
40-1	421.0	597.	702.69	701.27	2.08×10^{10}	3.7	686.	7.72×10^{10}
2	470.7	1408.	704.26	701.27	9.10	3.7	938.	33.7
3	647.3	2931.	705.83	701.30	9.94	3.71	1056.	36.9
4	951.8	4779.	706.42	701.39	17.9	3.75	1555.	67.2
5	1074.3	6995.	708.0	701.49	37.0	3.79	1758.	140.
6	1155.0	8931.	709.36	701.63	40.2	3.85	1896.	155.
7	1309.7	10915.	710.1	701.77	41.3	3.91	2156.	162.

1 Mil Test Section

Run	h_c $\frac{Btu}{hr.ft^2\ F}$	q'' $\frac{Btu}{hr.ft^2}$	t_w F	t_∞ F	$G_r'_\infty$	P_{r_∞}	N_{u_∞}	$R_a'_\infty$
70-2	396.8	1858.	697.05	692.37	3.12×10^{10}	1.99	572.8	6.21×10^{10}
3	491.8	3547.	699.61	692.4	4.92	1.99	710.0	9.79
4	533.4	5740.	703.26	692.5	8.23	2.00	770.8	16.4
5	559.8	7604.	706.24	692.66	12.5	2.01	810.1	25.1
7	760.5	12030.	708.88	693.06	20.9	2.04	1105.	42.5
8	898.3	15165.	710.11	693.23	34.2	2.05	1307.	70.2
71-1	1161.	731.	708.93	708.30	4.32×10^{10}	14.3	2256.	61.6×10^{10}
3	1567.	3552.	710.59	708.33	24.9	14.5	3051.	361.
4	1642.	5787.	711.84	708.32	30.8	14.4	3195.	444.
5	1514.	7674	713.43	708.36	34.0	14.8	2954.	503.
6	1583.	9837.	714.63	708.42	35.5	15.4	3102.	548.
7	1530.	12073.	716.35	708.45	37.1	15.8	3005.	587.
8	1409.	15127.	719.26	708.53	39.1	16.6	2786.	648.
73-2	1279.	1668.	710.84	709.54	14.7×10^{10}	34.95	3109.	$515. \times 10^{10}$
3	952.6	3007.	712.73	709.57	21.2	35.7	2332.	758.
4	1010.	4246.	713.76	709.55	23.5	35.3	2462.	829.
5	1043.	5759.	715.12	709.60	25.0	36.3	2569.	908.
6	978.0	7511.	717.26	709.58	27.4	36.0	2400.	987.
7	1037.	9824.	719.05	709.58	28.9	36.0	2547.	1041.
8	916.0	12211.	722.96	709.63	30.7	37.3	2275.	1144.
74-3	1027.	2928.	712.86	710.00	16.0×10^{10}	32.8	2771.	$524. \times 10^{10}$
4	862.9	4251.	714.94	710.02	19.6	32.7	2334.	640.
5	807.6	5777.	717.19	710.03	21.9	32.5	2191.	712.
6	708.0	7590.	720.76	710.04	24.7	32.4	1922.	803.
7	714.5	9762.	723.76	710.1	25.8	31.7	1962.	817.
8	676.7	12018.	727.89	710.13	27.4	31.3	1867.	858.

Run	h_c $\frac{Btu}{hr.ft^2 F}$	q'' $\frac{Btu}{hr.ft^2}$	t_w F	t_∞ F	$G_r'_\infty$	P_{r_∞}	N_{u_∞}	$R_a'_\infty$
76-1	184.3	744.	716.84	712.80	6.48×10^{10}	10.8	651.55	69.6×10^{10}
2	254.	1663.	719.4	712.85	8.74	10.5	900.0	91.8
3	270.1	2983.	723.95	712.91	11.5	10.2	959.6	117.
4	300.9	4267.	727.15	712.97	12.9	9.94	1071.	128.
5	300.0	5830.	732.49	713.05	14.8	9.70	1072.	143.
6	299.2	7752.	739.0	713.09	16.7	9.64	1071.	161.
7	305.3	9870.	745.57	713.24	18.0	9.41	1099.	169.
77-2	234.4	1674.	728.32	721.18	3.61×10^{10}	4.43	999.5	16.0×10^{10}
3	237.8	2988.	733.84	721.30	5.50	4.41	1016.	24.2
4	240.9	4307.	739.14	721.26	7.07	4.42	1028.	31.2
5	230.5	6048.	747.68	721.44	8.88	4.38	986.6	38.9

APPENDIX G

SAMPLE CALCULATION OF EXPERIMENTAL RESULTS

The computed data presented in Table 5 was calculated from the measured data presented in Table 4. The procedure will be shown below for the case 32-5.

The measured data was the following:

V_{2-5} = test section voltage across taps 2-5 = 0.04024 volts,

$V_{std.r.}$ = standard resistor voltage = 1.06064 volts,

R_t = Mueller bridge reading = 61.0456 ohms,

and P = pressure = 3225 $\frac{lb.}{in^2}$ gage.

The atmospheric pressure was taken as 15 $\frac{lb.}{in^2}$ as the gauge could not be measured within this error.

The bulk fluid temperature was calculated from the relationship for platinum resistance thermometers given by the National Bureau of Standards, viz.,

$$t = \frac{R_t - R_o}{a_1 R_o} + \delta\left(\frac{t}{100} - 1\right)\frac{t}{100} \quad ,$$

where

R_o = thermometer ice point resistance = 25.5571 ohms,

a_1 = 3.926685×10^{-3},

and δ = 1.49187.

The constants a and δ were determined by the National Bureau of Standards for the thermometer used. This expression was solved for temperature in Fahrenheit yielding,

$$t = \left(\frac{BK - \sqrt{BK^2 - CC}}{2} \right) 1.8 + 32 ,$$

where

$$BK = 10^2 + \frac{10^4}{\delta}$$

and $$CC = 4\left(\frac{10^4}{\delta}\right)\left(\frac{R_t - R_o}{a R_o}\right) .$$

For the bridge reading of 61.0456 ohms, the bulk fluid temperature was 695.09 F.

The resistance of the ribbon between taps 2-5 $R_{x_{2-5}}$ was determined from the voltage measurement of the ribbon between taps 2-5 and voltage of the standard resistor by

$$R_{x_{2-5}} = V_{x_{2-5}} \left(\frac{R}{V}\right)_{STD.\,R.} = 0.02636 \text{ ohms} .$$

The ribbon temperature was determined from the calibration relationship, viz.,

$$t_w = \left(\frac{\frac{R_{2-5}}{0.6017} - A}{B} \right) + 670$$

where A and B were the calibration constants. The number, 0.6017, corrected for the ratio of the ribbon resistance $\frac{R_{x_{2-5}}}{R_{x_{1-6}}}$ as the voltage

$V_{x_{1-6}}$ between taps 1-6 was used in calibration to determine A and B, but the data was taken using taps 2-5. This ratio was determined during the calibration procedure. The wall temperature was 705.79 F.

The heat flux was determined from the joulean heat generation and ribbon area yielding

$$q''_w = \frac{V_{x_{2-5}} \left(\frac{V}{R}\right)_{STD.R.}}{Area_{2-5}} \left(3.415 \frac{Btu.}{watt\,hr.}\right) = 6978 \frac{Btu.}{hr.\,ft^2}$$

This area was twice the width times the height and was

$$Area_{2-5} = \frac{2(0.5 \text{ in. width})(3.007 \text{ in. height})}{144 \frac{in^2}{ft^2}} = 0.02088 \text{ ft}^2$$

The edges of the ribbon were neglected.

The heat transfer coefficient was the heat flux divided by the temperature difference and was

$$h_c = \frac{q''_w}{t_w - t_\infty} = 651 \frac{Btu.}{hr.\,ft^2.\,F} .$$

The properties of specific heat and density were determined by linear interpolation of tabulated data and were

$$C_{p_\infty} = 3.375 \frac{Btu.}{lb.F},$$

$$\rho_\infty = 32.0 \frac{lb.}{ft^3},$$

and

$$\rho_w = 25.67 \frac{lb.}{ft^3} .$$

The bulk fluid viscosity and thermal conductivity were calculated from the equations

$$\mu = 32.17(3600)(0.04788t + 14.79 + 0.6066\rho^{1.48})\times 10^{-8} = 0.1744 \frac{lb.}{ft.hr.},$$

and

$$k = 0.246 + \left[0.4(t - 550) + 28.83\rho^{1.85}\right] \times 10^{-4} = 0.250 \frac{Btu.}{hr.ft.F}.$$

The thermal coefficient of expansion was found by the relationship

$$\beta = \frac{C_p - 1}{0.2079(t + 460)} = 9.893 \times 10^{-3} \frac{1}{F}.$$

The dimensionless numbers were then found from the proper grouping of the above properties.

All of the computation shown in this section was done by a digital computer.

APPENDIX H

TEST SECTION CALIBRATION

The platinum ribbon resistance-temperature relationship was experimentally determined in the following manner:

1. The pressure vessel and internal water were heated to a desired temperature.
2. A current of 200-300 milliamperes was passed through the ribbon.
3. A differential thermocouple across the vertical height of the ribbon was checked to ensure minimum vertical temperature gradient.
4. A series of readings were taken of the Mueller bridge, voltage across the ribbon, and voltage across the 0.10002 ohm standard resistor.

The readings were taken over a several minute period to ensure that steady state had been obtained with both the fluid temperature and calibration current remaining reasonably constant.

The resistance of the ribbon thus determined was fitted to a straight line curve by the method of least squares with temperature (bridge resistance converted to temperature) as the independent variable. Although the resistance of platinum is not exactly linear with temperature, a linear curve may be used over a reasonable temperature increment.

The temperature of the platinum ribbon was then

$$t = \frac{R_x - A}{B} + 670$$

where R was the test section resistance, A was its resistance at 670 F, and B was the slope of the curve.

The absolute value of the error between the data points and generated curve was then determined.

The one mil test section was calibrated daily and the individual calibrations are shown for each group of data runs.

The voltage across taps 1-6 was used for calibration of the two mil ribbon, while the voltage across taps 2-5 was used for the one mil ribbon.

The voltage across the adjacent taps was also measured to determine the fractional resistance of each local section. As the ribbon was essentially uniform in thickness, this fractional resistance was used to determine the temperature of the individual section by proper correction of the measured voltage. The fractional resistance was also used to determine distance between individual taps from a measurement across taps 1-6 made by a steel rule.

A tabulation of the fractional resistance is given in Table 7. The distance tabulated is the height from the leading edge of the ribbon to the midpoint of the adjacent taps except for 1-6 and 2-5, where it is the height from the leading edge to the top tap.

Table 6. Calibration Measurements

Two Mil Ribbon

Standard R. Volts	Ribbon Volts	Bridge Ohms	Ribbon Ohms	Error F
0.028826	0.012848	62.65379	0.04458	0.196
0.028821	0.012942	63.13304	0.044913	0.048
0.028564	0.012364	60.85852	0.043296	0.047
0.028876	0.012605	61.3678	0.043661	0.062
0.028486	0.012668	62.53571	0.044483	0.164

$A = 0.42533 \times 10^{-1}$ $B = 0.35747 \times 10^{-4}$

One Mil Ribbon

Runs 70-73

0.028789	0.012997	61.78642	0.045155	0.0
0.028294	0.012913	60.93571	0.04456	0.0

$A = 0.43752 \times 10^{-1}$ $B = 0.35267 \times 10^{-4}$

Runs 74-77

0.028763	0.013094	62.35627	0.045531	0.001
0.028863	0.013033	61.83237	0.045164	0.001

$A = 0.43729 \times 10^{-1}$ $B = 0.35239 \times 10^{-4}$

Table 7. Experimental Constants

	Two Mil Ribbon		One Mil Ribbon	
taps	x Distance ft.	Ratio	x Distance ft.	Ratio
1-2	0.417	0.19946		
2-3	0.3336	0.20046		
2-4	0.2503	0.20129		
4-5	0.167	0.19995		
5-6	0.08366	0.19899		
1-6	0.4583	1.0		
2-5	0.3748	0.6017	0.3755	0.9994*

* Correction for ratio box.

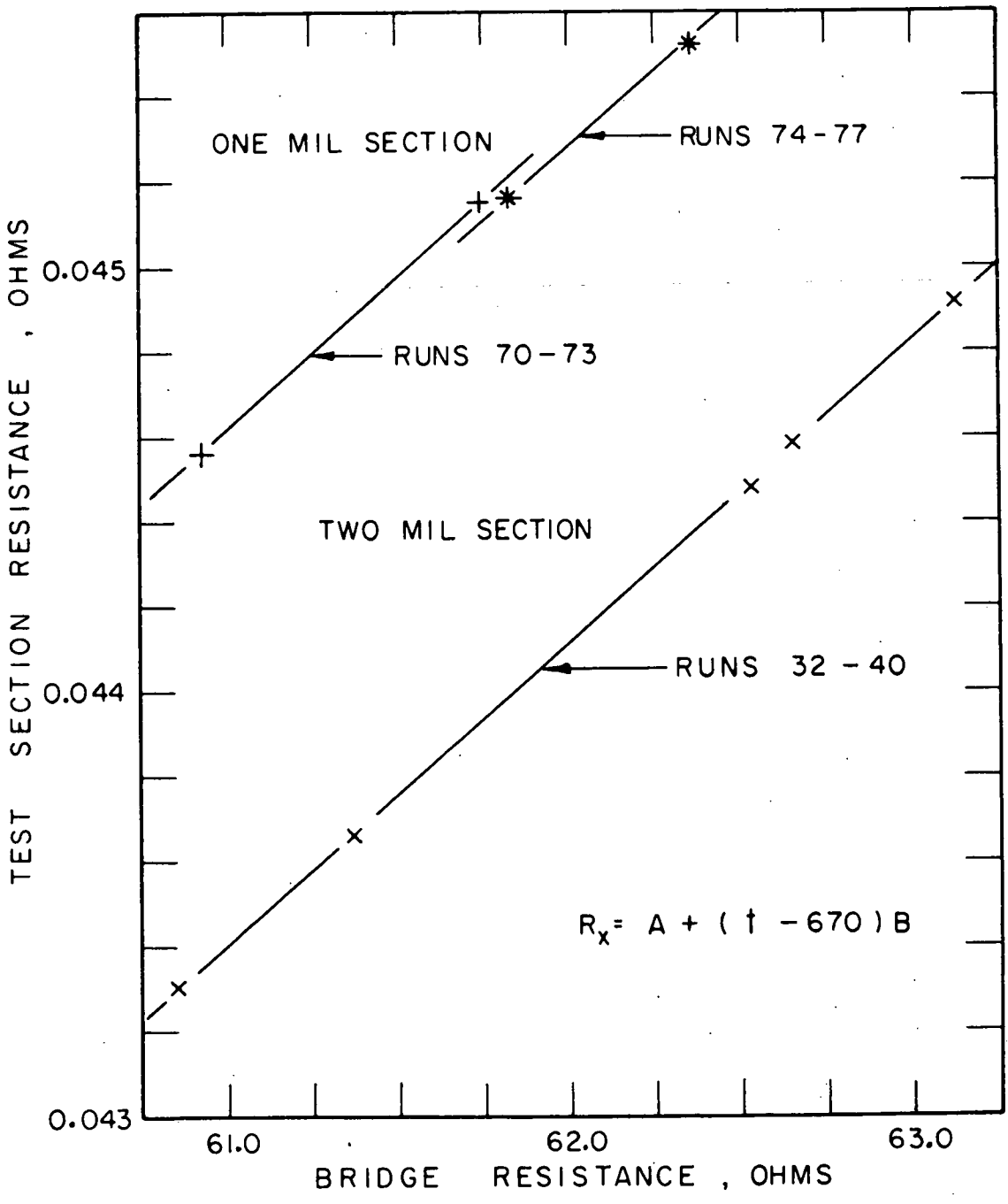

FIG. 32 TEST SECTION RESISTANCE VERSUS BRIDGE RESISTANCE

APPENDIX I

ERROR ANALYSIS

Measurement Error

The accuracy of the Mueller bridge was stated to be 0.02 percent by the manufacturer. This could yield a maximum absolute error of about 0.24 Fahrenheit at a temperature of 700 Fahrenheit. It is felt that the bridge was probably more consistent than this and any error was probably of near constant magnitude. However, this placed a severe limit on anticipated accuracy. The bridge was read to the closest 0.0001 ohm. Temperature fluctuations and drifts were normal but were less than 0.05 Fahrenheit during calibration but sometimes larger during data taking.

The potentiometer used to measure voltage was accurate to 0.01 percent on the scale used for taking data and 0.015 percent on the scale used for calibration. This would allow an error of about one-tenth degree in the test section temperature.

The calibration data was fitted to a straight line by a least squares fit and then the individual errors were computed. This largest computed error was about 0.20 F and was of reasonable magnitude.

During data taking runs fluctuations and drifts of the power supply occurred above 20 amperes. This was noted visually by watching the null detector when the potentiometer was measuring the voltage across the standard resistor. Larger fluctuations were noted of the

voltage drop across the test section. This effect was somewhat reduced by shifting to a less sensitive scale of the null detector. However, some visual averaging of dial readings was necessary at high current settings yielding an error with possible magnitude of 0.03 to 0.05 percent.

The procedure of correcting the ribbon fractional resistances to obtain a local ribbon temperature introduced a possible error estimated less than two-tenths degree for the two mil ribbon. An error in using the voltage ratio box in parallel with the one mil ribbon was estimated at less than two-tenths degree. A correction for the ratio box was determined by voltage measurement with the ratio box in the circuit compared to the same measurement with the box out of the circuit.

Thus the possible error in temperature differences was estimated around 25 percent for differences less than one degree and less than five percent above a difference of ten degrees.

The error introduced by excluding the ribbon edges in the area calculation was less than one-half percent and therefore negligible.

Error Analysis for a Thermocouple Attached to a Plate of Finite Thickness

The following analysis is made in order to obtain an approximate magnitude for the error caused by attaching a thermocouple to a plate of finite thickness. Consider a plate of unit radius with a long thermocouple lead attached to the center of the plate. The edge of the plate is at a uniform temperature, T_m. The thermocouple is exposed to an ambient fluid of temperature, T_∞. The temperature at the junction is T_1. The plate is shown in Figure 33.

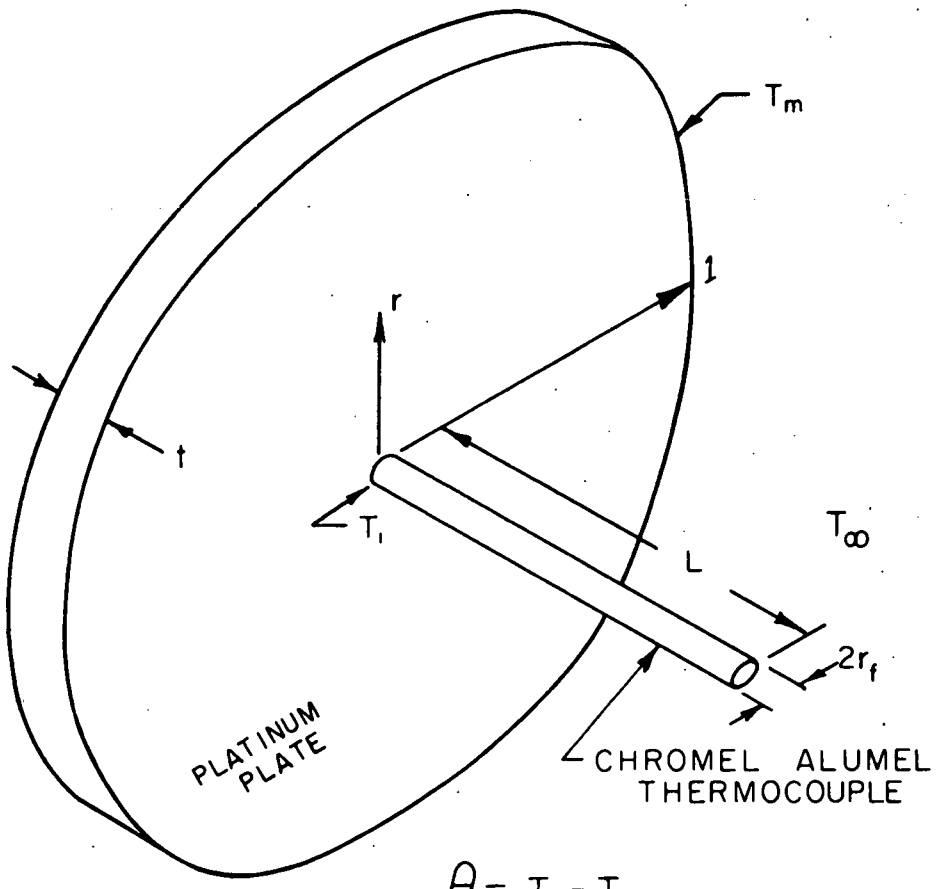

$$\theta = T - T_\infty$$

k_p = CONDUCTIVITY OF THE PLATE , 44 $\frac{\text{Btu}}{\text{hr} \cdot \text{ft} \cdot \text{F}}$

k_f = CONDUCTIVITY OF THE THERMOCOUPLE , 15 $\frac{\text{Btu}}{\text{hr} \cdot \text{ft} \cdot \text{F}}$

$P = 2\pi r_f$

FIG. 33 NOMENCLATURE FOR ANALYSIS OF THERMOCOUPLE ATTACHED TO A THIN PLATE

The equation for the temperature distribution in the plate may be written as

$$\frac{\partial}{\partial r}\left(r\frac{\partial \theta}{\partial r}\right) = 0 \quad ,$$

for a plate with symmetrical boundary conditions at steady state with no heat generation and no convection or radiation losses.

Upon integrating, a solution of the form

$$\theta = A \ln r + B$$

is obtained, where A and B are constants. Using the boundary conditions.

$$\theta = \theta_m \quad \text{at} \quad r = 1 \quad ,$$

and

$$\theta = \theta_1 \quad \text{at} \quad r = r_f \quad ,$$

the equation becomes

$$\theta = \theta_m - (\theta_m - \theta_1) \ln \frac{r}{r_f} \quad .$$

The heat flowing into the fin may be written as

$$q\Big|_{r=r_f} = -2\pi r_f t k_p \frac{\partial \theta}{\partial r}\Big|_{r=r_f} \quad .$$

Using the temperature distribution expression to determine the derivative, the equation becomes

$$q\Big|_{r=r_f} = -2\pi t k_p \frac{(\theta_m - \theta_1)}{\ln r_f} \quad .$$

Now considering the thermocouple length as infinite, the heat transferred by the fin effect is

$$q = (h_c P k_f A_f)^{1/2} \theta_1 = -2\pi t k_p \frac{\theta_m - \theta_1}{\ln r_f} .$$

Defining a collection of terms by

$$C = - \frac{(h_c P k_f A_f)^{1/2} \ln r_f}{2\pi k_p t} ,$$

a relationship expressing the ratio of temperature differences is found to be

$$\frac{T_m - T_1}{T_m - T_\infty} = \frac{C}{1 + C}$$

This expresses a temperature error caused by attaching the thermocouple to the plate.

For water at 690 F and 3300 psia, and with a five mil thermocouple wire the Grashof number equals about ten for a temperature difference of one degree. The Nusselt number according to Jakob Vol. I, Fig. 25-1, equals about two for a Prandtl number of unity. The coefficient of heat transfer is then about $1.2 \times 10^3 \frac{\text{Btu}}{\text{hr.ft}^2 \text{ F}}$. For this coefficient and a plate two mils thick, the parameter C equals 0.332. and the corresponding temperature error is

$$\frac{C}{1 + C} = 25\% .$$

For a one mil plate the error would be nearly 40 percent; for a five mil plate it would be about 12 percent.

A parameter similar to C for a thermocouple attached to a semi-infinite wall is given by Jakob, Vol. II, p. 153 as

$$C' = \frac{\pi}{k_p}\left(\frac{k_f h_c r_f}{8}\right)^{1/2} .$$

This expression gives an error of 4.3 percent.

This analysis indicates that the thermocouple correction for a wire attached to a semi-infinite solid is not valid when applied to a thin foil. The additional effects of convection and joulean heat generation would undoubtedly change the magnitude of the correction. To analytically study their effect is beyond the scope of this analysis.

Heat Loss Due to Lead Wires

For a specific heat generation rate in the test ribbon a fraction of the heat will be transferred to the ambient fluid by the lead wires. This heat transferred by each wire may be calculated approximately by

$$q = \left(h_c k 2\pi^2 r^3\right)^{1/2}(t_w - t_\infty)$$

where each wire is considered infinite in length with no internal heat generation.

Assuming k equal to 44 $\frac{\text{Btu}}{\text{hr.ft.}^\circ\text{F}}$ for platinum and h_c equal to 1200 $\frac{\text{Btu}}{\text{hr.ft}^2\,^\circ\text{F}}$ for six, five mil wires and equal to 600 $\frac{\text{Btu}}{\text{hr.ft}^2\,^\circ\text{F}}$ for two,

40 mil wires, this total heat loss may be computed equal to $4.9 \times 10^{-2} (t_w - t_\infty)$. If the heat transfer coefficient from the ribbon surface to the fluid is uniform and equal to 200 $\frac{Btu}{hr.ft^2.F}$, for a six inch long ribbon the heat transfer is 8.3 $(t_w - t_\infty)$ $\frac{Btu}{hr.}$. The fraction of heat transferred by the wires may be easily computed by the ratio and is 0.014.

This effect was neglected since the heat transfer coefficient of the ribbon was usually above 200 and the temperature at the wire-ribbon contact point will be significantly lower than the remainder of the ribbon.